

國立交通大學

電子物理研究所

博士論文

週期性分散式砷化鋁鎵銦多量子井的光學特性：
自發輻射、受激輻射及飽和吸收特性

Optical Properties of the Periodically Distributed AlGaInAs
Multiple-Quantum-Wells: Spontaneous Emission, Stimulated
Emission and Saturable Absorption

研究生：陳毅帆

指導教授：陳永富 教授

中華民國一百零二年六月

週期性分散式砷化鋁鎵銦多量子井的光學特性：自發輻射、受
激輻射及飽和吸收特性

Optical Properties of the Periodically Distributed AlGaInAs
Multiple-Quantum-Wells: Spontaneous Emission, Stimulated Emission and
Saturable Absorption

研究生：陳毅帆

Student : Yi-Fan Chen

指導教授：陳永富

Advisor : Yung-Fu Chen

國立交通大學

電子物理學系

博士論文

A Dissertation

Submitted to Department of Electrophysics

College of Science

National Chiao Tung University

in partial Fulfillment of the Requirements

for the Degree of

Doctor of Philosophy

in

Electrophysics

June 2013

Hsinchu, Taiwan, Republic of China

中華民國一百零二年六月


週期性分散式砷化鋁鎵銻多量子井的光學特性： 自發輻射、受激輻射及飽和吸收特性

學生：陳毅帆

指導教授：陳永富

國立交通大學電子物理學系博士班

摘 要



週期性排列的半導體多量子井結構作為半導體雷射的增益介質上相較於傳統的異質結構具有波長可調、低激發放射的閾值及較好的載子侷限特性。而相較於離子摻雜的晶體，其作為被動式 Q 開關固態雷射的飽和吸收體上也具有非飽和損失較小及作用長度極短的優點。結合以上特性半導體多量子井結構很有潛力作為一個同時進行飽和吸收及波長轉換的光學元件。此外由其近似二維的量子侷限結構加上高強度的激發使得受激載子間的多體效應相當顯著。因此本論文架構基本上可分為三個部份，第一部份首先討論高濃度電子電洞對在近似二維侷限的多量子井結構下展現的多體效應，藉由較高的侷限能障及週期性排列的多量子井結構我們觀察到了常溫下重整化能隙的自發輻射頻譜，相較於過去文獻僅對此輻射頻譜作不同受激載子濃度下的探討，我們對此多體效應下新發生的態對溫度的頻譜變化及輻射頻譜的集成強度作詳細的探討，並配合其發生的閾值強度隨溫度增加指數提升的結果驗證了週期性的多量子井結構對常溫下重整化態自發輻射頻譜的觀察的重要性。

在了解了高激發強度下多量子井結構的螢光特性後，本論文的第二部份則是實現以砷化鋁鎵銻多量子井結構作為光激發半導體雷射的增益介質。首先藉由摻鈦光纖的功率放大器作為激發光源實現了出光波長在 1220 nm 的高重覆率及高尖

峰功率光激發半導體雷射，在脈衝頻率及寬度可調的激發光源下可優化最佳的雷射輸出條件。接著在相同的激發光源下將同樣砷化鋁鎵銻半導體多量子井結構設計在光通訊及人眼安全波段以得到 1520 nm 的高重覆率及高尖峰功率光激發半導體雷射輸出，其中經由高透明度及高熱傳導率的單晶鑽石散熱片與半導體增益介質的鍵合技術解決了高重覆率及高激發功率下的熱反轉現象，使得最佳雷射操作重覆率從 30 kHz 提升到 200 kHz 且最高平均功率輸出提升了 4.7 倍，即使將重覆率提升到 500 kHz 仍有 2.32 W 的平均功率及 170 W 的尖峰功率輸出。

本論文最後一部份則是利用設計在 1530 nm 的砷化鋁鎵銻多量子井結構同時作為 1064 nm 摻釹釷酸鈣固態雷射的飽和吸收體及波長轉換元件，其多量子井結構 $n=2$ 的能階提供 1064 nm 的非線性飽和吸收作用而 $n=1$ 的能階搭配適當耦合共振腔則可進行增益轉換產生 1530 nm 的脈衝雷射輸出，此一架構結合了自調 Q 雷射、腔外脈衝式幫浦雷射及半導體多量子井結構的優點，由於被動式 Q 開關不需額外電子驅動元件且和受摻離子晶體飽和吸收體及非線性晶體相比量子井結構的作用長度相當短可縮減腔長，因此若搭配第二部份所述不同介質間的鍵合技術其相當具潛力作為低成本、簡單、一體成形且波長可設計範圍廣的微片被動式調 Q 雷射。



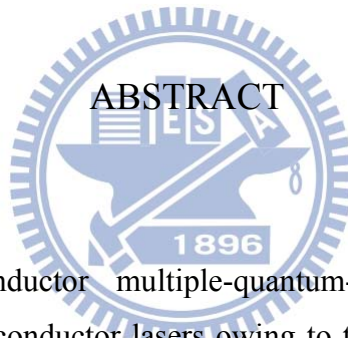
Optical Properties of the Periodically Distributed AlGaInAs Multiple-Quantum-Wells: Spontaneous Emission, Stimulated Emission and Saturable Absorption

Student : Yi-Fan Chen

Advisor : Yung-Fu Chen

Department of Electrophysics

National Chiao Tung University



Recently, the semiconductor multiple-quantum-wells (MQWs) structure is extensively used in the semiconductor lasers owing to the characteristics like versatile emission wavelength, lower laser threshold and excellent performance under room temperature operation. It is also applied as a promising saturable absorber in the diode-pumped passively Q-switched solid-state laser. Compared to the doped crystal saturable absorber, the MQWs absorber has lower non-saturable loss and allows the shorter cavity length. According to these characteristics, the MQWs structure has the potential to be designed simultaneously as a saturable absorber and an active medium in the intra-cavity pumped solid-state lasers. Besides, the many-body effect of the high density electron-hole plasma (EHP) under this quasi-2D confinement structure is also an interesting issue. Therefore, the contents of this dissertation are organized to be three parts. At the first part we investigate the many-body effect of the high density EHP in the quasi-2D confined MQWs structure. The room temperature spontaneous emission of the renormalized bandgap is observed under the designation of high confinement energy and periodically aligned gain structure. The temperature dependent luminescence features such as photoluminescence (PL) spectrum and the integrated PL intensity are

discussed and the threshold excitation intensity of the luminescence of renormalized band-edge is shown to be exponentially increased with increasing temperature. As a result we have confirmed that the periodically aligned MQWs structure is beneficial to the observation of room temperature many-body state emission

In the second part, an AlGaInAs MQWs structure is designed to be the gain chip of a high repetition rate and high peak power 1220 nm optically-pumped semiconductor laser (OPSL). By using an Yb-doped master oscillator fiber amplifier as the pump source, the output performance could be optimized with the free controlled pump conditions such as pump repetition rates and pulse durations. Then the same pump laser is used to excite the high repetition rate and high peak power AlGaInAs MQW OPSL at the communication and eye-safe spectral region of 1520 nm. By capillary bonding the highly transparent and thermal conductive single crystal diamond heat spreader to the gain chip, the thermal roll-over effect was eased at high average pump power under high repetition rate operation. The optimized repetition rate was raised from 30 to 200 kHz and the maximum average output power was scaled to be 4.7 times higher. When operated at as high as 500 kHz, the maximum average power of 2.32 W and peak power of 170 W were obtained.

At the end of this dissertation an AlGaInAs MQW structure is used simultaneously as the saturable absorber (SA) and wavelength-converted component in the Nd:GdVO₄ laser. It is fabricated to accommodate the pump level of 1064 nm and the emission level of 1530 nm in the quantum well region. The upper state is served as the nonlinear saturable absorption device at 1064 nm and the lower state is served as the active medium at 1530 nm with additional couple-cavity in the Nd:GdVO₄ laser. This configuration combines the advantages of the self-Q-switched lasers, pulse-pumped solid state lasers and the semiconductor MQW structures. Because there is no need of additional electronic drivers for passively Q-switches and the shorter action lengths of the MQWs compared to the bulk crystal SAs and nonlinear crystals, the device configuration could be simplified and cavity length is shortened, respectively. According to these characteristics and the capillary bonding technique in second part, this laser system has potential to be served as a low cost, simple and monolithic passively Q-switched microchip laser with broad achievable spectral range.

誌 謝

能完成這份博士論文及學位有許多需要感謝的對象，首先我最需要感謝的是我的指導老師-陳永富教授，陳老師除了指引我學習及研究的方向之外其在課堂上的教誨也讓我建立了立身處世的原則，其次要感謝的是黃凱風教授，除了提供實驗中最重要的半導體樣品外，黃老師對於我的研究也提供了許多想法及意見，而作為共同指導的蘇冠暉助理教授則是教導了我在研究上許多的基礎知識和經驗，而對於我許多想法上的反饋也促使我建立了邏輯性的思考。接著我想要感謝我的父母，除了生育養育我以及不辭辛勞的付出之外，自小至大對我的人格的培育有無可比擬的重要性，並且容忍及支持我人生中如此長的求學生涯，因此我每每思其恩德均不敢或忘。

除了師長及父母的影響之外，在研究所這段求學生涯中也受到實驗室許多同仁的幫助，在這裡感謝張漢龍博士指導我半導體雷射的概念、黃仕璋博士教導我架腔等實驗裝置的基礎、江柏毅學長提供我實驗上許多電子裝置的支援以及余彥廷博士和段必輝學弟協助我完成低溫下重整化能隙自發輻射頻譜的量測，也感謝其他同仁在實驗上及生活上提供的大大小的協助。最後要感謝的是政府及學校單位在網路、書籍及設施等資源上的提供以及國科會在實驗經費及個人工作費上的補助。

Contents

Abstract (Chinese)	i
Abstract	iii
Acknowledgement	v
Contents	vi
List of Figures	viii
List of Tables	xii
Chapter One Introduction	1
1.1 Semiconductor gain materials.....	1
1.2 Spontaneous emission of multiple-quantum-wells.....	7
1.3 Optically-pumped semiconductor lasers	11
1.4 Semiconductor saturable absorbers.....	15
Reference	20
Chapter Two Spontaneous Emission Properties of the AlGaInAs Multiple-Quantum-Wells under High Excitation Intensity	31
2.1 Device fabrication of the AlGaInAs multiple-quantum-wells.....	31
2.2 Experimental setup.....	35
2.3 Experimental results and discussions.....	44
2.4 Conclusions.....	53
Reference	55
Chapter Three High-Peak-Power and High-Repetition-Rate 1.2-1.6 μm Optically-Pumped Semiconductor Lasers	58
3.1 Thermal managements of the optically-pumped semiconductor lasers.....	58

3.2	1220 nm AlGaInAs multiple-quantum-wells lasers.....	63
3.2.1	Device fabrication and experimental setup.....	65
3.2.2	Experimental results and discussions.....	67
3.3	1520 nm AlGaInAs multiple-quantum-wells lasers.....	75
3.3.1	Device fabrication and experimental setup.....	78
3.3.2	Experimental results and discussions.....	81
3.4	Conclusions.....	89
Reference	89
Chapter Four	Simultaneous Q-switching and Wavelength Conversion of the AlGaInAs Multiple-Quantum-Wells.....	96
4.1	Simultaneously passively Q-switched and frequency-switched behaviors of the multiple-quantum-wells.....	96
4.2	Device fabrication and experimental setup.....	99
4.3	Experimental results and discussions.....	103
4.4	Conclusions.....	111
Reference	111
Chapter Five	Summary and Future Works.....	116
5.1	Summary.....	116
5.2	Future works.....	117
Reference	120
Curriculum Vitae	122
Publication List	123

List of Figures

Chapter One

Fig. 1.1-1	Schematic illustration of the structure of edge-emitting laser.....	3
Fig. 1.1-2	Schematic illustration of the structure of surface-emitting laser.....	4
Fig. 1.3-1	The typical gain mirror configuration of the OPSLs.....	14
Fig. 1.4-1	The pulse formation processes of typical passively Q-switched lasers..	18
Fig. 1.4-2	Typical device structure of A-FPSA used in the passively Q-switched microchip laser.....	19

Chapter Two

Fig. 2.1-1	The diagrams of the MQWs structures with (a) weak and (b) strong coupling of the light-QWs interaction.....	34
Fig. 2.2-1	Schematic diagram of the radiative recombination mechanisms of the AlGaInAs MQWs in the simplified single QW configuration.....	36
Fig. 2.2-2	Room temperature transmittance spectrum of the AlGaInAs MQWs chip excited at low intensity.....	37
Fig. 2.2-3	Room temperature reflectance spectrum of the AlGaInAs MQWs chip excited at low intensity.....	38
Fig. 2.2-4	Schematic illustration of constructive interference of waves A, B and C which are reflected from interfaces of three stacks of MQW structure.....	40
Fig. 2.2-5	Room temperature absorption spectrum of the AlGaInAs MQWs chip excited at low intensity.....	41
Fig. 2.2-6	The experimental configuration of the PL spectrum measurement.....	43
Fig. 2.3-1	Photo-luminescence spectra of the AlGaInAs MQWs chip with variance excitation intensity from 23 to 384 kW/cm ² at 253 K.....	45
Fig. 2.3-2	Integrated PL intensity of the many-body state emission line as the function of excitation intensity at 253, 193 and 123 K.....	46
Fig. 2.3-3	Photo-luminescence spectra of the AlGaInAs MQWs chip with the excitation intensity of 407 kW/cm ² measured at different temperatures	

	from 123 to 313 K.....	48
Fig. 2.3-4	Peak wavelength shift of the many-body state luminescence versus temperature at the excitation intensity of 407 kW/cm ²	49
Fig. 2.3-5	Plots of the integrated PL intensity of the many-body state luminescence versus temperature at the excitation intensity of 407 kW/cm ²	51
Fig. 2.3-6	Temperature dependence of the excitation threshold intensity of the EHP renormalized state emission.....	54
Chapter Three		
Fig. 3.1-1	The schematic illustrations of (a) barrier and (b) in-well pump configurations of MQWs.....	61
Fig. 3.1-2	The schematic configurations of the two thermal management using (a) thin-device and (b) intra-cavity heat spreader methods.....	62
Fig. 3.2-1	Experimental configuration of AlGaInAs/InP semiconductor laser at 1200 nm pumped by a 1.06 μm Yb-doped pulsed fiber amplifier in the single chip scheme.....	66
Fig. 3.2-2	Room temperature surface emitting spontaneous emission spectrum under 60 kHz pump repetition rate and 28 ns pump pulse width at average absorbed power of 0.38 W. Inset, the expanded lasing spectrum obtained with 0.85 W average absorbed power under the same pump conditions.....	68
Fig. 3.2-3	Redshift of peak lasing wavelength as a function of average absorbed power under 60 kHz pump repetition rate and 28 ns pump pulse width.....	70
Fig. 3.2-4	Laser output performances at fixed pump pulse width of 28 ns and different pump repetition rates ranged from 40-80 kHz.....	71
Fig. 3.2-5	Laser output performances under 60 kHz pump repetition rate with varied pump pulse width.....	73
Fig. 3.2-6	(a) Typical oscilloscope trace of a train of pump and output pulses and (b) expanded shapes of a single pulse.....	74
Fig. 3.2-7	Output performance with double gain chips at 60 kHz pump repetition rate and 28 ns pump pulse width.....	76

Fig. 3.3-1	Experimental setup of AlGaInAs eye-safe laser at 1525 nm with an intra-cavity diamond heat spreader and using an Yb-doped pulsed fiber amplifier as a pump source.....	79
Fig. 3.3-2	Room temperature surface emitting spontaneous emission spectrum under a 100-kHz pump repetition rate at an average absorbed power of 0.8 W.....	82
Fig. 3.3-3	Output performances of the eye-safe laser without and with the diamond heat spreader at a 30-kHz repetition rate.....	83
Fig. 3.3-4	Output performances without (a) and with (b) the diamond heat spreader for repetition rates in the range of 100-500 kHz.....	85
Fig. 3.3-5	(a) Lasing spectrum with the heat spreader under an average absorbed power of 2.5 W at a repetition rate of 100 kHz. (b) Dependence of the red-shift on the absorbed pump power for the laser operation without and with the heat spreader at a repetition rate of 100 kHz.....	86
Fig. 3.3-6	(a) Oscilloscope trace of a train of pump and output pulses obtained with an average absorbed power of 2.5 W at a repetition rate of 200 kHz. (b) Expanded shapes of a single pulse.....	88
Chapter Four		
Fig. 4.2-1	Experimental configuration of the diode-pumped Nd:GdVO ₄ laser simultaneously passively Q-switched and frequency-switched by the AlGaInAs/InP M.QWs.....	102
Fig. 4.3-1	Average output powers at 1064 nm and 1530 nm versus the incident pump power with 93% reflectivity of the 1064 nm output coupler.....	105
Fig. 4.3-2	Average output powers at 1064 nm and 1530 nm versus the incident pump power with 30% reflectivity of the 1064 nm output coupler.....	106
Fig. 4.3-3	Output lasing spectrum at (a) 1064 nm and (b) 1530 nm at incident pump power of 15 W.....	108
Fig. 4.3-4	Typical oscilloscope trace of the pump and output (a) pulse train and (b) expanded shape of a single pulse with output coupler of 93% reflectivity.....	109
Fig. 4.3-5	Typical oscilloscope trace of the pump and output (a) pulse train and (b) expanded shape of a single pulse with output coupler of 30%	

reflectivity..... 110

Chapter Five

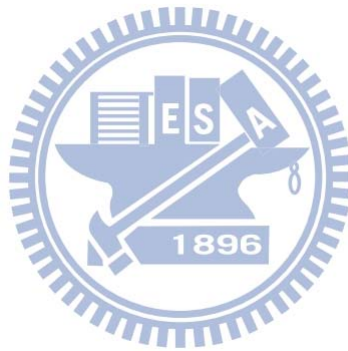
Fig. 5.2-1 Suppositional experimental setup of the simultaneously Q-switched and gain-switched Yb:YAG/AlGaInAs MQWs microchip laser..... 119



List of Tables

Chapter One

Table 1.1-1	Overview of the single-chip optical-pumped semiconductor lasers performance at different wavelength region and material systems under room-temperature operation.....	8
--------------------	---	---



Chapter One

Introduction

1.1 Semiconductor gain materials

Semiconductor materials are extensively used in electronics due to its specific electrical conductivity between conductors and insulators. It is also promising to be used in the optoelectronics such as the photo-detectors, light emitting diodes and semiconductor lasers. The development of semiconductor lasers is nearly as old as the advent of lasers. Compared to other laser sources, the semiconductor lasers have several advantages like good electrical-to-optical efficiency, compact and monolithic in fabrication and widely controlled emission spectral range. Mostly the gain mediums of the semiconductor lasers are direct bandgap semiconductor materials of III-V compounds. The light amplification is achieved by recombination of the electron-hole pairs in conduction band and valence band of active layers in semiconductor gain device induced by the propagating optical fields. The simplest form of semiconductor gain devices is p-n junction diodes in which the population inversion is brought about around junction area by a sufficiently large forward bias. To reduce pump threshold current and improve laser efficiency, the double heterostructure semiconductor laser diodes have been demonstrated with better carrier and photon confinement. More recently, a novel structure of multiple quantum wells (MQWs) has been demonstrated via advanced semiconductor growth techniques with the precision up to single atomic layer. They exhibit numerous excellent characteristics like lower optical loss, lower threshold current injection, better carrier confinement, superior room-temperature performance and the flexible tuning parameters in comparison to double heterostructure semiconductor lasers [1]. The

number of wells can be selected to fit the required gain or absorption coefficient and the emission wavelength can be adjusted by varying the bandgap of well layer, barrier height and well thickness.

Different types of semiconductor lasers could be classified as edge-emitting and surface-emitting lasers which will be mentioned in [section 1.3](#). The optical cavity of edge-emitting semiconductor lasers is formed by the cleaved facets perpendicular to plane of active layer structure. Therefore, the emitted photon is propagating in path normal to the epitaxial direction guided by the interfaces between active and confined layers. Schematic description of the edge-emitting lasers or the so-called Fabry-Pérot lasers is shown in [Fig. 1.1-1](#). Because of the long active region length L , the cavity gain of edge-emitting laser is pretty high and the output power is much higher than surface-emitting laser. But the active region height H , which is equivalent to active layer thickness, is typically two orders smaller than the width W and the output beam is elliptically shaped with poor beam quality. Alternatively, the surface-emitting lasers are developed with output light direction parallel to the epitaxial direction. The laser cavity is conventionally formed by two distributed Bragg mirror (DBR) structures which are parallel to the epitaxial layer on top and bottom side of semiconductor gain chip. A simplified schematic illustration of surface-emitting lasers is shown in [Fig. 1.1-2](#). Because there is no restriction of lateral dimensions and the cavity has circular cross-section geometry, the output laser beam could be a single transverse mode non-diffraction limit beam. But the low optical gain due to short active length and the small current injection aperture due to the ultra-short linear-linear cavity limited the output power to just several milli-watts. Therefore, the optical pumping instead of current injection is used in external-cavity surface-emitting lasers which has been developed to obtain high power and good beam quality semiconductor laser source.

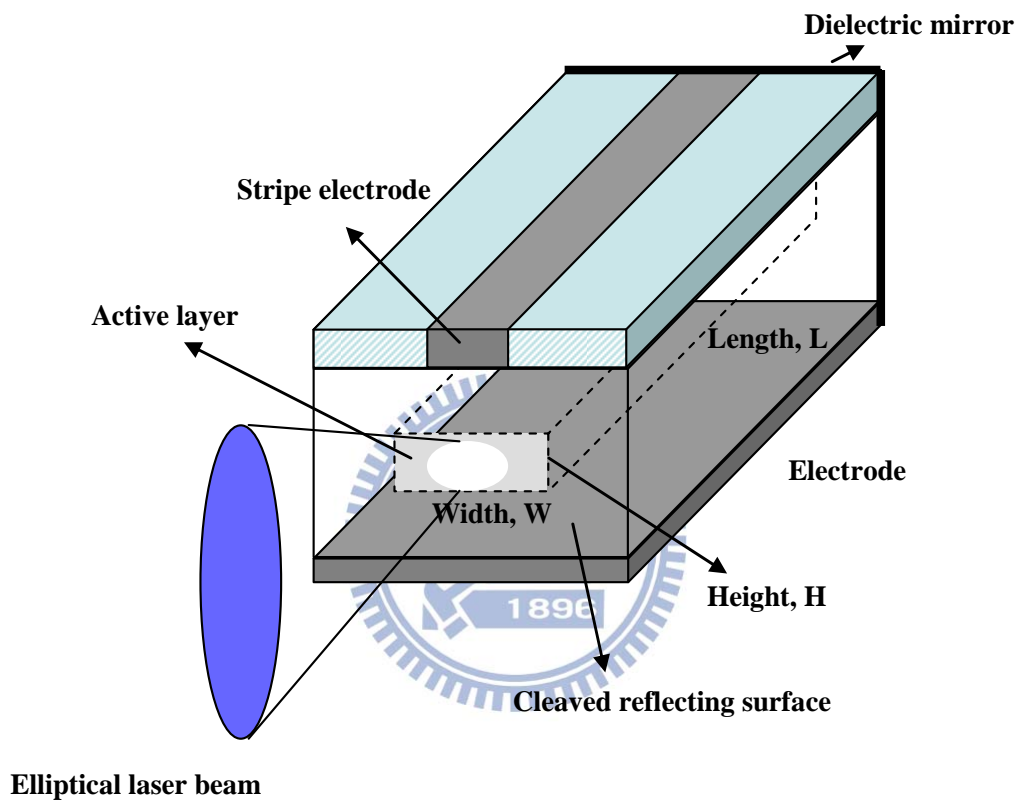


Fig 1.1-1 Schematic illustration of the structure of edge-emitting laser.

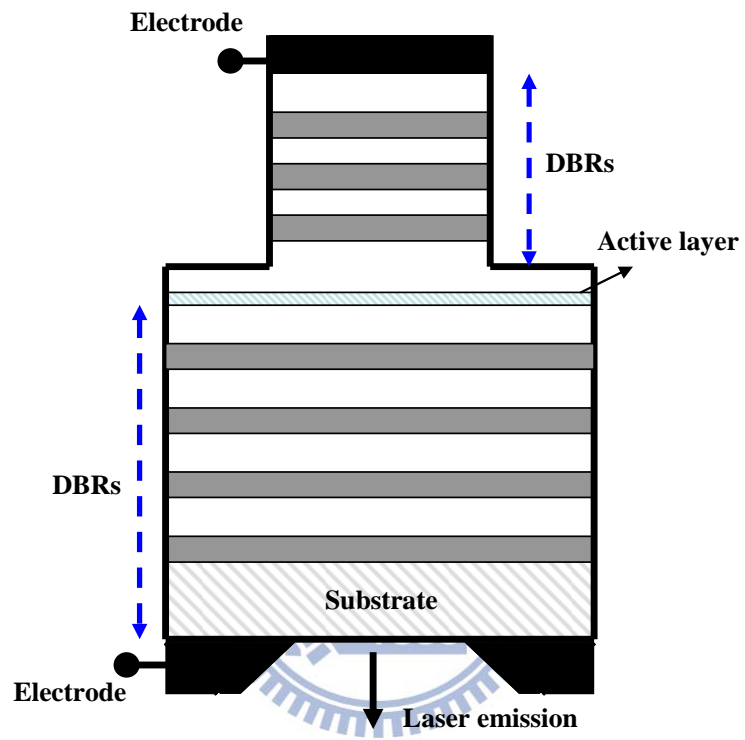


Fig 1.1-2 Schematic illustration of the structure of surface-emitting laser.

The detailed evolution of surface emitting lasers will be further discussed in [section 1.3](#).

The material system is important to the emission spectral range of semiconductor lasers which could be tuned from 400 nm in the ultraviolet by GaN-based system, to 2.3 μm by AlGaAsSb-based system. To select suitable substrate and semiconductor alloy epitaxial layers, the use of a lattice constant versus bandgap energy diagram is needed [2]. The chosen semiconductor materials in active layer should have direct bandgap matched to the objective emission photon energy. Besides, the lattice constant should be lattice-matched to the substrate and prevent the generation of large amount of defects. In using the approximation of Vegard's law, the lattice constant and bandgap shift could be continuously tuned via the mixed ternary or quaternary alloys instead of using binary compounds [3]. The mostly mature and used material system is the compounds composed by AlAs/GaAs/InAs alloys lattice-matched to the GaAs substrate. The wavelength range of $\text{Al}_x\text{Ga}_{1-x}\text{As}$ with mole fraction x could be varied from 780 nm to 900 nm with direct bandgap and nearly perfect lattice-matching to GaAs substrate. With the indium-doping in place of aluminum-doping, the compressive strain of the InGaAs on the GaAs substrate will make the bandgap shifted to around 1 μm . Although the more doping fraction of indium could alter the emission wavelength to be longer than 1 μm , the more serious strain effect will introduce more defects which will result in much scattering loss and lower the semiconductor laser efficiency. But this restriction could be eased by low temperature growth or by alternating growth of large and small lattice constant material to cancel the built-in energy of the MQWs which is called "strain compensation" [4]. The high refractive index difference and high thermal conductivity of the AlAs/GaAs distributed Bragg reflectors (DBRs) for GaAs-based system is also beneficial to the

development in surface-emitting lasers.

Semiconductor lasers at 1.3 and 1.55 μm are of great importance in remote sensing, laser ranging and optical communication. The InGaAsP and AlGaInAs quaternary compounds based on InP substrate and InGaNAs quaternary compound based on GaAs substrate are typically used in this spectral region. Although the InGaAsP/InP system is developed earlier than AlGaInAs/InP system, the conduction band offset of the former is smaller than the latter. This means that the carrier confinement and thermal stability under room temperature operation of InGaAsP/InP system is worse than AlGaInAs/InP system. Therefore, in this thesis we choose AlGaInAs/InP system as our MQWs material and a series of characteristics of photoluminescence, stimulated emission and saturable absorption in the surface-emitting scheme have been investigated in the following three chapters. But the DBRs lattice matched to the InP-based systems suffer from low refractive index contrast, low thermal conductivity and high complexity of growth to realize the surface-emitting laser. Alternatively, Fe-doped InP with good transparency at 1-2 μm is chosen as the substrate in our MQW sample instead of the conventionally used S-doped InP. Consequently, the transmitted AlGaInAs MQW chip is achieved and the function of DBRs could be replaced by an external mirror in the surface-emitting laser. Recently, a new GaAs-based nitride quaternary compound is applied in the semiconductor lasers in the spectral range of 1.1-1.6 μm . By introducing a few fraction of nitride to InGaAs the emission wavelength of this quaternary compound has potential shifted to longer wavelengths and the lattice-mismatching to GaAs can be reduced. However, because the nitrogen ion is smaller than the elements in the InGaAs material, the more doping concentration of nitride will result in the more defect in the alloys. It will give rise to strong scattering loss which is unfavorable to

the semiconductor lasers. So far, several InGaAs vertical-external-cavity surface-emitting lasers have been demonstrated at wavelength range at 1.2, 1.3 and 1.55 μm . Moreover, the wafer fusion technique which allows combining different semiconductor materials with variant lattice constant is used in the AlGaInAs/GaAs OPSLs and average output power of 2.6 W is obtained at 1.57 μm . Table 1.1-1 shows the performances and material systems of the OPSLs from visible to mid-infrared spectral region to date [5-27]. Because of the absence of efficient and mature commercial pump diode laser module, the semiconductor lasers at the spectral range below 640 nm are mostly realized by frequency-doubling of the infrared semiconductor lasers [28].

1.2 Spontaneous emission of multiple-quantum-wells

In the last section we have mentioned that the multiple-quantum-well (MQW) heterostructures have potential applications in the semiconductor lasers owing to the characteristics like versatile emission wavelength, lower laser threshold and excellent performance under room temperature operation [1,29,30]. The luminescence, absorption and carrier relaxation time of MQWs are the most important optical properties which are strongly related to material systems and epitaxial structures used in MQW samples. From the experimental point of view, MQW structures are extensively investigated by means of luminescence, absorption spectrum and optical transmittance under pump-and-probe configuration. Several characteristic features including band-edge energy, peak emission wavelength, emission linewidth, integrated luminescence intensity, and carrier lifetime as functions of temperature or excitation intensity have been studied in a variety of MQW materials [31-36]. From the theoretical aspect, the inter-band transition energy can be determined by a one-dimension Schrödinger-like equation with the envelope function approximation

Gain material	Substrate	λ_{lasing}	λ_{pumping}	P_{max}	Ref.
InGaN/GaN QW	Sapphire	337nm	397nm	-----	[5]
AlGaInP QD	GaAs	655nm	532nm	1.39W	[6]
AlGaInP QW	GaAs	665nm	532nm	1.2W	[7]
AlGaAs QW	GaAs	850nm	660nm	0.5W	[8]
InGaAs QW	GaAs	960nm	808nm	20W	[9]
InGaAs QW	GaAs	1000nm	808nm	8W	[10]
InGaAs QD	GaAs	1032nm	808nm	4.35W	[11]
InGaAs QW	GaAs	1040nm	808nm	23.8W	[12]
InGaAs QW	GaAs	1170nm	808nm	7W	[13]
GaInNAs QW	GaAs	1180nm	808nm	11W	[14]
InGaAs QD	GaAs	1180nm	808nm	4W	[15]
GaInNAs QW	GaAs	1220nm	808nm	5W	[16]
InGaAs QD	GaAs	1250nm	808nm	3W	[17]
AlGaInAs QW	GaAs (wafer fused)	1300nm	980nm	6.6W	[18]
GaInNAs QW	GaAs	1320nm	810nm	0.6W	[19]
AlGaInAs QW	GaAs (wafer fused)	1480nm	980nm	4.8W	[20]
InGaAsP QW	InP	1549nm	1250nm	170mW	[21]
AlGaInAs QW	InP	1550nm	980nm	77mW	[22]
AlGaInAs QW	GaAs (wafer fused)	1580nm	980nm	4.6W	[23]
GaInSb QW	GaSb	2 μ m	790nm	1W	[24]
GaInSb QW	GaSb	2 μ m	980nm	5W	[25]
GaInAsSb QW	GaSb	2.25 μ m	980nm	1.6W	[26]
GaInAsSb QW	GaSb	2.35 μ m	1.96 μ m	2W	[27]

Table 1.1-1 Overview of the single-chip optical-pumped semiconductor lasers performance at different wavelength region and material systems under room-temperature operation.

method as follows [37],

$$-\frac{\hbar^2}{2m_{rl}^*} \frac{d^2 \phi_{nrl}(z)}{dz^2} + V_r(z) \phi_{nrl}(z) = E_{nrl} \phi_{nrl}(z), \quad (1)$$

where the subscript n denotes subband levels of QWs and r is corresponding to electrons (conduction band) or holes (valence band), subscript l represents heavy or light holes, m_{rl}^* is the effective mass to rl value, z is the epitaxial direction, $V_r(z)$ is the potential height at position z , $\phi_{nrl}(z)$ is the wave function of confined carrier and E_{nrl} is the quantized energy to the nrl value. The first inter-band electron-heavy hole transition energy can then be obtained as,

$$E_{1h} = E_g(0) + E_{1Vh} + E_{1Ch}. \quad (2)$$

Despite of the fundamental band-to-band transition of quantized energy of MQWs, the luminescence and absorption features of exciton state which is characterized by bound electron-hole pairs have been investigated with high quality epitaxial films and under ultra-low temperature operation. However, above experiments are mostly focusing on small number of QWs below fifteen periods and low-level excitation intensity.

To further understand the behaviors of distinct luminescence features of the MQW structure under high intensity photo-excitation, much effort has been devoted to optical nonlinearities. One part of these effects is focusing on the exciton state like the phase-space filling of excitons due to the Pauli exclusion principle and the dissociation of high density excitons into the electron-hole pairs [38-40]. The other sorts of the nonlinear effects are mainly ascribed to the many-body interaction of the high density electron-hole plasma (EHP). These features include the progressive filling of higher quantized states and the band-gap renormalization [41-43]. Under

high excitation intensity, the exchange effects of the electrons and holes and the screening of Coulomb interaction will result in the band-gap reduction at no matter the occupied or vacant states [44,45]. The band-gap renormalization effects of the bulk semiconductor heterostructures have been studied experimentally and theoretically as the universal behavior independent of the band structure of materials but only in relation with the Bohr radius [46,47]. In contrast, the quasi-2D confinement of the MQW structure enhances the screening and exchange effects and strengthens the phenomenon of band-gap shrinkage [48,49]. A series of investigations have put attention on the carrier density dependence of the band-gap renormalization via the means of luminescence, absorption and line-shape analysis [48,50-53] and the optical transmission measurements by the pump-and-probe experiments [43,54,55] with high density EHP. In these investigations, the band-gap renormalization is just characterized by the slightly red-shifted band-edge below the lowest quantized state. But another typical luminescence phenomenon in several researches in use of a large number of MQWs is demonstrated in which a sharp emission band emanating below the lowest heavy-hole exciton state has been observed under high photo-excitation intensity [43,45,56,57]. This emanation mode is ascribed to be the high density EHP many-body state luminescence in which the peak intensity grows much faster with increasing excitation intensity and the linewidth are narrower than the fundamental band-to-band transition. The requirement of large number of quantum well pairs which is confirmed to be vital to the appearance of the EHP many-body state emission [57] elucidates that the strong optical confinement and amplified spontaneous emission effect play an important role in this particular radiative recombination process. So far, these observations are all limited to operate at cryogenic temperatures below 15 K in which the exciton single-particle state and the EHP many-body state are coexisted. This hinders the employment in practical applications such as lasers and

light emitting diodes which require high stability and thermal resistivity at room temperature.

1.3 Optically-pumped semiconductor lasers

High power and good beam quality all-solid-state lasers with circularly symmetric single transverse mode are in demand in a variety of applications like nonlinear optics and the optical communications. The diode-pumped, doped-dielectrics bulk solid-state or fiber lasers are developed to be a promising light source in these fields. However, the discrete energy level of the doped ions of these lasers limits the output wavelength coverage. In contrast, the semiconductor lasers enable the potential broad spectral range from ultra-violet to mid-infrared via the bandgap engineering. The traditional edge-emitting semiconductor lasers with high output power suffer from low beam quality which is mainly due to the extraction of light perpendicular to the growth direction. Alternatively, the surface-emitting scheme is applied in the well-known vertical-cavity surface-emitting lasers (VCSELs) to realize the single transverse mode output. The VCSELs are conventionally composed by a quantum-well (QW) active region clamped by two distributed Bragg mirrors (DBRs) with current-injection pumping. To obtain the single mode output beams the current aperture need to be smaller than 10 μm because of the short and flat-flat linear cavity. As a result, the maximum output power of the VCSELs is restricted to be lower than 15 mW.

In 1993, a new type of surface-emitting semiconductor laser in which one of the DBRs fabrication is replaced by a curved external output mirror is first reported by Hadley *et al* [58]. The single mode pulsed 100 mW output power of this laser which is also called the vertical-external-cavity surface-emitting laser (VECSEL) was obtained with an enlarged carrier injection aperture of 100 μm diameter in the InGaAs gain

region. In analogy to the diode-pumped solid-state lasers, the optically-pumped VECSELS, or named as optically-pumped semiconductor lasers (OPSLs), are demonstrated by Kuznetsov *et al* with further scaled output power greater than 0.5 W under single mode continuous-wave operation [59]. Nowadays, the OPSLs are confirmed to allow high power single mode operation in a wide spectral range via reliable semiconductor epitaxy design and growth and efficient thermal management [60-62].

The gain chips of the OPSLs are fabricated with QW structures grown on the latticed-matched substrate via the metal-organic chemical-vapor-deposition or molecular beam epitaxy. Several epitaxial growth configurations are presented depending on the ways of thermal management [63-65] which will be further discussed in section 3.1. In this section, a typical schematic of the OPSLs is shown in Fig. 1.3-1. The DBRs structure with 25-30 periods is first grown on the substrate with high reflection to the pump and lasing wavelengths to serve as the front mirror. Then the active region consisted of the QWs and the barrier structure is deposited on the top of DBRs. The designation that the QWs are separated by the pump absorption barriers with half lasing wavelength interval is the resonant periodic gain (RPG) structure. Under this frame the QWs active region is located at the anti-node of the lasing standing waves to enlarge the gain exploitation [66,67]. Finally, a cap layer which is transparent to the pump and lasing wavelengths is integrated on the top of QWs to avoid the surface recombination and the oxidation. Besides, the thickness of the cap layer could be tuned to control the sub-cavity resonance due to the Fabry-Perot interference between the semiconductor-air interface and the DBRs. Then the total assembly, which is called the gain mirror, is mounted on a heat sink with substrate side to activate the heat dissipation. The gain chips are usually pumped by the

commercial laser diode array in pairs with the focusing optics with an angle of 45° to the surface normal [64,68]. But the oblique incidence makes the pump spot to be elliptical shaped. This is unfavorable to obtain single transverse mode output and will decrease the degree of mode matching. Alternatively, the end-pump schemes of OPSLs have been demonstrated in use of the modified DBR or high transmittance substrate under CW and pulsed operation [69,70].

To complete the laser cavity, an external curved mirror is added as the output coupler to ensure the high power single transverse mode output as shown in Fig. 1.3-1. The radius of curvature and the distance to the gain mirror of the external mirror are assigned to let the laser cavity mode correspond to the pump mode. Because of the short active length, the semiconductor gain mirror is inherently a low gain device in comparison to the doped-crystals in the solid-state lasers. Consequently, the reflectivity of the output mirrors in the OPSLs is typically higher than 97% under CW-operation [64,71] and the RPG structure, as mentioned above, is applied to enhance the MQW gain. As an exception, the output reflectivity could be lowered to be 92-96% or even 70% under quasi-CW and pulsed pumping [72,73]. Using the separated external mirror makes the OPSLs capable of inserting various intra-cavity components such as the nonlinear elements, spectral filters and saturable absorbers.

Although many materials as the direct emitters at visible region like the AlInGaP and GaN based systems are presented, the absence of high power and high photon energy pump source hindered the developments of the OPSLs in this field. Therefore, the second harmonics generation of the mature and efficient NIR OPSLs draws lots of interests in producing visible OPSLs. So far, a variety of the frequency doubled OPSLs with blue, green and yellow-orange light emission [74-78] are realized with fundamental emission of 920-940 nm, 960-1100 nm and 1140-1250 nm, respectively.

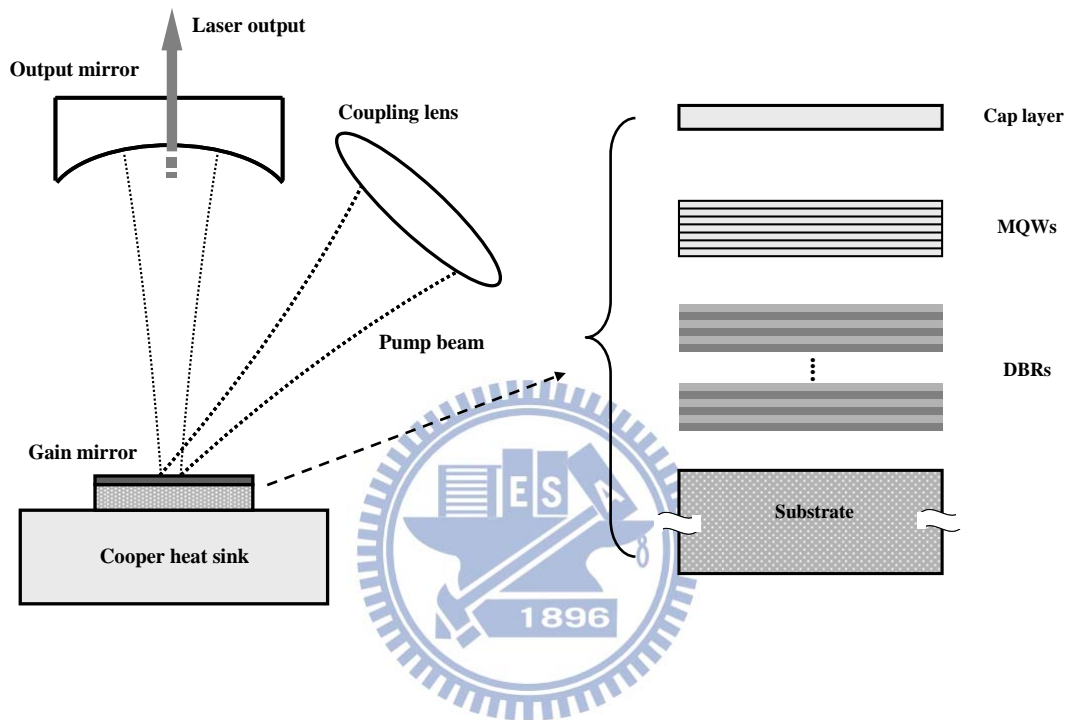


Fig. 1.3-1 The typical gain mirror configuration of the OPSLs.

To improve the wavelength conversion efficiency and enlarge the spectrum coverage, single frequency operation [79,80] and wavelength tunable OPSLs [81,82] have also been preceded. The large gain-bandwidth and gain cross-section of the semiconductor QW gain mirror are helpful in producing high-repetition rate and ultra-short passively mode-locked pulsed laser. Several passively mode-locked OPSLs with semiconductor saturable absorber mirrors (SESAMs) have demonstrated and supply giga-Hertz repetition rate and pico- to femto-seconds output pulses [83,84]. With these additional intra-cavity elements the 3- or 4- mirror SDL cavity in contrast to the traditional linear cavity as shown in Fig. 1.3-1 are applied [61] to provide intensive and focusing beam spots on these components.

1.4 Semiconductor saturable absorbers

Compact, rugged and all solid-state high peak power pulsed laser source is of great interests in many applications such as micro-processing, laser lidar, range finding and communication. To achieve the high peak power, high repetition rate and sub-nanosecond laser pulses, two intracavity modulation techniques have been extensively used. One way is using mode-locked laser in which the axial modes in the laser cavity are forced to be superimposed with a fixed phase. Consequently, the laser output will be forced to form a nearly delta function shaped pulse. The shortest duration of pulse is decided by the gain-bandwidth of the laser gain medium. The pulse-to-pulse period is equivalent to the cavity round-trip time. The other method is using the Q-switching techniques in which the population inversion density in cavity is accumulated by introducing additional loss and then release when the cavity Q value is restored to the usual large value at a suitable time interval. In general, the result of this process is the generation of a single short laser pulse with pulse duration typically several to a few tens of nanosecond long. Moreover, the practical modulation

methods of these two pulse formation techniques can be classified to active and passive modulation. The passive modulation technique is simple and no need of any electrical drivers and heat dissipation devices of the modulator. The primary method for passively Q-switched or mode-locked operation is to place a saturable absorber element inside the cavity to serve as a Q-switcher or phase modulator. The saturable absorber could be any materials with absorption band corresponding to the laser emission and has strong nonlinear saturable absorption properties. Although the organic dye solution is mostly used saturable absorber in the early stage due to its broad gain-bandwidth, the doped crystal and semiconductor saturable absorbers have taken place of it owing to the high toxicity and severely degradation under high power operation.

Mode locked laser is a promising method to produce high repetition rate and ultra-short laser pulse. But the pulse period of mode-locked laser which is equal to cavity round-trip time is too short and, as a result, the large number of pulse per second reduce the single pulse energy and could not produce pulses with high peak power even with high average output power [85,86]. Besides, the complexity and high expense and maintenance of the device configuration hinder the use in practical utilizations. Therefore, passive Q-switching of solid-state lasers which could provide high pulse energies with repetition rates in the kilo-Hz regime and nanosecond pulse width is a good alternation to produce high peak power pulsed lasers. The pulse formation process is depicted in Fig. 1.4-1. Although the pulse stabilities and periods are easy to control for the actively Q-switched lasers, the simple, low cost and monolithic fabrication and no need of high voltage electro- or acoustical-optical drivers and heat dissipation devices of passively Q-switches technique is more promising in applications requiring high peak power laser sources. Nowadays, the

bulk crystal saturable absorbers are extensively used in the passively Q-switched solid-state lasers such as Cr^{4+} :YAG at 0.9-1.2 μm , V^{3+} :YAG and Co^{2+} : MgAl_2O_4 at 1.3 μm and Er^{3+} :CaF and Co^{2+} :ZnSe at 1.5 μm [87-90]. But the discrete energy level of the doped ion limited the applications of the bulk crystal saturable absorber in the more versatile spectral region. In 1996, the Nd:LSB microchip laser is firstly passively Q-switched by an antiresonant Fabry-Perot SA (A-FPSA), or the so called semiconductor saturable absorber mirror (SESAM), by Braun *et al.* [91] with output pulse width shorter than 200 ps. In comparison to the bulk crystal saturable absorber, the advantage of SESAM is that high density of states makes the short absorption length and, therefore, the shorter cavity length even in several hundreds of microns. The Q-switching efficiency is also better because of the lower nonsaturable loss due to the shorter action length. The most important is that the absorption band of the SESAM which is decided by the bandgap of the semiconductor materials could be adapted to the gain medium at variant lasing wavelengths. Finally, there is enough design freedom of the saturable absorber parameters such as saturation fluence, modulation depth and recombination lifetime to adjust independently. Typical device structure of A-FPSAs is demonstrated in Fig. 1.4-2. In section 1.1 we have mentioned that the InP-based material system is conventionally used in the 1.3 and 1.5 μm semiconductor lasers. Because the absorption and emission wavelengths are all related to the bandgap of the semiconductors, the InGaAsP/InP and AlGaInAs/InP multiple-quantum-wells are also suitable to be fabricated as SESAMs at spectral region between 1.2-1.6 μm . But the distributed Bragg mirrors (DBRs) of InP-based semiconductor systems suffer from low refractive index contrast, low thermal conductivity or complexity in fabrication. As an alternative, semiconductor saturable absorbers (SESAs) have been developed by using an external mirror to replace the functions of DBRs. So far, numerous passively Q-switched solid-state lasers in use of

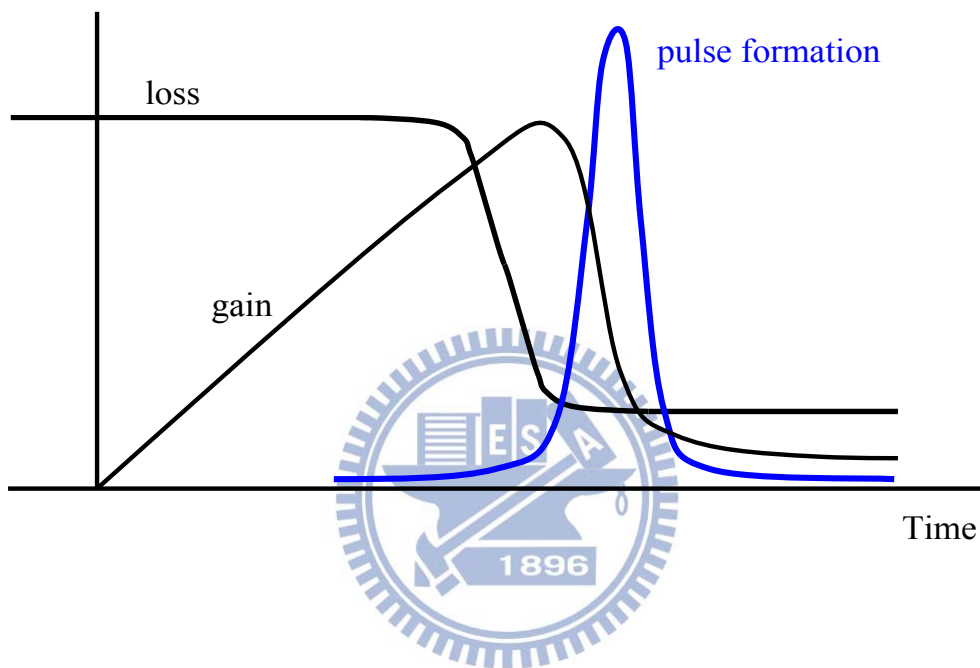


Fig. 1.4-1 The pulse formation processes of typical passively Q-switched lasers.

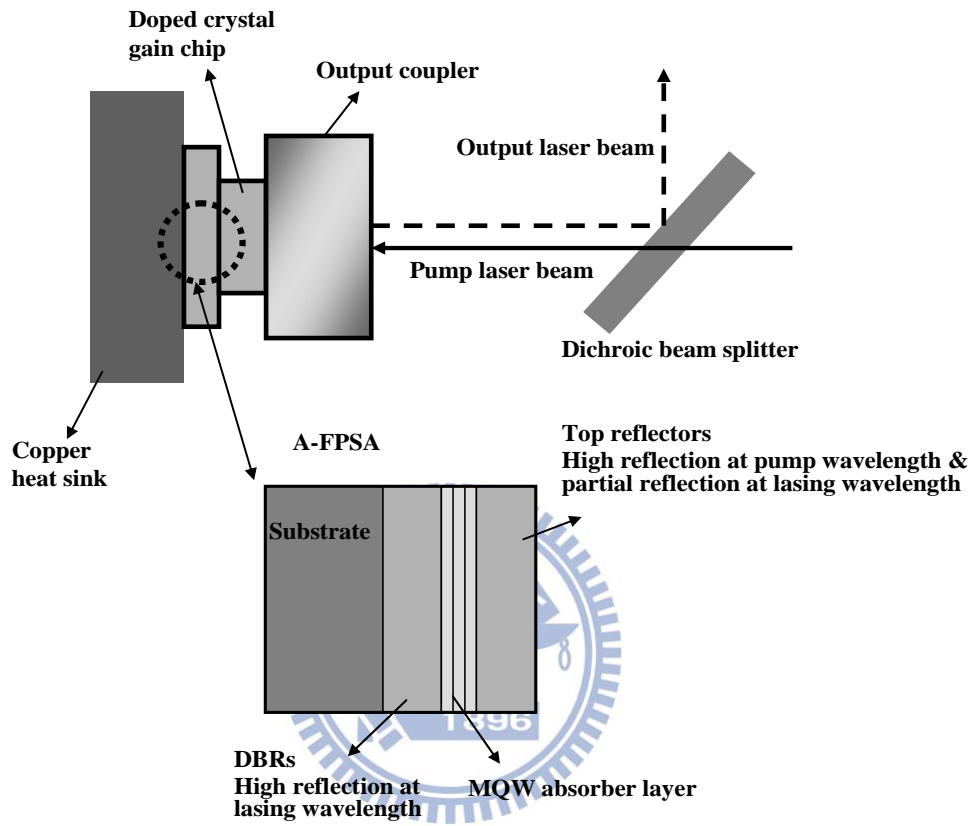


Fig. 1.4-2 Typical device structure of A-FPSA used in the passively Q-switched microchip laser.

SESAs with or without the DBRs have been demonstrated in the near-infrared spectral region [90-99].

Because the minimum pulse durations of the Q-switched lasers are inherently proportional to the resonator length [86,100,101], the microchip actively and passively Q-switched lasers have been developed with cavity length below 1 mm and, as a result, sub-nanosecond pulses output is obtained [86,102,103]. The ultra-short cavity length is beneficial to the single frequency operation in which the axial mode spacing is larger than the gain-bandwidth. In the early stage, the Nd³⁺:YAG bonded to thin piece of Cr⁴⁺:YAG saturable absorber [102] and Nd, Cr-codoped YAG crystal [104,105] are applied in the passively Q-switched microchip lasers with output pulse durations of 337 and 290 ps around 1- μ m, respectively. However, the limited doped concentration of bulk crystal SAs enlarged the cavity length and the restricted choices of the laser spectral region impede the further development as mentioned above. Therefore, high peak power and short pulse duration single frequency microchip lasers passively Q-switched by SESAM with divergent wavelength at 1 μ m and at the communication region of 1.34 and 1.5 μ m have been demonstrated [90-95]. By tuning reflectivity of the top reflector, the pulse width could be varied from tens of ps to several ns range and the repetition rate from kilo- to mega-Hz with changed modulation depth and saturation intensity. Recently, the passively Q-switched microchip lasers in use of SESAMs with shortest pulse duration of 22 ps [94] and peak power up to 20 kilo-watt [106] have been reported. However, the emission wavelengths of these lasers are mainly determined by the gain mediums which are limited to the discrete energy level of doped ions.

Reference

- [1] Y. Arakawa, and A. Yariv, "Quantum well lasers—Gain, spectra, dynamics,"

- IEEE J. Quantum Electron. **QE-22**, 1887-1899 (1986).
- [2] U. Keller and A. C. Tropper, "Passively modelocked surface-emitting semiconductor lasers," *Phys. Reports* **429**, 67-120 (2006).
- [3] A. R. Denton and N. W. Ashcroft, "Vegard's law," *Phys. Rev. A* **43**, 3161-3164 (1991).
- [4] N. J. Ekins-Daukes, K. Kawaguchi, and J. Zhang, "Strain-balanced criteria for multiple quantum well structures and its signature in X-ray rocking curves," *Cryst. Growth Des.* **2**, 287-292 (2002).
- [5] R. Debusmann, N. Dhidah, L. Weixelbaum, U. Brauch, T. Graf, M. Weyers, and M. Kneissl, "InGaN-GaN disk laser for blue-violet emission wavelengths," *IEEE Tech. Lett.* **22**, 652-654 (2010).
- [6] T. Schwarzbäck, R. Bek, F. Hargart, C. A. Kessler, and H. Kahle, "High-power InP quantum dot based semiconductor disk laser exceeding 1.3W," *Appl. Phys. Lett.* **102**, 092101 1-4 (2013).
- [7] T. Schwarzbäck, M. Eichfelder, W.-M. Schulz, R. RoBbach, M. Jetter, and P. Michler, "Short wavelength red-emitting AlGaInP-VECSEL exceeds 1.2 W continuous-wave output power," *Appl. Phys. B* **102**, 789-794 (2011).
- [8] J. E. Hastie, J.-M. Hopkins, S. Calvez, C. W. Jeon, D. Burns, R. Abram, E. Riis, A. I. Ferguson, and M. D. Dawson, "0.5-W single transverse-mode operation of an 850-nm diode-pumped surface-emitting semiconductor laser," *IEEE Photon. Tech. Lett.* **15**, 894-896 (2003).
- [9] B. Rudin, A. Rutz, M. Hoffmann, D. J. H. C. Maas, A.-R. Bellancourt, E. Gini, T. Südmeier, and U. Keller, "Highly efficient optically pumped vertical-emitting semiconductor laser with more than 20 W average output power in a fundamental transverse mode," *Opt. Lett.* **33**, 2719-2721 (2008).
- [10] S. Lutgen, T. Albrecht, P. Brick, W. Reill, J. Luft, and Späth, "8-W high-efficiency continuous-wave semiconductor disk laser at 1000 nm," *Appl. Phys. Lett.* **82**, 3620-3622 (2003).
- [11] M. Butkus, K. G. Wilcox, J. Rautiainen, O. G. Okhotnikov, S. S. Mikhrin, I. L. Krestnikov, A. R. Kovsh, M. Hoffmann, T. Südmeier, U. Keller, and E. U. Rafailov, "High-power quantum-dot-based semiconductor disk laser," *Opt. Lett.* **34**, 1672-1674 (2009).
- [12] T.-L. Wang, Y. Kaneda, J. M. Yarborough, J. Harder, J. V. Moloney, A. Chernikov, S. Chatterjee, S. W. Koch, B. Kunert, and W. Stolz, "High-power

- optically pumped semiconductor laser at 1040 nm,” *IEEE Photon. Tech. Lett.* **22**, 661-663 (2010).
- [13] L. Fan, C. Hessenius, M. Fallahi, J. Harder, H. Li, J. V. Moloney, W. Stolz, S. W. Koch, J. T. Murray, and R. Bedford, “Highly strained InGaAs/GaAs multiwatt vertical-external-cavity surface-emitting laser emitting around 1170 nm,” *Appl. Phys. Lett.* **91**, 131114 1-3 (2007).
- [14] V.-M. Korpijärvi, T. Leinonen, J. Puustinen, A. Härkönen, and M. D. Guina, “11 W single gain-chip dilute nitride disk laser emitting around 1180 nm,” *Opt. Express* **18**, 25633-25641 (2010).
- [15] J. Rautiainen, I. Krestnikov, J. Nikkinen and O. G. Okhotnikov, “2.5 W orange power by frequency conversion from a dual-gain quantum-dot disk laser,” *Opt. Lett.* **35**, 1935-1937 (2010).
- [16] V.-M. Korpijärvi, M. Guina, J. Puustinen, P. Tuomisto, J. Rautiainen, A. Härkönen, A. Tukiainen, O. Okhotnikov, and M. Pessa, “MBE grown GaInNAs-based multi-watt disk lasers,” *J. Cryst. Growth* **311**, 1868-1871 (2009).
- [17] A. R. Albrecht, T. J. Rotter, C. P. Hains, A. Stintz, J. V. Moloney, K. J. Malloy, and G. Balakrishnan, “Multi-watt 1.25 μm quantum dot VECSEL,” *Electron. Lett.* **46**, 856-857 (2010).
- [18] A. Rantamäki, A. Sirbu, A. Mereuta, E. Kapon, and O. G. Okhotnikov, “3 W of 650 nm red emission by frequency doubling of wafer-fused semiconductor disk laser,” *Opt. Express* **18**, 21645-21650 (2010).
- [19] J.-M. Hopkins, S. A. Smith, C. W. Jeon, H. D. Sun, D. Burns, S. Calvez, M. D. Dawson, T. Jouhti, and M. Pessa, “0.6 W CW GaInNAs vertical external-cavity surface emitting laser operating at 1.32 μm ,” *Electron. Lett.* **40**, 30-31 (2004).
- [20] A. Sirbu, N. Volet, A. Mereuta, J. Lyytikäinen, J. Rautiainen, O. Okhotnikov, J. Walczak, M. Wasiak, T. Czyszanowski, A. Caliman, Q. Zhu, V. Iakovlev, and E. Kapon, “Wafer-fused optically pumped VECSELs emitting in the 1310-nm and 1550-nm wavebands,” *Adv. Opt. Technol.* **2011**, 209093 1-8 (2011).
- [21] H. Lindberg, A. Larsson, and M. Strassner, “Single-frequency operation of a high-power, long-wavelength semiconductor disk laser,” *Opt. Lett.* **30**, 2260-2262 (2005).
- [22] J. P. Turrenc, S. Bouchoule, A. Khadour, J. Decobert, A. Miard, J. C. Harmand, and J. L. Oudar, “High power single-longitudinal-mode OP-VECSEL at 1.55 μm

- with hybrid metal-metamorphic Bragg mirror,” *Electron. Lett.* **43**, 1-2 (2007).
- [23] A. Rantamäki, J. Rautiainen, J. Lyytikäinen, A. Sirbu, A. Mereuta, E. Kapon, and O. G. Okhotnikov, “1 W at 785 nm from a frequency-doubled wafer-fused semiconductor disk laser,” *Opt. Express* **20**, 9046-9051 (2012).
- [24] A. Härkönen, M. Guina, O. Okhotnikov, K. Rößner, M. Hümmer, T. Lehnhardt, M. Müller, A. Forchel, and M. Fischer, “1-W antimonide-based vertical external cavity surface emitting laser operating at 2- μm ,” *Opt. Express* **14**, 6479-6484 (2006).
- [25] J.-M. Hopkins, N. Hempler, B. Rösener, N. Schulz, M. Rattunde, C. Manz, K. Köhler, J. Wagner, and D. Burns, “High-power, (AlGaIn)(AsSb) semiconductor disk laser at 2.0 μm ,” *Opt. Lett.* **33**, 201-203 (2008).
- [26] B. Rösener, N. Schulz, M. Rattunde, C. Manz, K. Köhler, and J. Wagner, “High-power high-brightness operation of a 2.25- μm (AlGaIn)(AsSb)-based barrier-pumped vertical-external-cavity surface-emitting laser,” *IEEE Photon. Technol. Lett.* **20**, 502-504 (2008).
- [27] N. Schulz, M. Rattunde, C. Ritzenthaler, B. Rösener, C. Manz, K. Köhler, and J. Wagner, “Resonant optical in-well pumping of an (AlGaIn)(AsSb)-based vertical-external-cavity surface-emitting laser emitting at 2.35 μm ,” *Appl. Phys. Lett.* **91**, 091113 1-3 (2007).
- [28] S. Calvez, J. E. Hastie, M. Guina, O. G. Okhotnikov, and M. D. Dawson, “Semiconductor disk lasers for the generation of visible and ultraviolet radiation,” *Laser & Photon. Rev.* **3**, 407-434 (2009).
- [29] K. Iga, “Surface-emitting lasers—Its birth and generation of new optoelectronics field,” *IEEE J. Sel. Top. Quantum Electron.* **6**, 1201-1215 (2000).
- [30] S. Lutgen, T. Albrecht, P. Brick, W. Reill, and J. Luft, “8-W high-efficiency continuous-wave semiconductor disk laser at 1000 nm,” *Appl. Phys. Lett.* **82**, 3620-3622 (2003).
- [31] D. S. Jiang, H. Jung, and K. Ploog, “Temperature dependence of photoluminescence from GaAs single and multiple quantum-well heterostructure grown by molecular-beam epitaxy,” *J. Appl. Phys.* **64**, 1371-1377 (1988).
- [32] C. Y. Liu, S. Yuan, J. R. Dong, S. J. Chua, M. C. Y. Chan, and S. Z. Wang, “Temperature-dependent photoluminescence of GaInP/AlGaInP multiple

- quantum well laser structure grown by metalorganic chemical vapor deposition with tertiarybutylarsine and tertiarybutylphosphine,” *J. Appl. Phys.* **94**, 2962-2967 (2003).
- [33] X. H. Zhang, R. E. Doezema, N. Goel, S. J. Chung, M. B. Santos, N. Dai, F. H. Zhao, and Z. S. Shi, “Photoluminescence study of InSb/Al_xIn_{1-x}Sb quantum wells,” *Appl. Phys. Lett.* **89**, 021907 1-3 (2006).
- [34] E. O. Göbel, H. Jung, J. Kuhl, and K. Ploog, “Recombination enhancement due to carrier localization in quantum well structures,” *Phys. Rev. Lett.* **51**, 1588-1591 (1983).
- [35] P. Michler, A. Hangleiter, M. Moser, M. Geiger, and F. Scholz, “Influence of barrier height on carrier lifetime in Ga_{1-y}In_yP/(Al_xGa_{1-x})_{1-y}In_yP single quantum wells,” *Phys. Rev. B* **46**, 7280-7283 (1992).
- [36] Y. J. Wang, S. J. Xu, Q. Li, D. G. Zhao, and H. Yang, “Band gap renormalization and carrier localization effects in InGaN/GaN quantum-wells light emitting diodes with Si doped barriers,” *Appl. Phys. Lett.* **88**, 041903 1-3 (2006).
- [37] S. Yuan, Y. Kim, H. H. Tan, C. Jagadish, P. T. Burke, L. V. Dao, M. Gal, M. C. Y. Chan, E. H. Li, J. Zou, D. Q. Cai, D. J. H. Cockayne, and R. M. Cohen, “Anodic-oxide-induced interdiffusion in GaAs/AlGaAs quantum wells,” *J. Appl. Phys.* **83**, 1305-1311 (1998).
- [38] S. Schmitt-Rink, D. S. Chemla, and D. A. B. Miller, “Theory of transient excitonic optical nonlinearities in semiconductor quantum-well structures,” *Phys. Rev. B* **32**, 6601-6609 (1985).
- [39] S. Schmitt-Rink, C. Ell, and H. Haug, “Many-body effects in the absorption, gain, and luminescence spectra of semiconductor quantum-well structures,” *Phys. Rev. B* **33**, 1183-1189 (1986).
- [40] S. Schmitt-Rink and C. Ell, “Excitons and electron-hole plasma in quasi-two-dimensional systems,” *J. Lumin.* **30**, 585-596 (1985).
- [41] E. O. Göbel, R. Höger, J. Kuhl, H. J. Polland, and K. Ploog, “Homogeneous gain saturation in GaAs/AlGaAs quantum well lasers,” *Appl. Phys. Lett.* **47**, 781-783 (1985).
- [42] Z. Y. Xu, V. G. Kreismanis, and C. L. Tang, “Stimulated emission of GaAsAl_{0.6}Ga_{0.4}As multiple quantum well structures grown by metalorganic chemical vapor deposition,” *Appl. Phys. Lett.* **44**, 136-138 (1984).
- [43] R. Cingolani, H. Kalt, and K. Ploog, “Observation of transient band-gap

- renormalization in quantum wells,” *Phys. Rev. B* **42**, 7655-7658 (1990).
- [44] C. Delalande, G. Bastard, J. Orgonasi, J. A. Brum, H. W. Liu, M. Voos, G. Weimann, and W. Schlapp, “Many-body effects in a modulation-doped semiconductor quantum well,” *Phys. Rev. Lett.* **59**, 2690-2692 (1987).
- [45] J. A. Levenson, I. Abram, R. Raj, G. Dolique, J. L. Oudar, and F. Alexandre, “Optical nonlinearities in multiple quantum wells: New insight on band-gap renormalization,” *Phys. Rev. B* **38**, 13443-13446 (1988).
- [46] M. Cappizzi, S. Modesti, A. Frova, J. L. Staehli, M. Gussi, and R. A. Logan, “Electron-hole plasma in direct-gap Ga_{1-x}Al_xAs and k-selection rule,” *Phys. Rev. B* **29**, 2028-2035 (1984).
- [47] P. Vashishta and R. K. Kalia, “Universal behavior of exchange-correlation energy in electron-hole liquid,” *Phys. Rev. B* **25**, 6492-6495 (1982).
- [48] G. Tränkle, A. Forchel, H. Haug, C. Ell, and G. Weimann, “Dimensionality dependence of the band-gap renormalization in two- and three-dimensional electron-hole plasmas in GaAs,” *Phys. Rev. Lett.* **58**, 419-422 (1987).
- [49] S. D. Sarma, R. Jalabert, and S.-R. E. Yang, “Band-gap renormalization in quasi-two-dimensional systems induced by many-body electron-electron and electron-phonon interactions,” *Phys. Rev. B* **39**, 5516-5519 (1989).
- [50] H. Haug and S. Schmitt-Rink, “Basic mechanisms of the optical nonlinearities of semiconductors near the band edge,” *J. Opt. Soc. Am. B* **2**, 1135-1142 (1985).
- [51] D. A. Kleinman and R. C. Miller, “Band-gap renormalization in semiconductor quantum wells containing carriers,” *Phys. Rev. B* **32**, 2266-2272 (1985).
- [52] G. Tränkle, E. Lach, A. Forchel, F. Scholz, C. Ell, H. Haug, and G. Weimann, “General relation between band-gap renormalization and carrier density in two-dimensional electron-hole plasmas,” *Phys. Rev. B* **36**, 6712-6714 (1987).
- [53] E. Lach, A. Forchel, D. A. Broido, T. L. Reinecke, G. Weimann, and W. Schlapp, “Room-temperature emission of highly excited GaAs/Ga_{1-x}Al_xAs quantum wells,” *Phys. Rev. B* **42**, 5395-5398 (1990).
- [54] C. Webber, C. Klingshirn, D. S. Chemla, D. A. B. Miller, J. E. Cunningham, and C. Ell, “Gain measurements and band-gap renormalization in GaAs/Al_xGa_{1-x}As multiple-quantum-well structures,” *Phys. Rev. B* **38**, 12748-12751 (1988).
- [55] B. Deveaud, F. Clérot, K. Fujiwara, and K. Mitsunaga, “Radiative properties of a highly excited quantum well,” *Appl. Phys. Lett.* **58**, 1485-1487 (1991).
- [56] H. Q. Le, B. Lax, B. A. Vojak, and A. R. Calawa, “High-density excitonic state

- in two-dimensional multiple quantum wells,” *Phys. Rev. B* **32**, 1419-1422 (1985).
- [57] R. Cingolani, K. Ploog, A. Cingolani, C. Moro, and M. Ferrara, “Radiative recombination processes of the many-body states in multiple quantum wells,” *Phys. Rev. B* **42**, 2893-2903 (1990).
- [58] M. A. Hadley, G. C. Wilson, K. Y. Lau, and J. S. Smith, “High single-transverse-mode output from external-cavity surface-emitting laser diodes,” *Appl. Phys. Lett.* **63**, 1607-1609 (1993).
- [59] M. Kuznetsov, F. Hakimi, R. Sprague, and A. Mooradian, “Design and characteristics of high-power (>0.5-W CW) diode-pumped vertical-external-cavity surface-emitting semiconductor lasers with circular TEM₀₀ beams,” *IEEE J. Sel. Top. Quantum Electron.* **5**, 561-573 (1999)
- [60] M. Guina, T. Leinonen, A. Härkönen, and M. Pessa, “High-power disk lasers based on dilute nitride heterostructures,” *N. J. Phys.* **11**, 125019 (2009).
- [61] S. Calvez, J. E. Hastie, M. Guina, O. G. Okhotnikov, and M. D. Dawson, “Semiconductor disk lasers for the generation of visible and ultraviolet radiation,” *Laser & Photon. Rev.* **3**, 407-434 (2009).
- [62] S. Calvez, J. E. Hastie, A. J. Kemp, N. Laurand, and M. D. Dawson, “Thermal management, structure design, and integration considerations for VECSELs,” in *Semiconductor Disk Lasers: Physics and Technology*, O. G. Okhotnikov, Ed. Darmstadt, Germany: Wiley-VCH Verlag GmbH, 2010, pp. 73-117.
- [63] S. Lutgen, T. Albrecht, P. Brick, W. Reill, J. Luft, and W. Spath, “8-W high-efficiency continuous-wave semiconductor disk laser at 1000 nm,” *Appl. Phys. Lett.* **82**, 3620-3622 (2003).
- [64] W. J. Alford, T. D. Raymond, and A. A. Allerman, “High power and good beam quality at 980 nm from a vertical external-cavity surface-emitting laser,” *J. Opt. Soc. Am. B* **19**, 663-666 (2002).
- [65] R. Häring, R. Paschotta, A. Aschwanden, E. Gini, F. Morier-Genoud, and U. Keller, “High-power passively mode-locked semiconductor laser,” *IEEE J. Quantum Electron.* **38**, 1268-1275 (2002).
- [66] M. Y. A. Raya, S. R. J. Brueck, M. Osinsky, C. F. Schaus, J. G. Mcinery, T. M. Brennan, B. E. Hammons, “Resonant periodic gain surface-emitting semiconductor lasers,” *IEEE J. Quantum Electron.* **QE-25**, 1500-1512 (1989).
- [67] M. Y. A. Raya, S. R. J. Brueck, M. O. Scully, and C. Lee, “Resonant

- periodic-gain surface-emitting semiconductor lasers and correlated emission in a ring cavity,” *Phys. Rev. A* **44**, 4599-4607 (1991).
- [68] H. Lindberg, M. Strassner, J. Bengtsson, and A. Larsson, “High-power optically pumped 1550-nm VECSEL with a bonded silicon heat spreader,” *IEEE Photonics Technol. Lett.* **16**, 1233-1235 (2004).
- [69] J. H. Lee, J. Y. Kim, S. M. Lee, J. R. Yoo, K. S. Kim, S. H. Cho, S. J. Lim, G. B. Kim, S. M. Hwang, T. Kim, and Y. J. Park, “9.1-W high-efficient continuous-wave end-pumped vertical-external-cavity surface-emitting semiconductor laser,” *IEEE Photonics Technol. Lett.* **18**, 2117-2119 (2006).
- [70] K. W. Su, S. C. Huang, A. Li, S. C. Liu, Y. F. Chen, and K. F. Huang, “High-peak-power AlGaInAs quantum-well 1.3- μ m laser pumped by a diode-pumped actively Q-switched solid-state laser,” *Opt. Lett.* **31**, 2009-2011 (2006).
- [71] B. Rudin, A. Rutz, M. Hoffmann, D. J. H. C. Maas, A.-R. Bellancourt, E. Gini, T. Südmeyer, and U. Keller, “Highly efficient optically pumped vertical-emitting semiconductor laser with more than 20 W average output power in a fundamental transverse mode,” *Opt. Lett.* **15**, 2719-2721 (2008).
- [72] A. Laurain, T.-L. Wang, M. J. Yarborough, J. Harder, J. V. Moloney, S. W. Koch, B. Kunert, and W. Stolz, “High peak power operation of a 1- μ m GaAs-based optically pumped semiconductor laser,” *IEEE Photonics Technol. Lett.* **24**, 380-382 (2012).
- [73] Y.-F. Chen, K. W. Su, W. L. Chen, K. F. Huang, and Y. F. Chen, “High-peak-power optically pumped AlGaInAs eye-safe laser at 500-kHz repetition rate with an intracavity diamond heat spreader,” *Appl. Phys. B* **108**, 319-323 (2012).
- [74] G. B. Kim, J.-Y. Kim, J. Lee, J. Yoo, and K.-S. Kim, “End-pumped green and blue vertical external cavity surface emitting laser device,” *Appl. Phys. Lett.* **89**, 181106 1-3 (2006).
- [75] L. Fan, T.-C. Hsu, M. Fallahi, J. T. Murray, and R. Bedford, “Tunable watt-level blue-green vertical-external-cavity surface-emitting lasers by intracavity frequency doubling,” *Appl. Phys. Lett.* **88**, 251117 1-3 (2006).
- [76] S. Cho, G. B. Kim, J.-Y. Kim, K.-S. Kim, S.-M. Lee, J. Yoo, T. Kim, and T.Y. Park, “Compact and efficient green VECSEL based on novel optical end-pumping scheme,” *IEEE Photon. Tech. Lett.* **19**, 1325-1327 (2007).

- [77] M. Fallahi, L. Fan, Y. Kaneda, C. Hessenius, J. Harder, H. Li, J. V. Moloney, B. Kunert, W. Stolz, S. W. Koch, J. Murray, and R. Bedford, "5-W yellow laser by intracavity frequency doubling of high-power vertical-external-cavity surface-emitting laser," *IEEE Photon. Tech. Lett.* **20**, 1700-1702 (2008).
- [78] J. Rautiainen, A. Härkönen, V.-M. Korpijärvi, P. Tuomisto, M. Guina, and O. G. Okhotnikov, "2.7 W tunable orange-red GaInNAs semiconductor disk laser," *Opt. Express* **15**, 18345-18350 (2007).
- [79] M. Jacquemet, M. Domenech, G. Lucas-Leclin, P. Georges, J. Dion, M. Strassner, I. Sagnes, and A. Garnache, "Single-frequency cw vertical external cavity surface emitting semiconductor laser at 1003 nm and 501 nm by intracavity frequency doubling," *Appl. Phys. B* **86**, 503-510 (2007).
- [80] H. Lindberg, A. Larsson, and M. Strassner, "Single-frequency operation of a high-power, long-wavelength semiconductor disk laser," *Opt. Lett.* **30**, 2260-2262 (2005).
- [81] A. J. Maclean, A. J. Kemp, S. Calvez, J.-Y. Kim, T. Kim, M. D. Dawson, and D. Burns, "Continuous tuning and efficient intracavity second-harmonic generation in a semiconductor disk laser with an intracavity diamond heatspreader," *IEEE J. Quantum Electron.* **44**, 216-225 (2008).
- [82] L. Fan, C. Hessenius, M. Fallahi, J. Harder, H. Li, J. V. Moloney, W. Stolz, S. W. Koch, J. T. Murray, and R. Bedford, "Highly strained InGaAs/GaAs multiwatt vertical-external-cavity surface-emitting laser emitting around 1170 nm," *Appl. Phys. Lett.* **91**, 131114 1-3 (2007).
- [83] R. Häring, R. Paschotta, A. Aschwanden, E. Gini, F. Morier-Genoud, and U. Keller, "High-power passively mode-locked semiconductor lasers," *IEEE J. Quantum Electron.* **38**, 1268-1275 (2002).
- [84] U. Keller and A. C. Tropper, "Passively modelocked surface-emitting semiconductor lasers," *Phys. Reports* **429**, 67-120 (2006).
- [85] J. J. Zayhowski and C. Dill III, "Diode-pumped passively Q-switched picosecond microchip lasers," *Opt. Lett.* **19**, 1427-1429 (1994).
- [86] J. J. Zayhowski, "Passively Q-switched Nd:YAG microchip lasers and applications," *J. Alloys and Compounds* **303**, 393-400 (2000).
- [87] Y. F. Chen and Y. P. Lan, "Diode-pumped passively Q-switched Nd:YAG laser at 1123 nm," *Appl. Phys. B* **79**, 29-31 (2004).

- [88] A. Agnesi, A. Guandalini, G. Reali, J. K. Jabczynski, K. Kopczynski, and Z. Mierczyk, "Diode pumped Nd:YVO₄ laser at 1.34 μm Q-switched and mode locked by a V³⁺:YAG saturable absorber," *Opt. Commun.* **194**, 429-433 (2001).
- [89] K. V. Yumashev, I. A. Denisov, N. N. Posnov, P. V. Prokoshin, and V. P. Mikhailov, "Nonlinear absorption properties of Co²⁺:MgAl₂O₄ crystal," *Appl. Phys. B* **70**, 179-184 (2000).
- [90] R. Häring, R. Paschotta, R. Fluck, E. Gini, H. Melchior, and U. Keller, "Passively Q-switched microchip laser at 1.5 μm ," *J. Opt. Soc. Am. B* **18**, 1805-1812 (1998).
- [91] B. Braun, F. X. Kärtner, U. Keller, J.-P. Meyn, and G. Huber, "Passively Q-switched 180-ps Nd:LaSc₃(BO₃)₄ microchip laser," *Opt. Lett.* **21**, 405-407 (1996).
- [92] B. Braun, F. X. Kärtner, G. Zhang, M. Moser, and U. Keller, "56-ps passively Q-switched diode-pumped microchip laser," *Opt. Lett.* **22**, 381-383 (1997).
- [93] G. J. Spühler, R. Paschotta, M. P. Kullberg, M. Graf, M. Moser, E. Mix, G. Huber, C. Harder, and U. Keller, "A passively Q-switched Yb:YAG microchip laser," *Appl. Phys. B* **72**, 285-287 (2001).
- [94] A. C. Butler, D. J. Spence, and D. W. Coutts, "Scaling Q-switched microchip lasers for shortest pulses," *Appl. Phys. B* **109**, 81-88 (2012).
- [95] R. Fluck, B. Braun, E. Gini, H. Melchior, and U. Keller, "Passively Q-switched 1.34- μm Nd:YVO₄ microchip laser with semiconductor saturable-absorber mirrors," *Opt. Lett.* **22**, 991-993 (1997).
- [96] R. Fluck, R. Häring, R. Paschotta, E. Gini, H. Melchior, and U. Keller, "Eyesafe pulsed microchip laser using semiconductor saturable absorber mirrors," *Appl. Phys. Lett.* **72**, 3273-3275 (1998).
- [97] A. Li, S. C. Liu, K. W. Su, Y. L. Liao, S. C. Huang, Y. F. Chen, and K. F. Huang, "InGaAsP quantum-wells saturable absorber for diode-pumped passively Q-switched 1.3- μm lasers," *Appl. Phys. B* **84**, 429-431 (2006).
- [98] S. C. Huang, S. C. Liu, A. Li, K. W. Su, Y. F. Chen, and K. F. Huang, "AlGaInAs quantum-well as a saturable absorber in a diode-pumped passively Q-switched solid-state laser," *Opt. Lett.* **32**, 1480-1482 (2007).
- [99] J. Y. Huang, H. C. Liang, K. W. Su, H. C. Lai, Y.-F. Chen, and K. F. Huang, "InGaAs quantum-well saturables for a diode-pumped passively Q-switched

- Nd:YAG laser at 1123 nm,” *Appl. Opt.* **46**, 239-242 (2007).
- [100] J. J. Zayhowski and P. L. Kelley, “Optimization of Q-switched lasers,” *IEEE J. Quantum Electron.* **27**, 2220-2225 (1991).
- [101] G. J. Spühler, R. Paschotta, R. Fluck, B. Braun, M. Moser, G. Zhang, E. Gini, and U. Keller, “Experimentally confirmed design guidelines for passively Q-switched microchip lasers using semiconductor saturable absorbers,” *J. Opt. Soc. Am. B* **16**, 376-388 (1999).
- [102] J. J. Zayhowski and C. Dill III, “Diode-pumped passively Q-switched picosecond microchip lasers,” *Opt. Lett.* **19**, 1427-1429 (1994).
- [103] J. J. Zayhowski and C. Dill III, “Couple-cavity electro-optically Q-switched Nd:YVO₄ microchip lasers,” *Opt. Lett.* **20**, 716-718 (1995).
- [104] S. Zhou, K. K. Lee, Y. C. Chen, and S. Li, “Monolithic self-Q-switched Cr,Nd:YAG laser,” *Opt. Lett.* **18**, 511-512 (1993).
- [105] P. Wang, S.-H. Zhou, K. K. Lee, and Y. C. Chen, “Picosecond laser pulse generation in a monolithic self-Q-switched solid-state laser,” *Opt. Commun.* **114**, 439-441 (1993).
- [106] D. Nodop, J. Limpert, R. Hohmuth, W. Richter, M. Guina, and A. Tünnermann, “High-pulse-energy passively Q-switched quasi-monolithic microchip lasers operating in the sub-100-ps pulse regime,” *Opt. Lett.* **32**, 2115-2117 (2007).

Chapter Two

Spontaneous Emission of AlGaInAs Multiple-Quantum-Wells under High Level Excitation

2.1 Device fabrication of AlGaInAs multiple-quantum-wells

In [section 1.2](#), we have mentioned that the high density electron-hole plasma (EHP) will give rise to the band-gap renormalization due to the many-body effect [\[1,2\]](#). Despite the investigations of carrier density dependence of the band-gap reduction via the photo-luminescence (PL) and absorption spectrum [\[3-6\]](#), the prominent luminescence features of the high density EHP many-body state have been observed in the large number of quasi-2D confined multiple-quantum-wells (MQWs) under cryogenic temperature [\[7-10\]](#). This emanation mode is appeared with the linewidth much narrower than the fundamental $n=1$ state transition and the peak intensity grows super-linearly with the increase of excitation intensity [\[9\]](#). However, the requirement of operation temperature below 15 K in which the exciton single-particle state and the EHP many-body state are coexisted hinders the employment in practical applications such as lasers and light emitting diodes which require high stability and thermal resistivity at room temperature. Besides, the evolution of spectral features and the integrated PL intensity of the EHP many-body state luminescence have not been studied as the function of temperature up to now.

Nowadays, the semiconductor surface-emitting lasers in use of the MQWs structure as the active medium have been developed to be a promising laser source providing the high power, versatile wavelength, low divergence and high quality single transverse mode beams [\[11-13\]](#). The resonant-periodical-gain (RPG) structure extensively applied in these lasers is not only used to improve the wavelength

selection and optical gain but also to avoid the amplified spontaneous emission in the lateral direction via the better spatial overlap of the MQWs gain region and the anti-node of the lasing standing waves [14,15]. The requirement of large number of quantum well pairs which is confirmed to be vital to the appearance of the EHP many-body state emission [9] elucidates that the strong optical confinement and amplified spontaneous emission effect play an important role in this particular emanation process. Based on these reasons, the designation of RPG structure to the MQWs sample in which the effective number of the QWs is significantly increased should be contributive to the observation of this many-body state luminescence. Therefore, the reduction of the luminescence intensity due to the thermally-induced non-radiative recombination could be eased in virtue of the enhanced light-QWs interaction.

The previous investigations of the prominent luminescence features below the band-edge induced by the many-body interaction in the quasi 2-D EHP systems are mainly focusing on the AlGaAs/GaAs MQWs [7-10]. The GaAs QWs are spaced by the AlGaAs barrier regions with thickness nearly comparable to the QWs width. In this composition, the coupling between the emitted photons and the excited carriers is weak. The effective number of QWs for the formation of EHP emission is lower than the actual configuration. Therefore, the large amounts of QWs and ultra-low sample temperature below 15 K are needed to exhibit the EHP many-body state emission. In this chapter, we use 30 groups of the AlGaInAs triple QWs pairs which were grown on the Fe-doped InP and each pairs of the MQWs were spaced with $\lambda/2$ interval by the cladding layers via metalorganic chemical-vapor deposition. The cladding layers with half wavelength distributions are assigned to separate the MQWs and locate the gain region at the anti-node of the emission light standing wave to realize the RPG

structure. Therefore, the light-QWs interaction is strengthened and all of the MQWs are activated under this periodical aligned gain configuration. The schematic comparisons of above two arrangements are depicted in Fig. 2.1-1 (a) and (b) respectively.

In the following contents, an AlGaInAs/InP MQWs chip with $\lambda/2$ interval spaced gain region is used to investigate the specific radiative recombination phenomenon of the high density EHP many-body state under the quasi-2D confined system. Each pairs of the MQWs contained three 8 nm InGaAs QWs layers and two 6 nm InAlAs barrier layers. The total confinement energy of the electron-hole pairs is assigned to be 0.717 eV which is much higher than in the AlGaAs/GaAs systems specified in *literature* with confinement energy around 0.15 to 0.22 eV [7-10]. The higher confined energy will prevent the carrier leakage from the QWs to barrier region and the thermal induced nonradiative recombination could be strongly reduced. Although the evolution of the electron-hole pairs band-to-band luminescence with respect to the temperature in MQWs structure has been investigated for a long time, the temperature dependence of the many-body state luminescence has not been studied so far. In this chapter, we first demonstrate the intensity dependent PL spectra of the AlGaInAs MQWs with excitation intensity varied from 23 to 384 kW/cm² at 253 K. The luminescence features of the EHP many-body state beneath the typical quantized state emission of the MQWs is observed with threshold intensity of 80 kW/cm² and the schematics of integrated PL intensity as the function of excitation intensity are also shown at different temperatures. Then the evolution of this emission mode is verified to be a strong function of the temperature via the temperature-dependent PL spectra from 123 to 313 K at excitation intensity of 407 kW/cm². The peak wavelength of the many-body state emission is also shown to be linearly shifted with

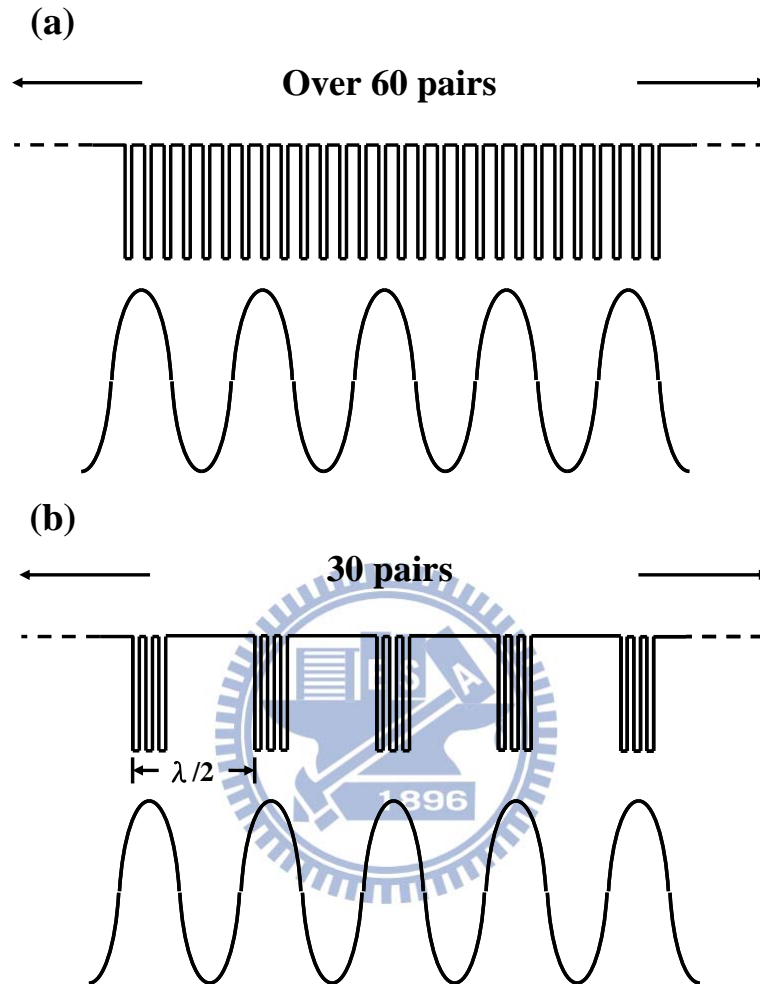
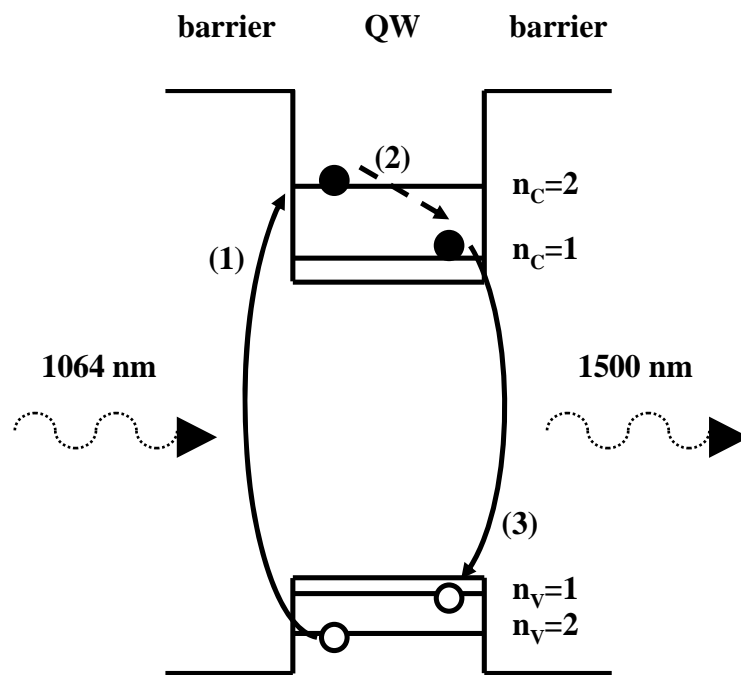


Fig. 2.1-1 The diagrams of the MQWs structures with (a) weak and (b) strong coupling of the light-QWs interaction.

increasing temperature from 93 to 313 K. At the end the integrated PL intensity and threshold excitation intensity are presented at a broad temperature range and, via the analytical model using three-level Boltzmann distribution, the effectiveness of the periodically aligned MQWs structure is confirmed contributing to the enhancement of the EHP many-body state emission at high temperature. To our knowledge, this is the first demonstration of high density EHP many-body state luminescence of AlGaInAs MQWs under room temperature.

2.2 Experimental setup

In contrast to the conventional barrier pump scheme, the MQWs sample used in our experiment is fabricated to be in-well pumped at the second quantized state ($n=2$) of QWs to prevent the carrier capture time from barrier to the QWs region [16,17]. Then the excited carriers relax to the ground state ($n=1$) and the intrinsic PL is radiated. The schematic demonstration of the radiative recombination processes is shown in Fig. 2.2-1 in use of a simplified single QW configuration. The room temperature transmission spectrum of the AlGaInAs MQWs chip is shown in Fig. 2.2-2 under low power excitation. The first and second quantum states can be recognized obviously due to the step-like density of state structure. But there is a deep valley of transmittance spectrum near the band-edge. Therefore, we performed reflectance spectrum measurement of MQW chip to fully understand this specific feature. In Fig. 2.2-3, the reflectance spectrum depicted by solid curve reveals that the relatively low transmission at 1500 nm is mainly resulted from the strong reflectance peak. This phenomenon could be explained by the interference of multi-reflected wave from periodic layers. In Fig. 2.2-4 we illustrated three stacks of MQW layers with propagating optical waves A, B and C which are reflected by three MQW interface units. Because the lengths of MQW stacks are much shorter than space



- (1) Pump absorption
- (2) Nonradiative relaxation
- (3) Ground state luminescence

Fig. 2.2-1 Schematic diagram of the radiative recombination mechanisms of the AlGaInAs MQWs in the simplified single QW configuration.

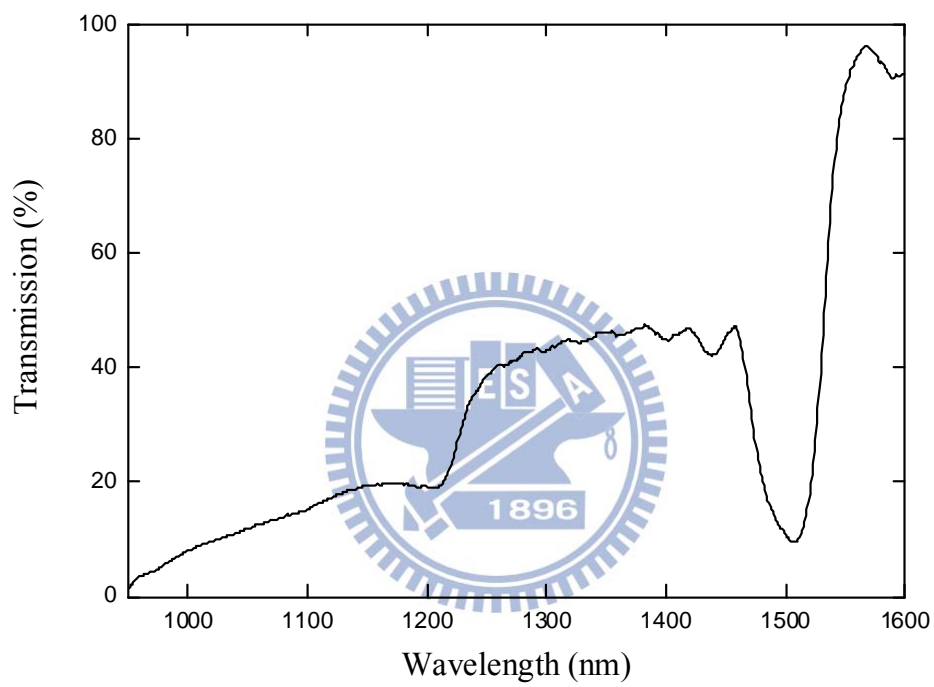


Fig. 2.2-2 Room temperature transmittance spectrum of the AlGaInAs MQWs chip excited at low intensity.

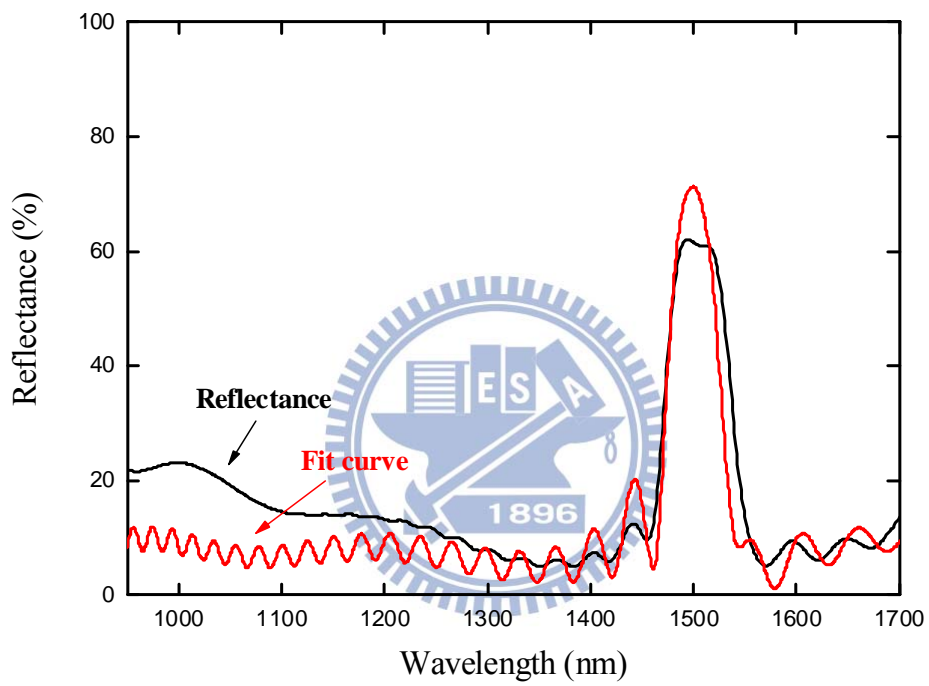


Fig. 2.2-3 Room temperature reflectance spectrum of the AlGaInAs MQWs chip excited at low intensity.

layers, phase difference of single unit of MQW interface give rise to phase change of $\Delta\varphi$. Consequently, the three reflected wave A, B and C are all in-phase at the incident surface and the constructive interference will result in the reflectance peak as seen in Fig. 2.2-3. This characteristic reflection band due to periodically distributed semiconductor structure can be modeled in use of the transfer matrix method [18]. When a light wave with wavelength λ is incident to the periodically layered MQW structure from air, the scattering matrix T_j at (j-1)- to j-th semiconductor material interface and propagation matrix P_j for wave traveling in the j-th semiconductor material element could be expressed as follows,

$$T_j = \frac{1}{2} \begin{bmatrix} 1 + \frac{k_j}{k_{j-1}} & 1 - \frac{k_j}{k_{j-1}} \\ 1 - \frac{k_j}{k_{j-1}} & 1 + \frac{k_j}{k_{j-1}} \end{bmatrix}; P_j = \frac{1}{2} \begin{bmatrix} e^{-ik_j d_j} & 0 \\ 0 & e^{ik_j d_j} \end{bmatrix}, \quad (1)$$

where $k_j = 2\pi/\lambda_j$ and d_j denote the wave vector and thickness at j-th element, respectively. Consequently, the total equivalent transfer matrix Q is obtained by multiplying the scattering and propagation matrices the incident light passing through. The square value of reflection coefficient R at wavelength λ is calculated to be,

$$R = |r|^2 = \frac{|Q_{21}|^2}{|Q_{11}|^2}. \quad (2)$$

The fitted curve of reflection spectrum with incident light wavelength from 950 to 1700 nm is shown in Fig. 2.2-3 and in good agreement with the experimentally measured data. Finally, the absorption spectrum can be obtained using reflection and transmission spectrum and is shown in Fig. 2.2-5. The band-edge of n=1 quantized state is indicated to be located around 1500 nm at room temperature.

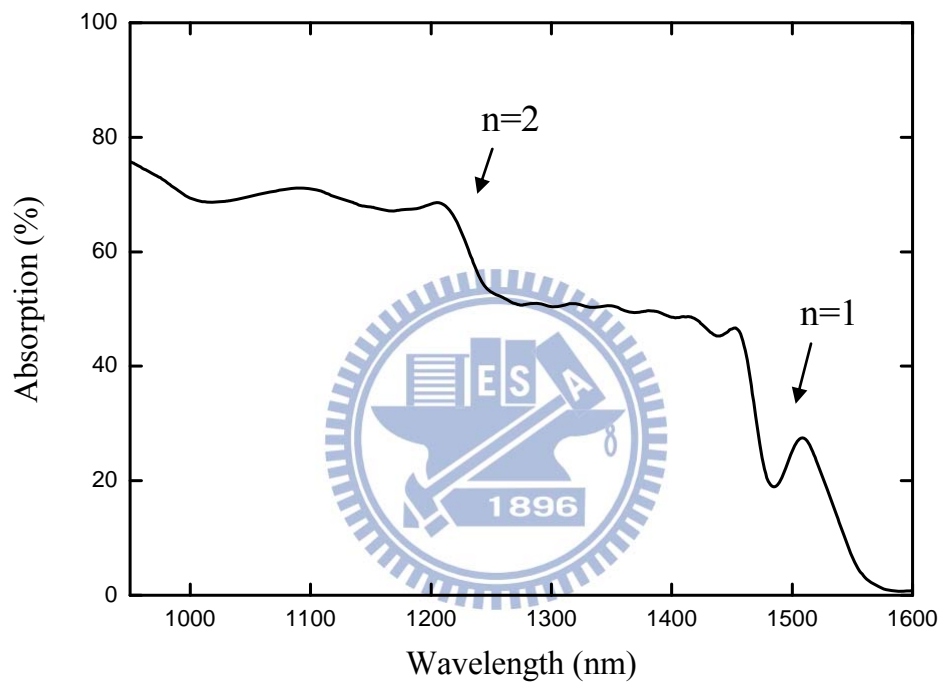


Fig. 2.2-5 Room temperature absorption spectrum of the AlGaInAs MQWs chip excited at low intensity.

In the proceeding experiments, excitation was performed by an Yb-doped master oscillator fiber amplifier (SPI redENERGY G3) with emission wavelength at 1.06 μm which is beyond the band-edge of $n=2$ quantized state. This pulsed fiber laser source supplies 12-200 ns pulses and the pulse repetition rates could be ranged from 10-500 kHz. The following experimental results are obtained under the pulse repetition rate of 20 kHz and pulse duration of 30 ns. The experimental configuration of the PL measurement is shown in Fig. 2.2-6. A focusing lens with 95% coupling efficiency was used to reimage the output beam of the pump fiber laser. The incident pump light was normal to the surface of the MQWwafer at a spot radius of 420 μm and the maximum pump intensity is 1 MW/cm^2 . To investigate the luminescence spectrum of MQW sample at the broad temperature range from 93 to 313 K, the MQW chip was cooled down by the cryogenic system (Janis VPF-100) in which the temperature could be ranged from 77 to 500 K and the stability is ± 50 mK. The epitaxial side of MQW chip was bonded to a single-crystal diamond plate with thickness of 450 μm via the liquid capillary bonding [19] to improve the heat dissipation in the lateral direction. The entire composite was clamped by the copper blocks with 2 mm diameter aperture in each side. The MQW sample was excited at the epitaxial side which is directly in contact with the diamond heat spreader to decrease the thermal resistance. The spectral information is recorded by an optical spectrum analyzer (Advantest Q8381A) with the diffraction monochromator which can be used to perform the high speed measurement of pulsed light with 0.1 nm resolution. The luminescence light of the MQW sample was collected from the substrate side by a multimode fiber with 75 μm core size and an angle of 50° to the surface normal. The size of aperture on the copper heat sinks and transparent windows on the vacuum chamber are large enough to prevent sheltering the luminescence light from the sample surface. Thus the

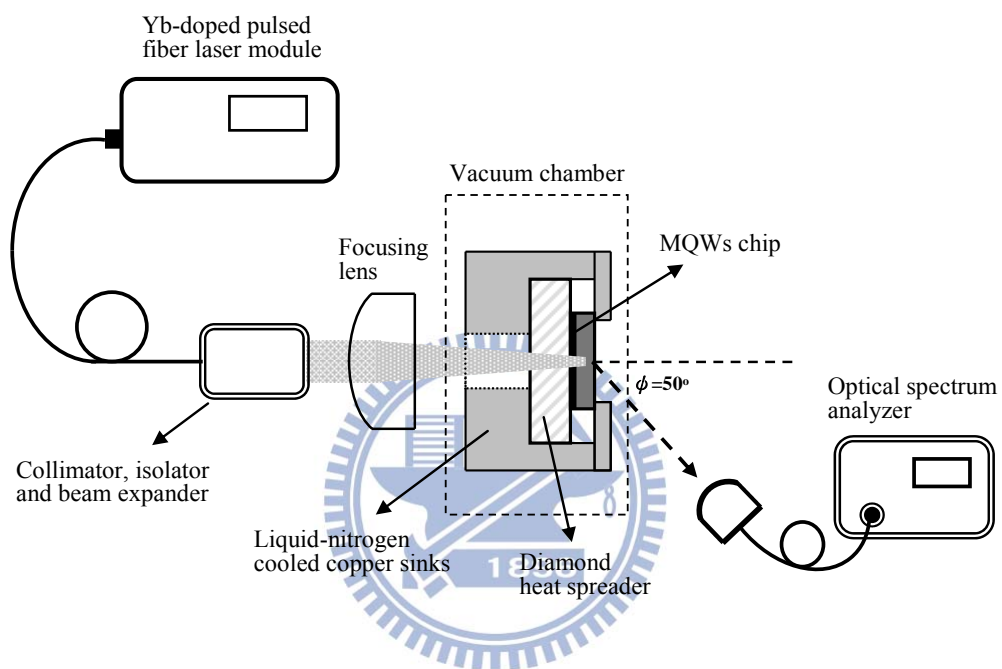


Fig. 2.2-6 The experimental configuration of the PL spectrum measurement.

collected light is composed of the radiation emanating from the entire excited region. The Fe-doped InP substrate is transparent at the wavelength region longer than 950 nm and polished to 300 μm . This means that the substrate will not alter the emission light from the MQW region except for a little scattering loss.

2.3 Experimental results and discussions

Figure 2.3-1 shows the intensity-dependent PL spectra of the AlGaInAs MQWs from 23 to 384 kW/cm^2 at 253 K. At the lowest excitation intensity of 23 kW/cm^2 only the emission line of fundamental $n=1$ transition exists. The peak wavelength of this emission line is located at around 1500 nm and with linewidth of 58 nm. However, above the threshold excitation intensity of 80 kW/cm^2 , a new and relatively sharp luminescence spectral feature appears at the low energy side of the $n=1$ transition with the full width at half maximum (FWHM) around 5.6-8.4 nm. This emanation mode is attributed to the many-body state luminescence of the renormalized band-edge induced by the high density EHP under high intensity photo-excitation. With increasing excitation intensity, the many-body state emission line grows superlinearly and, in contrast, the $n=1$ transition varies slowly with linear tendency. The integrated PL intensities of many-body state emission line as the functions of excitation intensity are shown in Fig. 2.3-2 at various temperatures of 253, 193 and 123 K. In this plot the integrated intensities of three curves are all increased rapidly at low excitation intensity and become saturated at relatively high excitation intensity. This means that when the excitation intensity is high enough the many-body states will be all filled and the luminescence intensity will be held unchanged with increasing pump intensity. In addition, this plot also indicates that the saturated luminescence intensity could be raised via the reduction of temperature which will be mentioned in the following.

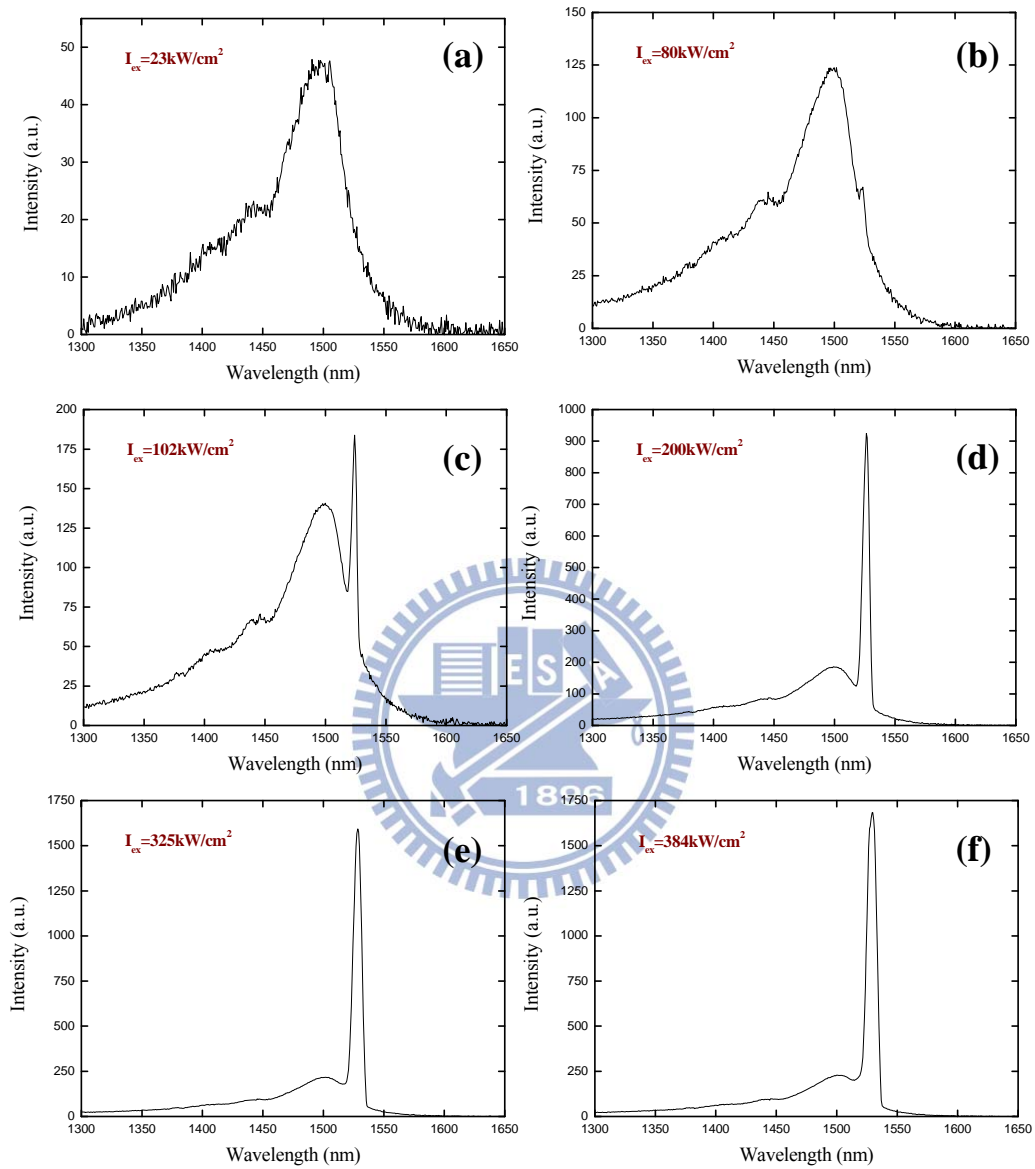


Fig. 2.3-1 Photo-luminescence spectra of the AlGaInAs MQWs chip with variance excitation intensity from 23 to 384 kW/cm^2 at 253 K.

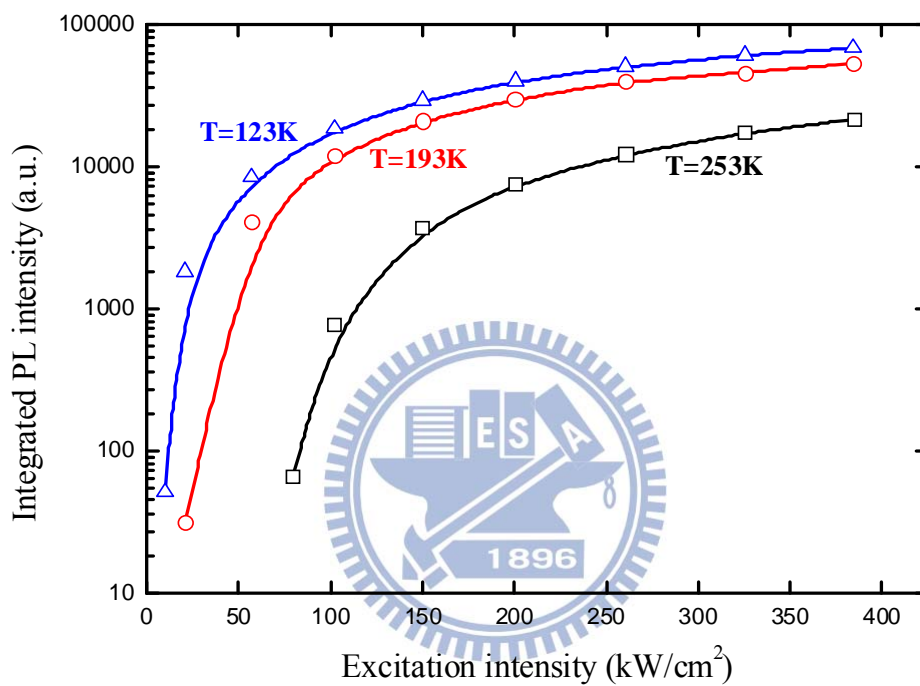


Fig. 2.3-2 Integrated PL intensity of the many-body state emission line as the function of excitation intensity at 253, 193 and 123 K.

To further investigate the temperature dependence of the many-body state luminescence, Fig. 2.3-3 shows the PL spectra of the AlGaInAs MQWs with the setting temperatures of 123, 193, 253 and 313 K at a fixed excitation intensity of 407 kW/cm². The peak of fundamental n=1 transition line is red-shifted from 1422 to 1510 nm due to the thermally induced band-gap shrinkage. When the temperature is decreased, the bandwidths of the n=1 transition line are narrowed significantly as the peak intensities hold unchanged. Because the excitation intensity of 407 kW/cm² is far from the threshold at temperature range up to 253 K which has been shown in Fig. 2.2-2, the emission line of many-body state could be observed clearly at 123, 193 and 253 K. The tendency of decreasing luminescence intensity with arising temperature is also corresponding to the results demonstrated in Fig. 2.3-2. Besides, the many-body state emission line still exists even at the temperature which is scaled up to 313 K as shown in Fig. 2.3-3. To our knowledge, this is the first demonstration of high density EHP many-body state luminescence of AlGaInAs MQWs under room temperature operation. The peak wavelength of many-body state emission line follows the reduction of band-edge of the fundamental ground state in MQWs and shifts to the low energy side as the temperature arising. Figure 2.3-4 depicts the variance of many-body state peak wavelength as the function of temperature from 93 to 313 K. The peak wavelength shift rate of 0.59 nm/K with diamond heat spreader is nearly the same with respect to the framework without diamond heat spreader. Therefore, the peak wavelength offset of 10.7 nm between these two schemes at the identical setting temperatures indicates that the sample temperature in use of the diamond heat spreader was 18 K lower than the case without diamond heat spreader. This suggests that the use of diamond heat spreader is not to promote the heat dissipation but to lessen the difference between the sample temperature and setting

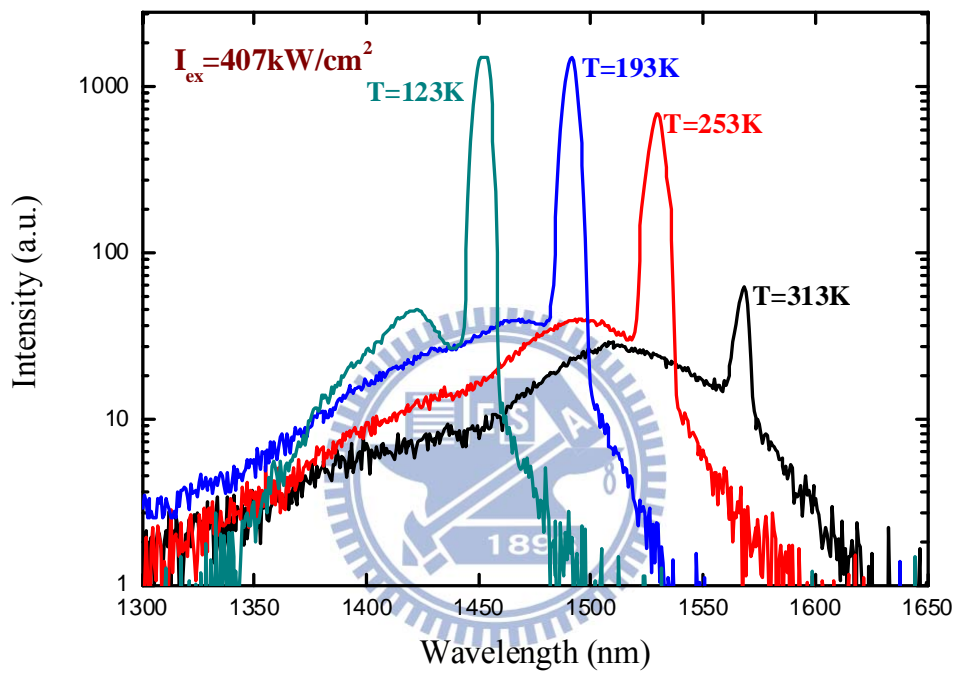


Fig. 2.3-3 Photo-luminescence spectra of the AlGaInAs MQWs chip with the excitation intensity of 407 kW/cm^2 measured at different temperatures from 123 to 313 K.

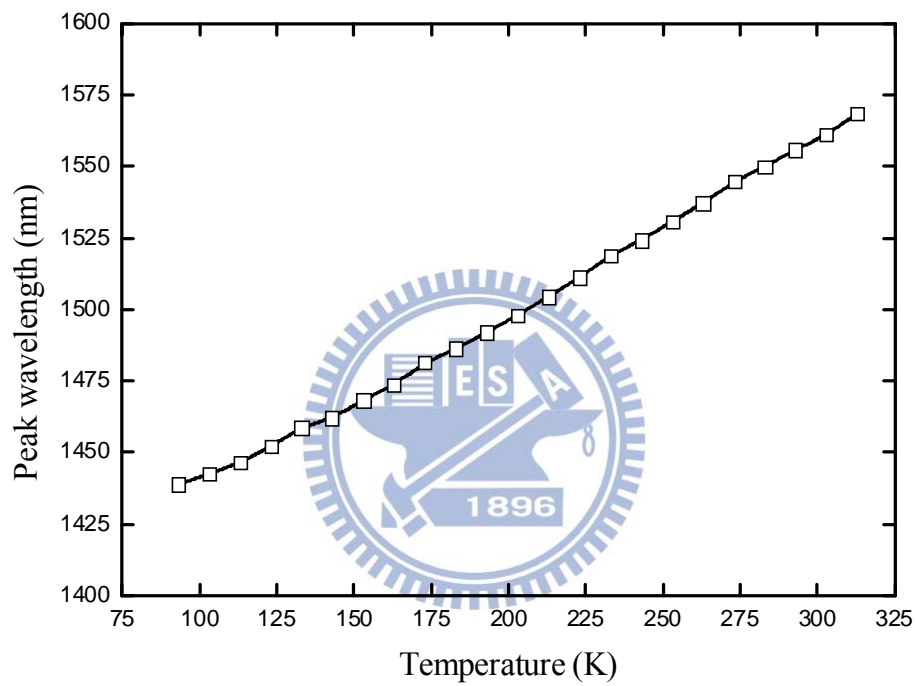


Fig. 2.3-4 Peak wavelength shift of the many-body state luminescence versus temperature at the excitation intensity of 407 kW/cm^2 .

temperature. Besides, the peak wavelength shift rate of 0.59 nm/K also elucidates that this specific emission line is not resulted from the particular reflection band depicted in Fig. 2.2-3 which has thermal induced shift rates about 0.1 nm/K.

In Fig. 2.3-2 we have revealed that the luminescence intensity of the many-body state is strongly related to the temperature. To obtain more information about this topic, the integrated PL intensity of many-body state emission line is depicted as a function of temperature from 93 to 313 K as in Fig. 2.3-5. It could be seen that the integrated PL intensity of the many-body state emission line exhibits three variant trends in the different portion of temperature regimes. At low temperature, the integrated PL intensity held unchanged up to 173 K. As the temperature operated above 253 K, a strong luminescence quenching was appeared with exponentially decay of the integrated intensity. In addition, the transition stage of the integrated intensity dropped slowly with increasing temperature between 173 to 253 K. This PL quenching phenomenon could be attributed to the presence of two nonradiative recombination mechanisms which are characterized by two different activation energies in variant temperature regions. To determine the activation energies a simple model using the three-level Boltzmann distribution is developed by Bimberg *et al.* [20] as follows,

$$I = I_0[1 + C_1 \exp(-E_1 / k_B T) + C_2 \exp(-E_2 / k_B T)]^{-1} , \quad (1)$$

where I is the integrated PL intensity at particular temperature, I_0 is the saturated integrated PL intensity at low temperature limit, k_B is the Boltzmann constant, T is the sample temperature, E_1 and E_2 are the specific activation energies for different nonradiative recombination centers, and C_1 and C_2 are the corresponding constants in connection with the density of states of E_1 and E_2 . The best fit to the integrated

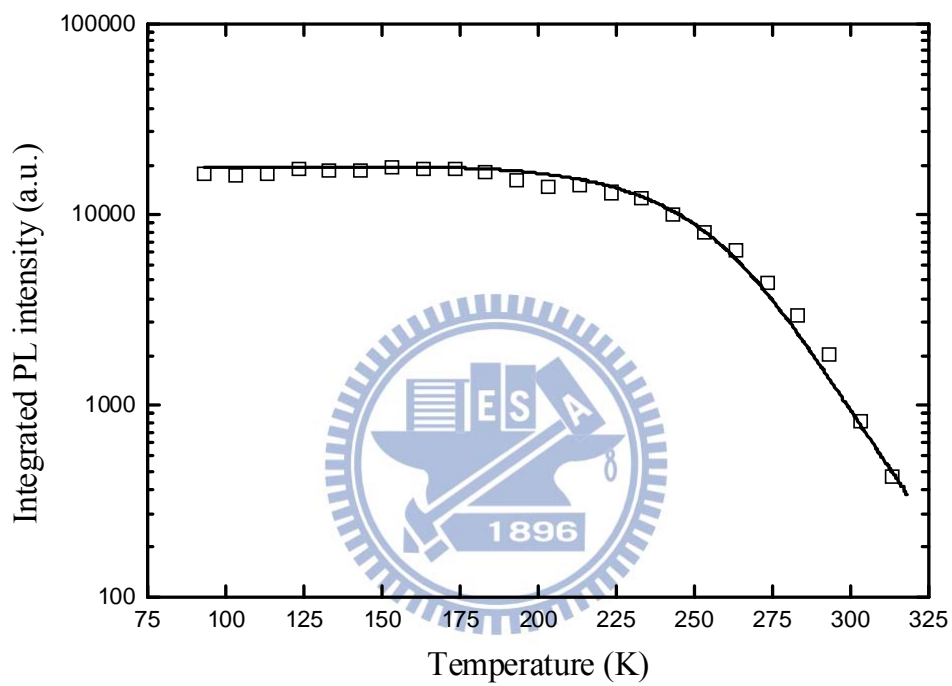
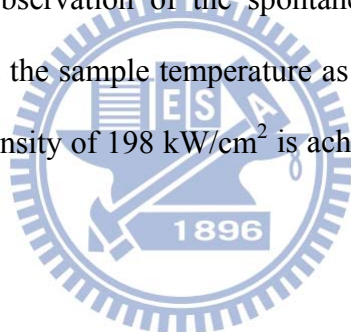


Fig. 2.3-5 Plots of the integrated PL intensity of the many-body state luminescence versus temperature at the excitation intensity of 407 kW/cm^2 .

intensity of the many-body state emission line is shown in Fig. 2.3-5 as the solid curve. By fitting the experimental data the value of activation energies E_1 and E_2 are yielded to be 0.19 and 0.52 eV, corresponding to the integrated PL intensity drop at intermediate and high temperature region, respectively. Similar behaviors are reported with exciton state or electron-hole pair luminescence in various MQWs samples [21,22]. Because E_2 is much larger than the possible inter-particle interaction energies, the luminescence quenching above 253 K is inferred to be resulted from the strengthened nonradiative recombination processes due to thermally induced carrier leakage from the renormalized band to barrier region [23]. The activation energy of the thermal emission of excited carriers under high excitation intensity has been reported to be equal to half of the confined energy of the electron-hole pairs theoretically and experimentally for the single quantum well [23,24]. However, one half of the energy gap between the barrier layer and renormalized band in our experiment was found to be 0.33 eV which is two-thirds of the fitted activation energy. This result bears that the periodically aligned gain structure is contributive to the existence of many-body state luminescence under high temperature. Although the fitted value of C_1 is six-order smaller than C_2 , the insertion of E_1 is necessary in matching the fit curve to experimental data at the intermediate temperature regime from 173 to 253 K. The origin of activation energy E_1 is still not clear at this time but we believe that it may be connected to the dissociation of the many-body state interaction. At the end, the integrated luminescence intensity of the n=1 transition line stayed nearly invariant in comparison to the many-body state luminescence in the entire temperature range. This suggests that the carriers tend to be trapped by the renormalized band due to the reabsorption and reemission processes and the relatively low radiative recombination lifetime.

In Fig. 2.3-2 and 2.3-5 we have examined that the saturation luminescence intensity is a strong function of temperature. However, the threshold excitation intensity is also depending on the temperature as observed in Fig. 2.3-2. To further understand this phenomenon, the threshold excitation intensity versus temperature from 123 to 293 K is shown in Fig. 2.3-6 quantitatively. The solid curve is the exponential fit of the experimental results. The excitation threshold intensity grew exponentially with the increasing temperature. It is because the higher excitation intensity produces more heat which will result in the more serious carrier leakage. However, the enhanced luminescence by using the periodically-aligned gain structure compensates the thermally induced emanation gain reduction as the temperature raised. Consequently, the observation of the spontaneous EHP renormalized state emission is obtained even at the sample temperature as high as 313 K. The relatively low excitation threshold intensity of 198 kW/cm^2 is achieved under room temperature of 293 K.



2.4 Conclusions

In this chapter, we demonstrated the first observation of room-temperature many-body state luminescence in a quasi-2D confined system via the stronger confined energy and resonant periodical gain enhancement. The temperature dependence of the many-body state luminescence features have also been shown to investigate the nonradiative recombination effect. The evolution of the integrated PL intensity at different temperature segments exhibit same PL quenching phenomenon as in the exciton or electron-hole pair luminescence of other MQW structures. The reduction of radiation intensity at distinct portion could be characterized by two activation energies related to different nonradiative recombination mechanisms. Although the origin of the activation energy at the intermediate temperature region

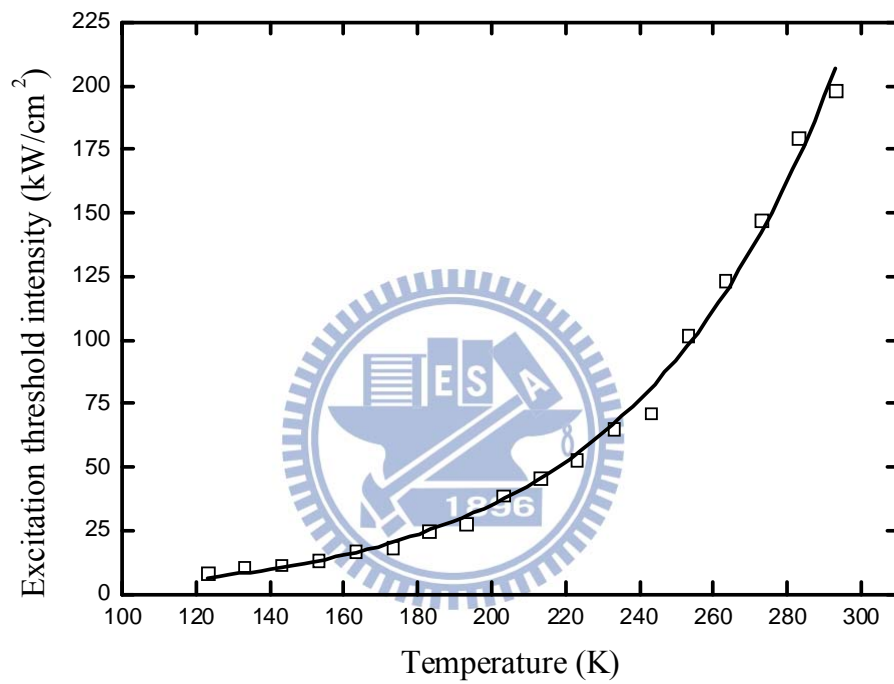
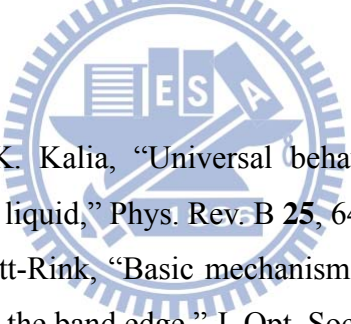


Fig. 2.3-6 Temperature dependence of the excitation threshold intensity of the EHP renormalized state emission.

which may be related to the dissociation of many-body state is still unclear, the decreasing PL intensity at high temperature is caused by thermally activated carrier leakage to the barrier state and, as a result, the nonradiative recombination process is strengthened. Because the activation energy of the thermal carrier emission has been reported to be equal to half of the total confined energy of electron and hole states, the half confined energy in our MQW sample found to be two thirds of the fitted activation energy confirms the gain enhancement of the periodically aligned MQW structure. At the end the excitation threshold of renormalized state is shown to be exponentially increased with increasing temperature. This result reveals the importance of the RPG structure in the MQW fabrication to the observation of the room-temperature spontaneous renormalized state emission.

Reference

- 
- [1] P. Vashishta and R. K. Kalia, "Universal behavior of exchange-correlation energy in electron-hole liquid," *Phys. Rev. B* **25**, 6492-6495 (1982).
 - [2] H. Haug and S. Schmitt-Rink, "Basic mechanisms of the optical nonlinearities of semiconductors near the band edge," *J. Opt. Soc. Am. B* **2**, 1135-1142 (1985).
 - [3] D. A. Kleinman and R. C. Miller, "Band-gap renormalization in semiconductor quantum wells containing carriers," *Phys. Rev. B* **32**, 2266-2272 (1985).
 - [4] G. Tränkle, H. Leier, A. Forchel, H. Haug, C. Ell, and G. Weimann, "Dimensionality dependence of the band-gap renormalization in two- and three-dimensional electron-hole plasmas in GaAs," *Phys. Rev. Lett.* **58**, 419-422 (1987).
 - [5] G. Tränkle, E. Lach, A. Forchel, F. Scholz, C. Ell, H. Haug, and G. Weimann, "General relation between band-gap renormalization and carrier density in two-dimensional electron-hole plasmas," *Phys. Rev. B* **36**, 6712-6714 (1987).
 - [6] E. Lach, A. Forchel, D. A. Broido, T. L. Reinecke, G. Weimann, and W. Schlapp, "Room-temperature emission of highly excited GaAs/Ga_{1-x}Al_xAs quantum wells," *Phys. Rev. B* **42**, 5395-5398 (1990).
 - [7] H. Q. Le, B. Lax, B. A. Vojak, and A. R. Calawa, "High-density excitonic state

- in two-dimensional multiple quantum wells,” *Phys. Rev. B* **32**, 1419-1422 (1985).
- [8] J. A. Levenson, I. Abram, R. Raj, G. Dolique, J. L. Oudar, and F. Alexandre, “Optical nonlinearities in multiple quantum wells: New insight on band-gap renormalization,” *Phys. Rev. B* **38**, 13443-13446 (1988).
- [9] R. Cingolani, K. Ploog, A. Cingolani, C. Moro, and M. Ferrara, “Radiative recombination processes of the many-body states in multiple quantum wells,” *Phys. Rev. B* **42**, 2893-2903 (1990).
- [10] R. Cingolani, H. Kalt, and K. Ploog, “Observation of transient band-gap renormalization in quantum wells,” *Phys. Rev. B* **42**, 7655-7658 (1990).
- [11] M. Kuznetsov, F. Hakimi, R. Sprague, and A. Mooradian, “High-power (> 0.5 W CW) diode-pumped vertical-external-cavity surface-emitting semiconductor lasers with circular TEM₀₀ beams,” *IEEE Photon. Technol. Lett.* **9**, 1063-1065 (1997).
- [12] B. Rudin, A. Rutz, M. Hoffmann, D. J. H. C. Maas, A.-R. Bellancourt, E. Gini, T. Südmeier, and U. Keller, “Highly efficient optically pumped vertical-emitting semiconductor laser with more than 20 W average output power in a fundamental transverse mode,” *Opt. Lett.* **33**, 2719-2721 (2008).
- [13] T.-L. Wang, Y. Kaneda, J. M. Yarborough, J. Harder, J. V. Moloney, A. Chernikov, S. Chatterjee, S. W. Koch, B. Kunert, and W. Stolz, “High-power optically pumped semiconductor laser at 1040 nm,” *IEEE Photon. Technol. Lett.* **22**, 661-663 (2010).
- [14] M. Y. A. Raja, S. R. J. Brueck, M. Osinski, C. F. Schaus, J. G. McInerney, T. M. Brennan, and B. E. Hammons, “Surface-emitting, multiple quantum well GaAs/AlGaAs laser with wavelength-resonant periodic gain medium,” *Appl. Phys. Lett.* **53**, 1678-1680 (1988).
- [15] S. W. Corzine, R. S. Geels, J. W. Scott, R.-H. Yan, and L. A. Coldren, “Design of Fabry-Perot surface-emitting lasers with a periodic gain structure,” *IEEE J. Quantum Electron.* **25**, 1513-1524 (1989).
- [16] E. O. Göbel, H. Jung, J. Kuhl, and K. Ploog, “Recombination enhancement due to carrier localization in quantum well structures,” *Phys. Rev. Lett.* **51**, 1588-1591 (1983).
- [17] D. S. Jiang, H. Jung, and K. Ploog, “Temperature dependence of

- photoluminescence from GaAs single and multiple quantum-well heterostructures grown by molecular-beam epitaxy,” *J. Appl. Phys.* **64**, 1371-1377 (1988).
- [18] D. Y. K. Ko and J. R. Sambles, “Scattering matrix method for propagation of radiation in stratified media: attenuated total reflection studies of liquid crystals,” *J. Opt. Soc. Am. A* **5**, 1863-1866 (1988).
- [19] Z. L. Liao, “Semiconductor wafer bonding via liquid capillarity,” *Appl. Phys. Lett.* **77**, 651-653 (2000).
- [20] D. Bimberg, M. Sondergeld, and E. Grobe, “Thermal dissociation of exciton bounds to neutral acceptors in high-purity GaAs,” *Phys. Rev. B* **4**, 3451-3455 (1971).
- [21] D. S. Jiang, H. Jung, and K. Ploog, “Temperature dependence of photoluminescence from GaAs single and multiple quantum-well heterostructures grown by molecular-beam epitaxy,” *J. Appl. Phys.* **64**, 1371-1377 (1988).
- [22] C. Y. Liu, S. Yuan, J. R. Dong, S. J. Chua, and M. C. Y. Chan, “Temperature-dependent photoluminescence of GaInP/AlGaInP multiple quantum well laser structure grown by metalorganic chemical vapor deposition with tertiarybutylarsine and tertiarybutylphosphine,” *J. Appl. Phys.* **94**, 2962-2967 (2003).
- [23] S. Weber, W. Limmer, K. Thonke, R. Sauer, K. Panzlaff, and G. Bacher, “Thermal carrier emission from a semiconductor quantum well,” *Phys. Rev. B* **52**, 14739-14747 (1995).
- [24] P. Micher, A. Hangleiter, M. Moser, M. Geiger, and F. Scholz, “Influence of barrier height on carrier lifetime in $\text{Ga}_{1-y}\text{In}_y\text{P}/(\text{Al}_x\text{Ga}_{1-x})_{1-y}\text{In}_y\text{P}$ single quantum wells,” *Phys. Rev. B* **46**, 7280-7283 (1992).

Chapter Three

High-Peak-Power and High-Repetition-Rate

1.2-1.6 μm Optically-Pumped Semiconductor

Lasers

3.1 Thermal management of the optically-pumped semiconductor lasers

The optically-pumped semiconductor lasers (OPSLs) introduced in [section 1.3](#) are capable of producing the high power, diffraction limited and single transverse mode beam output with the wide wavelength diversity. To achieve power scalability, the thermal management of the OPSLs should be efficient to prevent thermal degradation of the output performance under high pump power. The origin of thermal roll-over effect in OPSLs is mainly resulted from two factors. First, the cavity gain of the OPSLs is decided by the peak of the photo-luminescence (PL), micro-cavity resonance formed by the air-DBRs and air-cap layer interfaces and the resonant-periodic-gain structure. Under high power excitation, the quantum-wells (QWs) emission peak will red-shift at the rate three or four times faster than the later two issues in which the offset rates are determined by the optical thickness [1]. Consequently, the PL peak will deviate from the sub-cavity resonance and the assigned periodic gain structure and the output power will be lowered with increasing pump power. Second, the thermally-activated carriers in the QWs region will acquire additional kinetic energy to overcome the confined potential and escape away from the wells to barrier region. As a result, the nonradiative recombination process such as surface recombination or the Auger recombination will be enhanced under the large amount of thermal load. To prevent these thermal degradation mechanisms, the

efficient thermal management is required which will be elucidated in detail in the following.

The conventional pump approach of the OPSLs is exciting the carriers from the barrier regions and the excited carriers will relax to the QW region to provide the emission gain. The inherent quantum defect between the energy difference of the barrier and QW area is inevitable and leads to a large amount of heat. Recently, a novel optical pumping method in which the carriers are directly excited at the QW region and the thermal load resulted from the quantum defect is significantly lowered is demonstrated by Schmid *et al* [2]. This in-well pump scheme is of practical importance in the long wavelength OPSLs which have a large energy difference between the barrier potential height and the QW ground state confined energy [3,4]. The comparison between the barrier and in-well pump scheme under the same MQW fabrication but different pump absorption photon energy is also presented [3,5] and the schematic illustrations are shown in Fig. 3.1-1 (a) and (b).

Despite the reduction of the inherent heat generation, the effective heat dissipation method is more vital for power scalable OPSLs. There are two mostly used heat removal methods which are deployed in a variety of OPSLs successfully to date. One is the “substrate removal” technique in which the MQW gain mirror is fabricated in reverse order in comparison to the configuration depicted in Fig. 1.3-1. Under this so called “thin-device” method, an etch-stop layer is first grown on the substrate then the cap layer and the periodically aligned MQW structure are deposited in turn. At the end the top of the gain mirror is finished by packaging pairs of distributed Bragg reflector (DBR) structure on it. After the epitaxial growth, the gain chip is soldered on the diamond heat sink at the DBR side and substrate of the total composite is removed by chemical etching process to reduce the intra-cavity loss. The

total configuration is shown in Fig. 3.1-2 (a). Under this framework, the heat generated at the active region could be transmitted to the heat sink via the DBR stack with thickness of several of microns. As a comparison, the mirror-on-substrate configuration depicted in Fig. 1.3-1 with thickness of several tens to hundreds of microns contributes tremendous thermal impedance to the OPSLs. Several efficient OPSLs with output power higher than 5 W have been presented under substrate removal method [6-9]. But these lasers are concentrated on the spectral region around 1 μm with GaAs-based substrate system. It is because the mostly used GaAs/AlAs DBRs in GaAs-based system have good thermal conductivity and high refractive index difference. The DBRs at spectral range longer than 1 μm based on the InP substrate system suffers from low thermal conductivity and large number of pairs of DBR layers due to low refractive index difference and longer $\lambda/4$ length. This situation will give rise to high thermal impedance and pretty low heat dissipated efficiency. To conquer this dilemma, the so called “intracavity heat spreader” method has been demonstrated in optically-pumped edge-emitting [10,11] and surface-emitting [12-18] lasers. In this approach the gain chip is fabricated in the same direction as shown in Fig. 1.3-1 and an intra-cavity transparent plate with high thermal conductivity is liquid capillary bonded on the epitaxial side of MQWs. This intra-cavity element need to be transparent with low absorption and scattering and polarization loss to the pump and lasing emission and should have high thermal conductivity to bypass the heat from the substrate region [1,19-21]. Beside, the thickness of the heat spreader could be adjusted to complete single frequency operation or turning spectral range of the OPSLs [22,23]. Several materials such as sapphire, silicon carbide and diamond are applied as the heat spreader in the OPSLs [2,12-18,24]. However, the single crystal CVD diamond with thermal conductivity as high as $2000 \text{ Wm}^{-1}\text{K}^{-1}$ and controlled birefringence is mostly used to be the heat

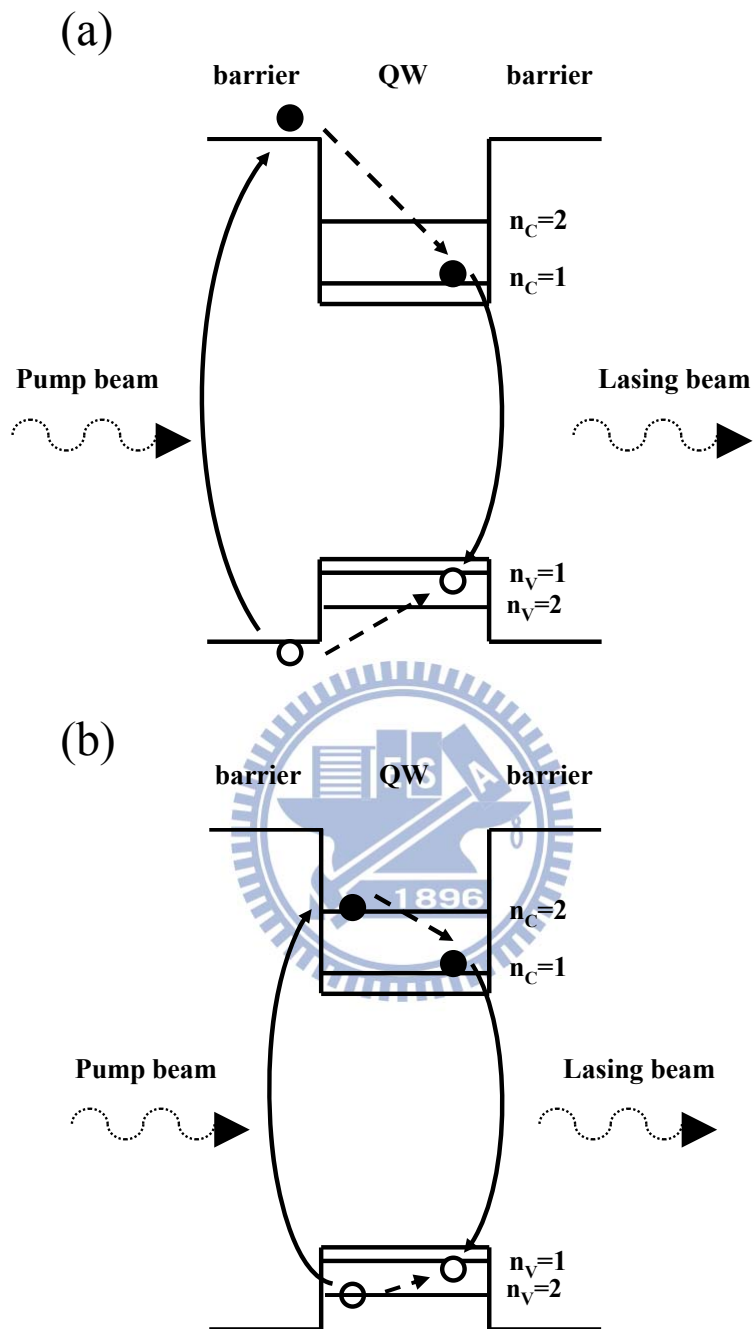


Fig. 3.1-1 The schematic illustrations of (a) barrier and (b) in-well pump configurations of MQWs.

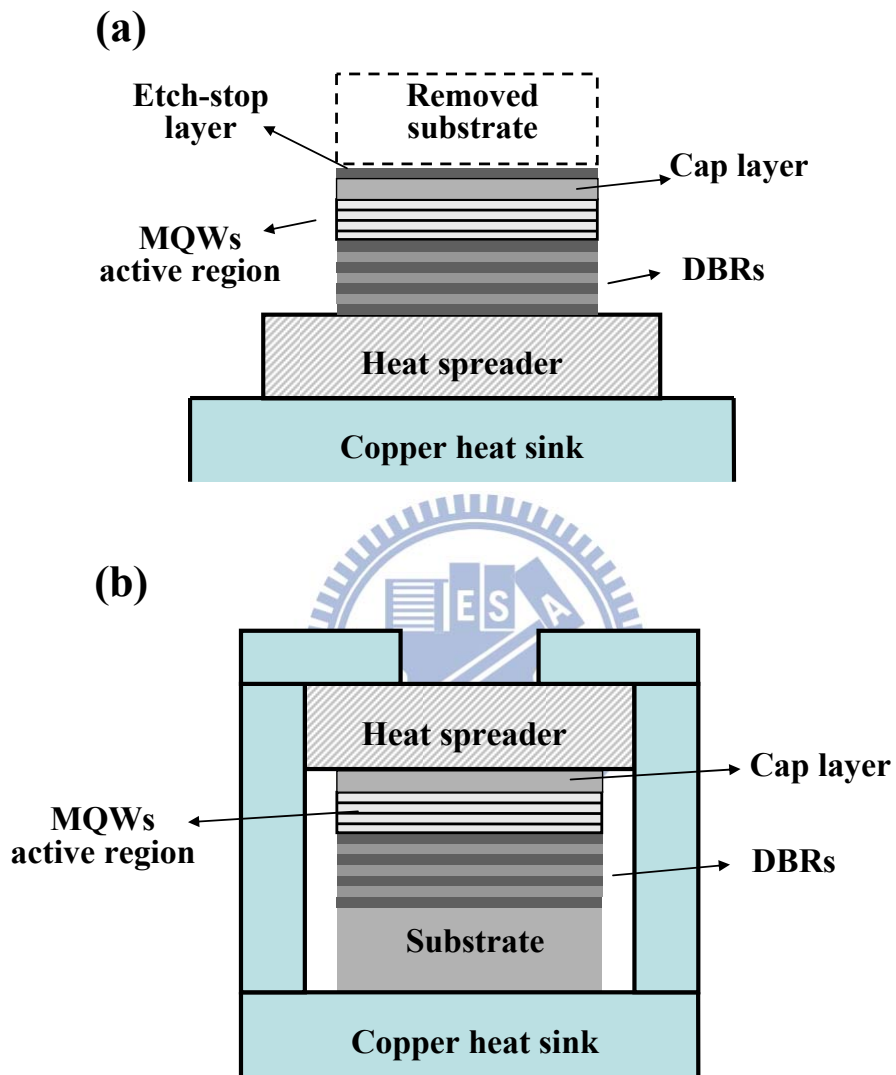


Fig. 3.1-2 The schematic configurations of the two thermal management using (a) thin-device and (b) intra-cavity heat spreader methods.

spreader to date. Many experimental and theoretical investigations have compared the performance of these two methods under different thermal conditions and pump-spot radius [1,20,25,26]. Although the highest output power record of the OPSLs is achieved using the thin device method at around 1 μm , the heat spreader method without post-processing and independent of the construction of DBRs is suitable for the heat dissipation in the OPSLs operated beyond 1 μm . The typical configuration of this heat dissipation method is depicted in Fig. 3.1-2 (b).

3.2 1220 nm AlGaInAs multiple-quantum-wells lasers

High-peak-power all-solid-state lasers operating at 1.14-1.25 μm are desirable for producing yellow-orange lights for many applications such as astronomy community, biomedical optics and laser absorption spectroscopy [27,28]. Light sources in this spectral range could be realized by Raman-shifted Nd- (Yb-) doped solid-state lasers or directly using the Yb- (Bi-) doped fiber lasers [29-31]. However, the performance of solid-state lasers is limited by the discrete energy level of the doped ions of the dielectrics. Alternatively, OPSLs have been developed to provide flexible choice of emission wavelength via bandgap engineering with scalable output power as mentioned in [second 1.3](#) and also offer a variety of advantages like broad gain curves and a low-divergence, circular and high quality nearly-diffraction-limited output beam [6-9,12-18,32,33]. So far, the lasers based on the quantum confined structure with GaAs material systems including InGaAs/GaAs and GaInNAs/GaAs have been demonstrated in the 1.14-1.25 μm spectral range under continuous-wave operation [15,16,34,35]. But these lasers are pumped by exciting the electrons from the barrier region and the quantum defect between pump and lasing photons leads to a large amount of heat. Recently, a novel method based on the in-well pumping scheme has been demonstrated to reduce the heat as described in [section 3.1](#). However, the

OPSLs at 1.14-1.25 μm based on the in-well pumping scheme have not been explored until now.

The quaternary alloys lattice matched to InP such as AlGaInAs and InGaAsP are employed in the semiconductor lasers in the near-infrared (NIR) spectral region. The AlGaInAs systems have been verified to have higher conduction band offset and better carrier confinement than the InGaAsP systems. This means that the resistance to heat of AlGaInAs based materials is stronger than InGaAsP. Several high-peak-power AlGaInAs OPSLs have been demonstrated in the NIR region driven by the actively Q-switched (AQS) solid-state lasers [5,36,37]. With the pulsed pumping operation, not only the heat generation is significantly reduced but the high-peak-power output is obtained. Because the pulse width of conventional AQS solid-state lasers depends on the pulse repetition rate and the average pump power. Consequently, it is difficult to optimize the output performance of the semiconductor disk lasers. Therefore, a light source with fixed pulse duration under various repetition rates can be a more suitable pump source for optimizing the performance of OPSLs. High-power pulsed fiber amplifiers are a light source to satisfy this requirement [38].

In this section, we present a high-peak-power AlGaInAs multiple-quantum-well (MQW) semiconductor laser grown on a Fe-doped InP transparent substrate and pumped by a 1.06 μm Yb-doped pulsed fiber amplifier. With in-well pumping, the thermal and roll-over effect could be reduced by lowering the quantum defect. We obtained an average output power of 810 mW at 1225 nm with slope efficiency up to 46.7 % to the average absorbed power in the single-chip scheme. The pump conditions of 60 kHz pulse repetition rate and 28 ns pulse width are used. To increase the average absorbed power, the double-chips scheme is used under the same pump conditions. The maximum average output power could be scaled up to 1.28 W with

slope efficiency of 37.5% at 1225 nm lasing wavelength. The maximum peak output power of 0.76 kW is obtained with 2.37 kW peak pump power.

3.2.1 Device fabrication and experimental setup

Figure 3.2-1 shows the experimental configuration of the AlGaInAs MQW 1220 nm semiconductor disk laser pumped by a SPI 1.06 μm Yb-doped master oscillator fiber amplifier. This pump source provides 9-200 ns pulse with repetition rate ranged from 10-500 kHz. Compared to the AQS solid-state laser, this laser module can provide fixed pulse width of output pulse even when the output power is changed. We controlled pump spot diameter to be about 800 μm to have efficient spatial overlap with the lasing mode. The gain region is composed of an AlGaInAs QW/barrier structure grown on a Fe-doped InP transparent substrate by metalorganic chemical-vapor deposition. It consisted of 30 groups of triple QWs spaced at half-wavelength intervals by AlGaInAs barrier layers as shown in the inset of Fig. 3.2-1. This is a resonant-periodic-gain structure that barrier layers are used to locate the quantum well region at the anti-node of the lasing field standing wave as discussed in section 1.3. Under this framework, the wavelength and optical gain are enhanced and the amplified spontaneous emission in the lateral direction and spatial hole burning effect are inhibited. A window layer of InP was deposited on the gain structure to prevent surface recombination and oxidation. In contrast to the conventional barrier pumping scheme, our gain medium is in-well pumped by a 1.06 μm Yb-doped pulsed fiber amplifier. This pumping scheme results in the low absorption (58%) but high conversion efficiency due to the short active region and the small quantum defect, respectively.

The InP based systems suffer from the lack of good distributed-Bragg-reflector (DBR) and have been challenging to transfer from edge-emitting lasers to

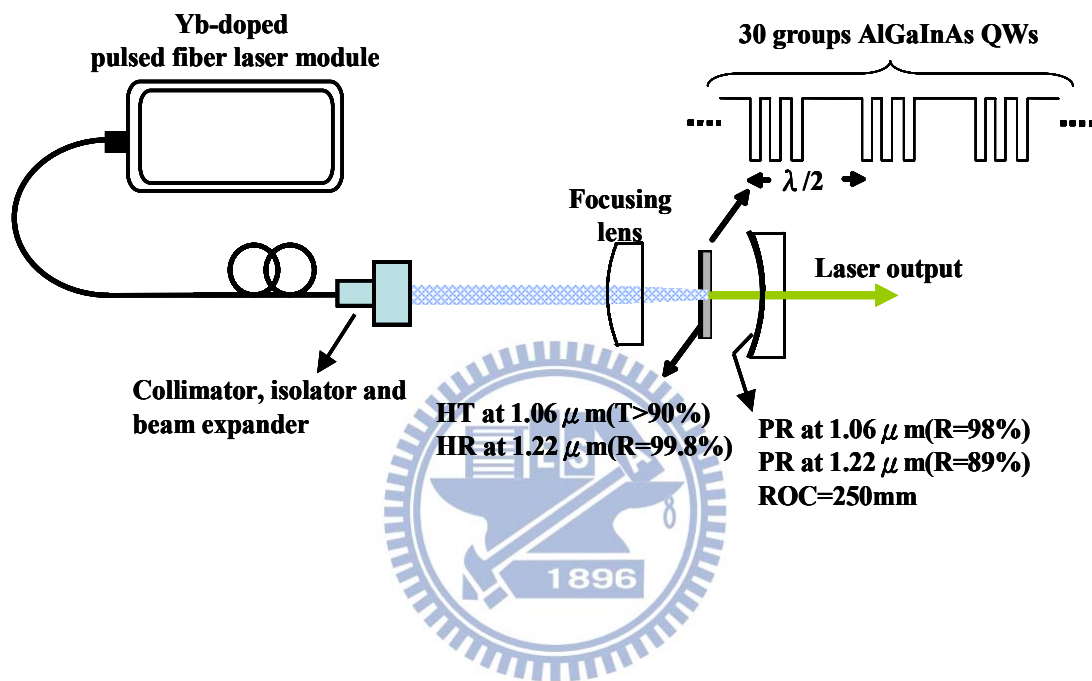


Fig. 3.2-1 Experimental configuration of AlGaInAs/InP semiconductor laser at 1220 nm pumped by a 1.06 μm Yb-doped pulsed fiber amplifier in the single chip scheme.

surface-emitting lasers. A number of lattice-matched DBRs such as AlGaInAs/AlInAs, AlGaInAs/InP, GaInAsP/InP, AlGaAsSb/AlAsSb and AlGaAsSb/InP have been demonstrated [39,40]. Unfortunately, these DBR systems suffer from the low refractive index contrast, low thermal conductivity or high complexity of growth. Therefore, Fe-doped InP with good transparency in the lasing wavelength is chosen as the substrate system instead of conventional S-doped InP with large absorption in the 1.0-2.0 μm spectral region. As a result, the function of DBRs could be replaced by an external mirror. In this configuration, the problem of fabrication of good DBRs has been resolved and the heat dissipation is improved by reducing the length of thermal conduction.

The laser gain medium is fabricated with dielectric coated mirror on the cap layer which is acted as a front mirror to simplify the device configuration. This forms high transmittance at 1.06 μm ($T > 90\%$) and high reflectance between 1.18-1.25 μm ($R > 99.8\%$) on the entrance face. We use an external mirror with radius of curvature of 250 mm and partial reflectance at 1.22 μm ($R = 89\%$) as output coupler. The overall cavity length is about 3 mm. With this plano-concave linear cavity, we could modulate the laser mode volume to have better efficiency. The gain medium is attached on a cooper heat sink with substrate side and is cooled down by water with temperature controlled to be 15 $^{\circ}\text{C}$.

3.2.2 Experimental results and discussions

Figure 3.2-2 shows the room temperature spontaneous-emission spectrum of AlGaInAs MQWs with dielectric coated mirror excited by the 1.06 μm Yb-doped pulsed fiber amplifier with average absorbed power of 0.38 W. The pump repetition rate is 60 kHz and the pump pulse width is 28 ns. This surface emitting photoluminescence (PL) spectrum is captured with the pump beam incident on the

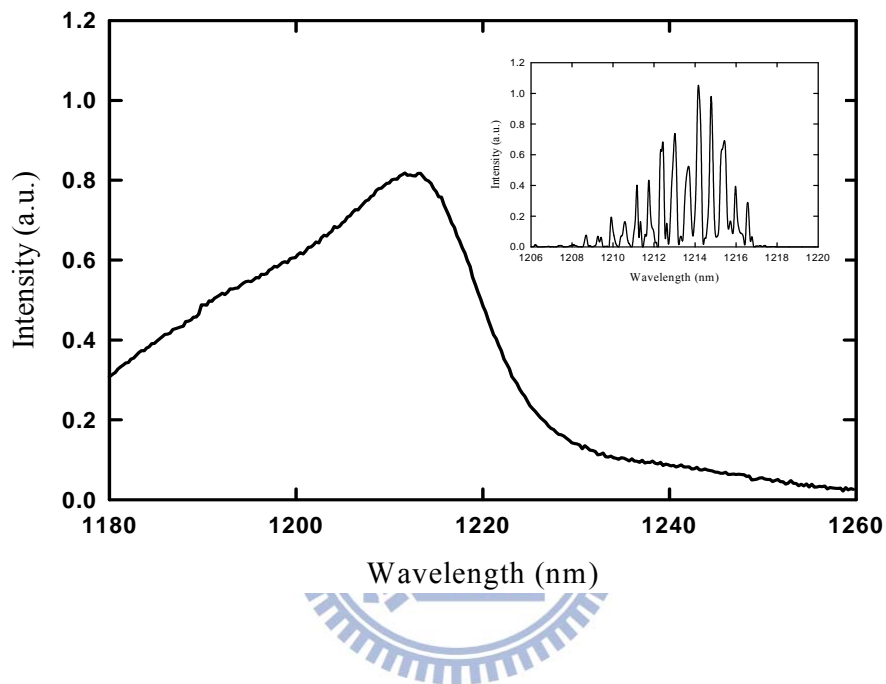


Fig. 3.2-2 Room temperature surface emitting spontaneous emission spectrum under 60 kHz pump repetition rate and 28 ns pump pulse width at average absorbed power of 0.38 W. Inset, the expanded lasing spectrum obtained with 0.85 W average absorbed power under the same pump conditions.

dielectric coated side, and the emitted light is collected into the multi-mode fiber on the other side. The spectral information was monitored by an optical spectrum analyzer (Advantest Q8381A) with a diffraction monochromator which can be used for high-speed measurement of pulsed light with a resolution of 0.1 nm. The PL peak is located at 1215 nm. The expanded lasing spectrum is shown in the inset of Fig. 3.2-2 at the average absorbed power of 0.85 W. The bandwidth of lasing spectrum is about 9 nm, and it comprises dense longitudinal modes due to the multiple interferences between the air-substrate interface and cavity mirrors. With increasing average pump power, the lasing spectrum will redshift due to the temperature induced shift of cavity resonance and MQW emission peak. In Fig. 3.2-3 the degree of redshift of peak lasing wavelength is shown as a function of average absorbed power. It will be shifted to 1225 nm at average absorbed power of 2.2 W as the roll-over effect happened.

Figure 3.2-4 shows the laser output performances with fixed pump pulse width of 28 ns and different pump repetition rates varied from 40-80 kHz. Under 40 kHz pump repetition rate, the average output power begins to saturate with absorbed power exceeded 2 W, i.e., the maximum allowed pump intensity is approximately 0.35 MW/cm². Since the saturation intensity of the MQW absorption was measured to be approximately 0.4 MW/cm², the power roll-over phenomenon at 40 kHz was attributed to the pump-saturation effect. On the other hand, the average output power at 80 kHz is also limited when the average absorbed power increased up to 2 W. This is mainly due to the local heating effect which is resulted from the high pump repetition rate. Consequently, the output performance at fixed pump pulse width of 28 ns can be optimized under 60 kHz pump repetition rate. The maximum average output power of 810 mW at 1225 nm is generated by the average absorbed power of 2 W.

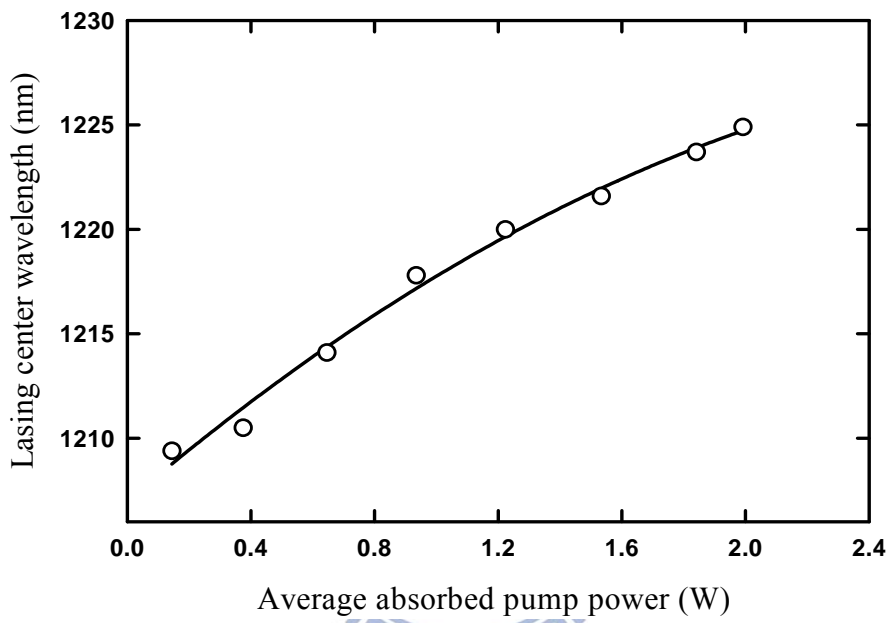


Fig. 3.2-3 Redshift of peak lasing wavelength as a function of average absorbed power under 60 kHz pump repetition rate and 28 ns pump pulse width.

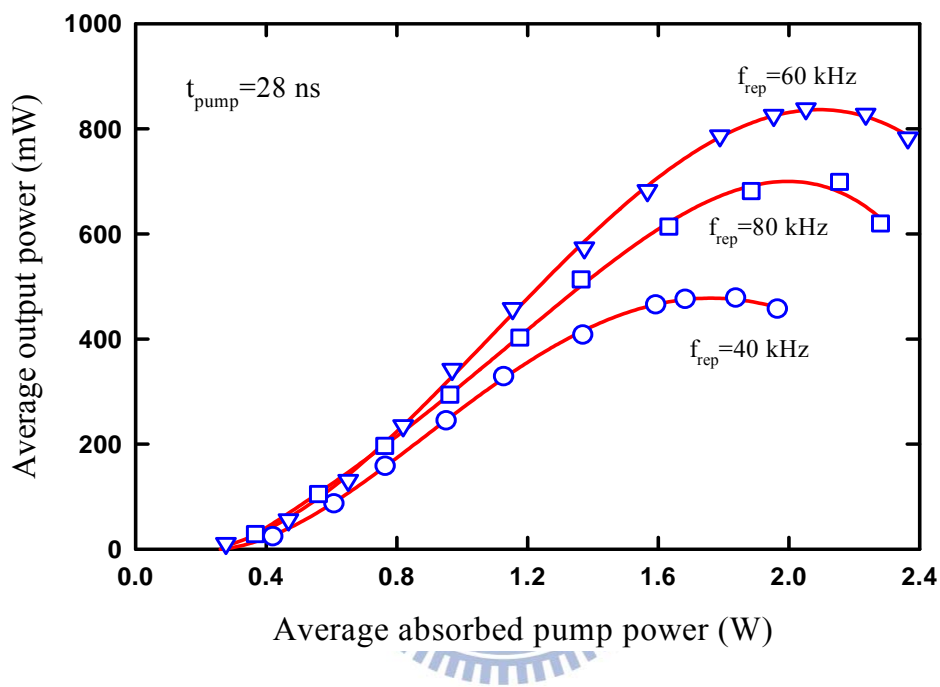


Fig. 3.2-4 Laser output performances at fixed pump pulse width of 28 ns and different pump repetition rates ranged from 40-80 kHz.

The slope efficiency to the average absorbed power is calculated to be 46.7%. The overall beam quality M^2 was found to be better than 1.3.

Figure 3.2-5 shows the laser output performance with fixed pump repetition rate of 60 kHz and different pump pulse width varied from 22-89 ns. For the given cavity and average absorbed power, the maximum average output power was limited using short pulse width which resulted in the pump-saturation effect [37]. When the pulse duration is long, the roll-over effect appeared due to the thermally induced carrier leakage. As a result, the best performance is obtained under 28 ns pump pulse width. The absorbed saturation intensity of 22 ns and 28 ns pump pulse width is calculated to be 0.3 MW/cm² and 0.24 MW/cm², respectively. The slightly lower saturation intensity of 28 ns pump pulse width is due to the larger amount of heat. By contrast, the maximum absorbed intensity of 89 ns pump pulse width is 0.07 MW/cm². This shows that the roll-over is mainly arisen from the considerable heat production with long pump pulse width. Moreover, the conversion efficiency is strongly affected by the thermal load before roll-over effect happens. Hence the slope efficiency is higher for lower pump pulse width under low average absorbed power.

With a LeCroy digital oscilloscope (Wave pro 7100, 10 G samples/s, 1 GHz bandwidth), the typical input and output pulse train as well as the extended pulse shape of single pulse are shown in Fig. 3.2-6. It can be seen that the output pulse shape tracked the input pulses with barely delayed turn-on time due to the in-well pump scheme [5]. And the pulse-to-pulse fluctuation was found to be within $\pm 5\%$, which is mainly attributed to the instability of the pump beam. To increase the average absorbed power of gain medium without the fabrication of more MQW, we insert another gain chip with the same MQW structure but without the dielectric coating and keep the same experimental setup as shown in Fig. 3.2-1. The absorption of

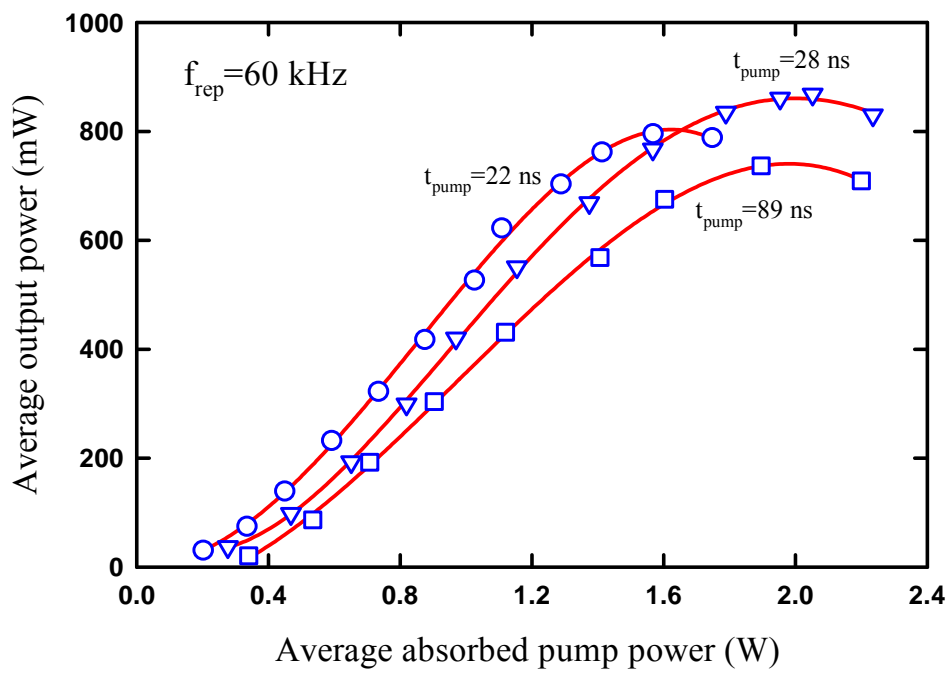


Fig. 3.2-5 Laser output performances under 60 kHz pump repetition rate with varied pump pulse width.

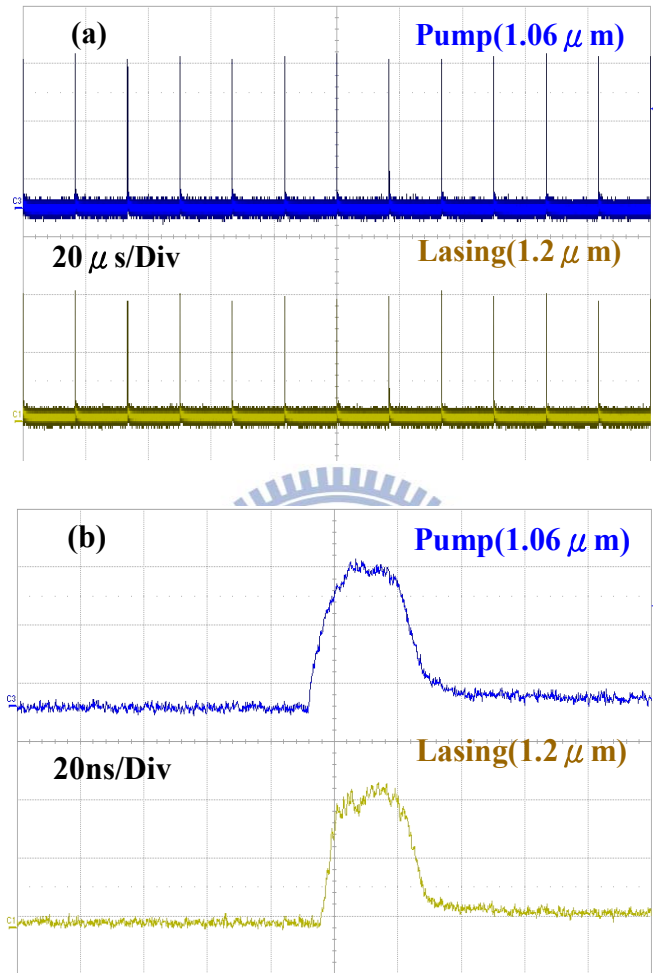


Fig. 3.2-6 (a) Typical oscilloscope trace of a train of pump and output pulses and (b) expanded shapes of a single pulse.

double-chips scheme (82%) is 1.41 times higher than the single-chip scheme (58%). The highest average absorbed power is increased to 4 W before the roll-over effect appeared. In this setup, the thermal load is distributed to the two chips. Figure 3.2-7 shows the output characteristic of double-chips scheme operated under 60 kHz pump repetition rate and 28 ns pump pulse width. The average output power could be scaled to 1.28 W with 4 W average absorbed power at 1225 nm. Although this method enhanced the absorption and dispersed the generated heat, the asynchronous PL emission due to the inhomogeneous heat distribution and the additional loss make the slope efficiency to be 37.5% which is lower than the single-chip scheme. With this setup, the peak output power is up to 0.76 kW at a peak pump power of 2.37 kW under the same pump conditions.

In summary, a high-peak-power semiconductor disk laser at 1.2 μm optically-pumped by the Yb-doped pulsed fiber amplifier has been presented. The gain medium is an AlGaInAs MQW structure grown on a Fe-doped InP substrate by metalorganic chemical-vapor deposition. With in-well pumping we could reduce the thermal and roll-over effect by lowering the quantum defect. The average output power of 810 mW at 1225 nm lasing wavelength is generated at an average absorbed power of 2 W under 60 kHz pump repetition rate and 28 ns pump pulse width in the single-chip scheme. With the double gain chips, the average output power could be scaled up to 1.28 W at an average absorbed power of 4 W. The peak output power of 0.76 kW is obtained with 2.37 kW peak pump power.

3.3 1520 nm AlGaInAs multiple-quantum-wells lasers

High-peak-power and high-repetition-rate laser sources have been in demand for the applications in the eye-safe wavelength regime beyond 1.44 μm such as free-space communication, gas sensing, spectroscopy, and medical treatment. The eye-safe laser

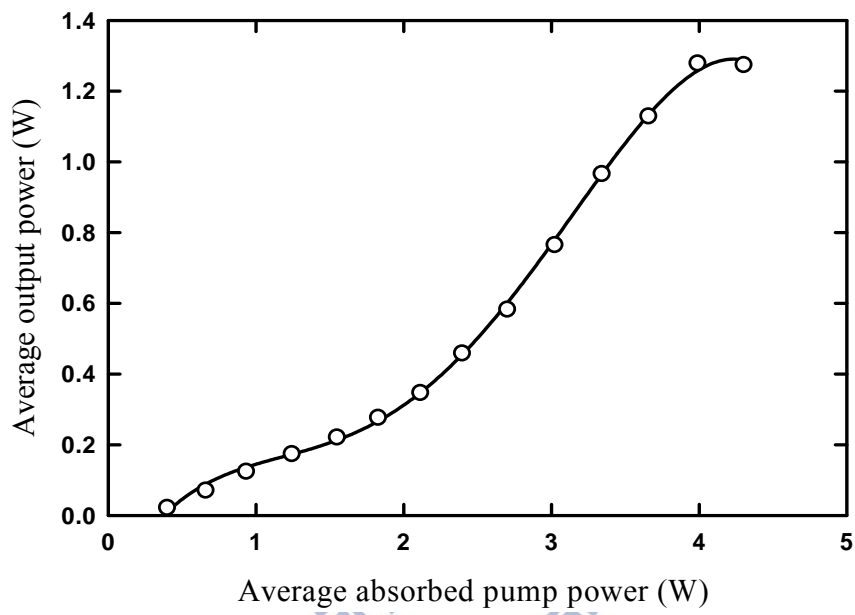


Fig. 3.2-7 Output performance with double gain chips at 60 kHz pump repetition rate and 28 ns pump pulse width.

sources can be realized in several ways including stimulated Raman scattering or optical parametric oscillation pumped by the high-peak-power Nd-doped lasers [41-47] and the solid state lasers directly use the Er^{3+} -doped or Cr^{4+} -doped gain media [48-51]. However, the spectral diversity of these lasers is restricted by the quantized energy level of the doped-dielectrics and the suitable nonlinear crystals.

Optically-pumped multiple-quantum-wells (MQWs) semiconductor disk lasers have been developed to provide low-divergence, circular and high quality nearly-diffraction-limited output beams with flexible choices of emission wavelengths via bandgap engineering as mentioned in [section 1.3](#). The quaternary alloys lattice matched to InP including InGaAsP and AlGaInAs are developed in the quantum confined structure of the semiconductor lasers for generating the radiation at the NIR region. Although the InGaAsP systems were commonly employed in the semiconductor lasers of the NIR region in the early stage, the AlGaInAs systems have been verified to have higher conduction band offsets and better carrier confinements. So far, the maximum average output power ever reported for the eye-safe laser based on the AlGaInAs material was found to be 2.6 W at the continuous-wave operation [52].

Recently, the AlGaInAs eye-safe pulsed laser was realized with an actively Q-switched 1.06- μm laser as a pump source [5,37] even under barrier or in-well pump scheme. However, the average output power and the pulse repetition rate were restricted to 0.52 W and 20 kHz, respectively, due to the poor heat dissipation from the pump area. Here we demonstrate, for the first time to our knowledge, on a high-repetition-rate (100-500 kHz) high-power optically pumped AlGaInAs nano-second eye-safe laser at 1525 nm with an intracavity diamond heat spreader to enhance the heat removal. We employ an Yb-doped pulsed fiber amplifier to be a

pump source for providing various pulse repetition rates with the same reason as in [Section 3.2](#). With a pump width of 28-ns at a repetition rate of 200 kHz, the average output power and peak output power under an average pump power of 13.3 W are found to be up to 3.12 W and 560 W, respectively. The maximum average power and peak power at a repetition rate 500 kHz are found to be 2.32 W and 170 W, respectively. The overall slope efficiency is maintained as high as 27.3% at a pulse repetition rate between 100 and 500 kHz.

3.3.1 Device fabrication and experimental setup

[Figure 3.3-1](#) shows the experimental configuration of the AlGaInAs MQW laser at the eye-safe region driven by a 1.06 μm Yb-doped pulsed fiber amplifier (SPI redENERGY G3). The pump source could be operated to provide consecutive pulses with the pulse duration in the range of 9-200 ns and the repetition rate ranging from 10-500 kHz. The pump spot diameter was controlled to be approximately $700\pm 20 \mu\text{m}$ to have a good spatial overlap with the lasing mode. The laser resonator was designed to be a linear plane-plane cavity which was stabilized by the thermally induced lens of the gain material. The flat mirror at the pump side was coated with anti-reflection coating at 1.06 μm ($R < 0.2\%$) at the entrance face and with high-reflection coating ($R > 99.8\%$) at 1.53 μm and high-transmission ($T > 95\%$) at 1.06 μm at the other face. The reflectivity of the flat output coupler was 70% at 1.53 μm . The overall cavity length is approximately 15 mm.

The gain structure is composed of 30 groups of triple QWs spaced at half-wavelength intervals by AlGaInAs barrier layers as shown in the inset of [Fig. 3.3-1](#). The thickness of the quantum wells are designed to be 8 nm. The resonant-periodic-gain (RPG) structure was designed to locate the QWs at the anti-nodes of the lasing field standing wave as discussed in [section 1.3](#). The periodic

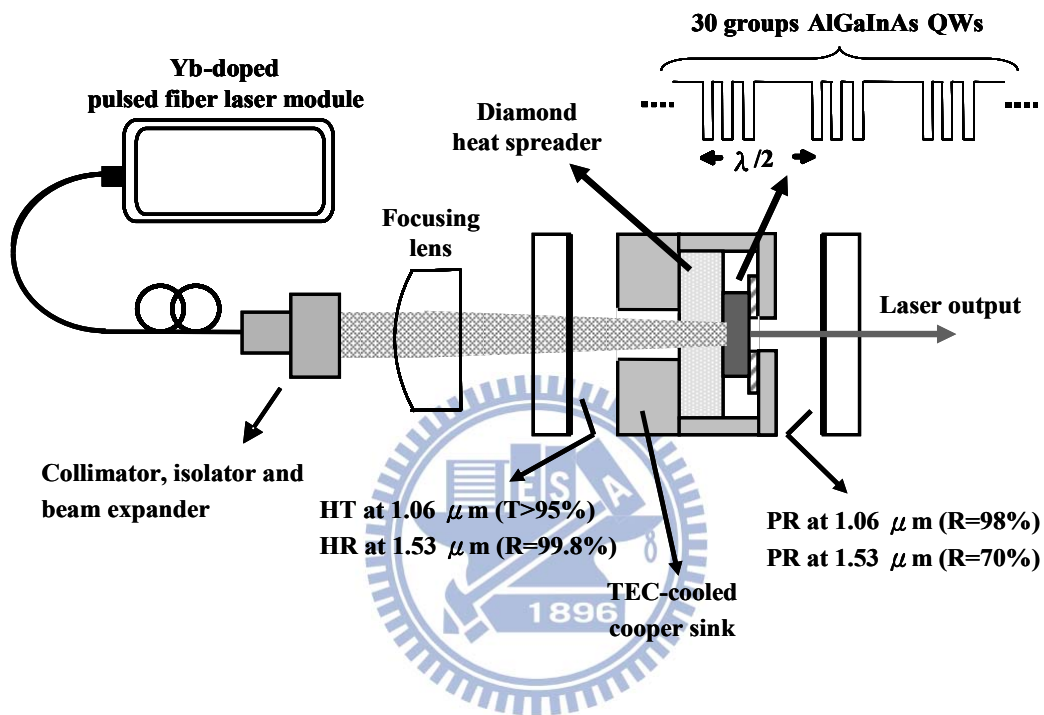


Fig. 3.3-1 Experimental setup of AlGaInAs eye-safe laser at 1525 nm with an intra-cavity diamond heat spreader and using an Yb-doped pulsed fiber amplifier as a pump source.

AlGaInAs QW/barrier layers were grown on a Fe-doped InP transparent substrate by metalorganic chemical-vapor deposition. The Fe-doped InP transparent substrate with high transmission at the pump and lasing wavelength is used to solve the problem of the lack of good distributed Bragg reflectors (DBRs) for the InP-based systems. The function of conventional DBRs was replaced with an external reflective mirror. A window layer of InP was deposited on the gain structure to prevent surface recombination and oxidation. In contrast to the conventional barrier pumping scheme, the present gain medium was designed to be suitable for in-well pumping to enhance the quantum efficiency as mentioned in [section 3.1](#). It has been confirmed that the slope efficiency with the in-well pumping scheme was significantly higher than that with the barrier pumping scheme [\[5\]](#). In the experiment, the single-pass absorption of this gain chip is 81-84% for repetition rate ranged from 30-500 kHz under 28 ns pump pulse width.

Based on the intra-cavity heat spreader method discussed in [section 3.1](#), a 4.5-mm square, 0.5-mm thick piece of uncoated single crystal diamond heat spreader was bonded to the MQW side of the cleaved 2.5-mm square piece of the gain chip to improve the heat removal. Although the heat spreader approach has been used in a variety of high power optically pumped semiconductor lasers [\[12-18\]](#), to the best of our knowledge, the diamond heat spreader is for the first time to be applied to the transparent semiconductor gain medium. The other side of the diamond was in contact with a copper heat sink which was cooled by a thermal-electric cooler (TEC), where the temperature was maintained at 15 °C. The substrate side of the gain chip was attached tightly to a copper plate with a hole of 2-mm diameter, where an indium foil was employed to be the contact interface. The contact uniformity was further confirmed by inspecting the interference fringe coming from the minute gap between

the gain chip and the diamond heat spreader. The package configuration of the gain medium can be seen in [Fig. 3.3-1](#).

3.3.2 Experimental results and discussions

We fixed the duration of pump pulses to be 28 ns for making a detailed comparison at different pulse repetition rates. The spectral information was monitored by an optical spectrum analyzer (Advantest Q8381A) with a diffraction monochromator which could be used for the high-speed measurement of pulsed light with a resolution of 0.1 nm. [Figure 3.3-2](#) shows the room temperature spontaneous-emission spectrum of AlGaInAs MQWs pumped with an average absorbed power of 0.8 W at a pulse repetition rate of 100 kHz. It can be seen that the photoluminescence peak at a low pump power was approximately at 1500 nm.

To investigate the losses introduced by the intracavity diamond heat spreader, we make a comparison between the performance of the AlGaInAs eye-safe laser without and with the diamond at the repetition rate of 30 kHz, as shown in [Fig. 3.3-3](#). Note that the thermal effect at the repetition rate of 30 kHz is not significant for the absorbed pump power less than 2 W. It can be seen that the output power without the heat spreader displays a thermally induced roll-over effect for the average absorbed power higher than 2.3 W. In contrast, the slope efficiency obtained with the heat spreader can remain nearly constant for the absorbed pump power up to the maximum pump power of 3.3 W, where the maximum pump power is just limited by the pump source at the repetition rate of 30 kHz. This result confirms the improvement of the power scalability by use of the diamond heat spreader. On the other hand, the slope efficiencies obtained without and with the heat spreader can be found to be 33% and 28%, respectively. With these slope efficiencies and the output reflectivity of 70%, the losses introduced by the heat spreader can be estimated to be 7.5%. Even though there

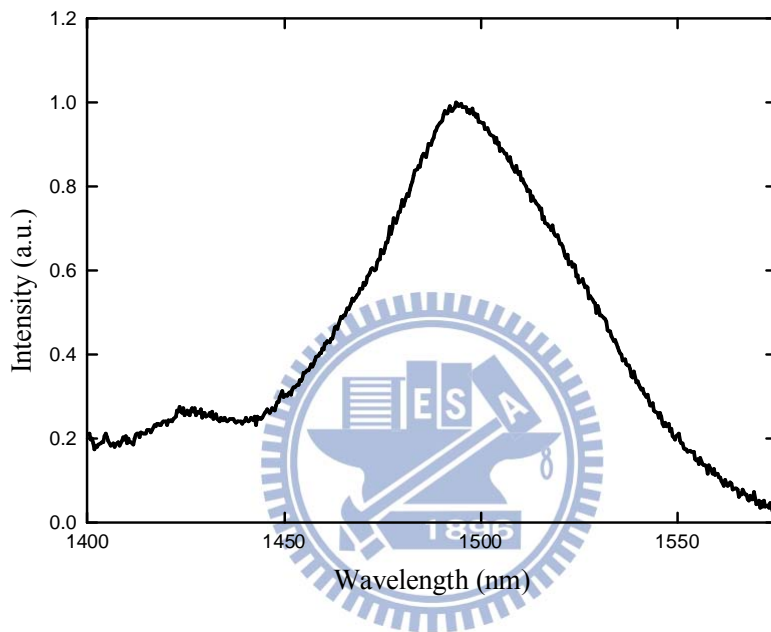


Fig. 3.3-2 Room temperature surface emitting spontaneous emission spectrum under a 100-kHz pump repetition rate at an average absorbed power of 0.8 W.

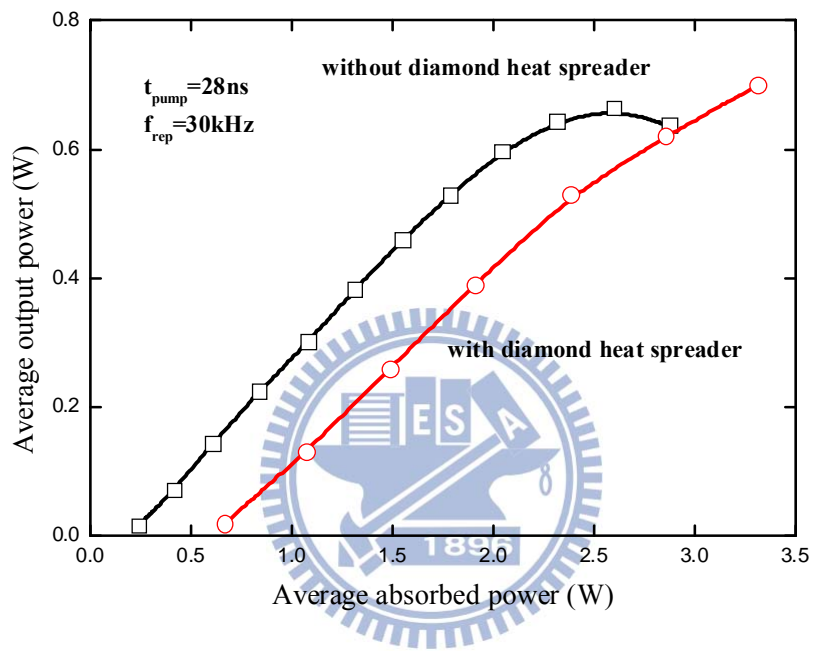


Fig. 3.3-3 Output performances of the eye-safe laser without and with the diamond heat spreader at a 30-kHz repetition rate.

is a room for improving the introduced losses, the diamond heat spreader can extend the operation frequency up to 500 kHz, as shown in the following results.

Figures 3.3-4 (a) and (b) show the output performances without and with the diamond heat spreader, respectively, for the repetition rate in the range of 100- to 500-kHz. The maximum average output powers without the heat spreader can be seen to decrease from 0.45 W down to 0.11 W for the repetition rate increasing from 100 kHz to 500 kHz. On the other hand, the average output powers with the heat spreader can be almost maintained linear for the absorbed pump power reaching the maximum value of 13.3 W at the repetition rate within the range of 200-500 kHz. The overall beam quality M^2 was found to be better than 1.3. The maximum average output powers can be found to be up to 3.12 W and 2.32 W for the repetition rates of 200 kHz and 500 kHz, respectively. The roll-over phenomenon observed in Fig. 3.3-4 (b) for the case of 100 kHz was attributed to the pump-saturation effect. With an absorbed pump power of 10 W and a pump diameter of 700 μm , the pump intensity for the pump duration of 28 ns at 100 kHz could be calculated to be $0.93 \text{ MW}/\text{cm}^2$. Since the saturation intensity of the MQW absorption was measured to be approximately within $0.8\text{-}1.0 \text{ MW}/\text{cm}^2$, the power roll-over phenomenon at 100 kHz was considered to come from the pump-saturation effect.

Figure 3.3-5 (a) depicts the lasing spectrum with the heat spreader under an average absorbed power of 2.5 W at a repetition rate of 100 kHz. The lasing spectrum can be seen to comprise dense longitudinal modes with the bandwidth to be approximately 10 nm and the center wavelength to be located at 1515 nm. With increasing the average absorbed power, the center wavelength has significant redshifts due to the pump power induced the local heating on the gain medium. Figure 3.3-5 (b) shows the dependence of the red-shift on the absorbed pump power for the laser

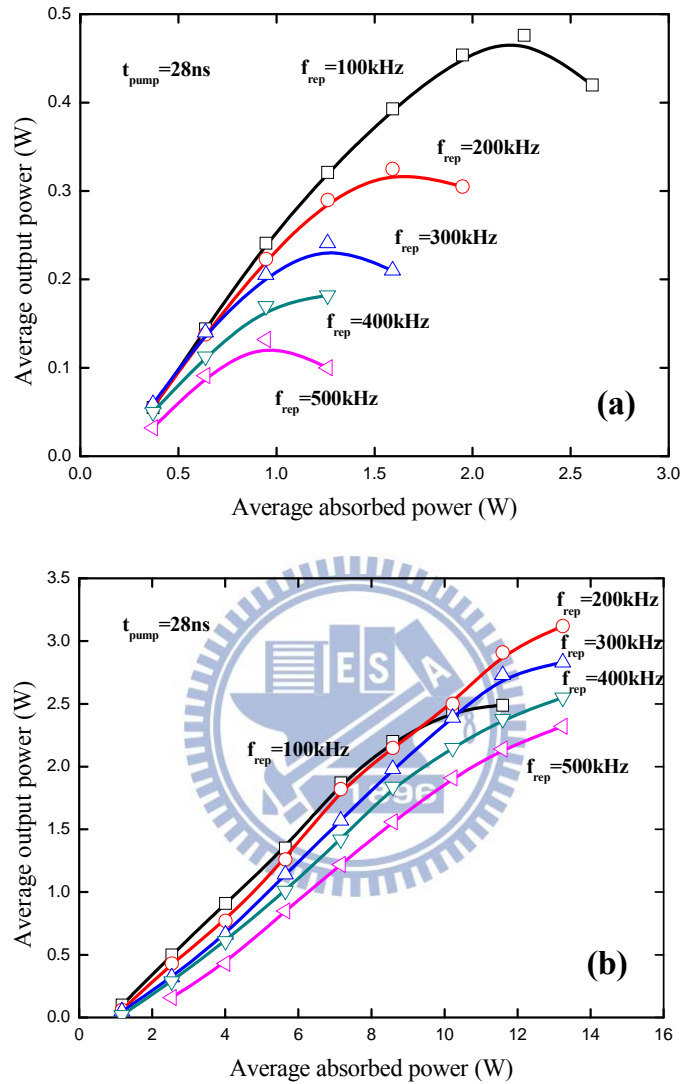


Fig. 3.3-4 Output performances without (a) and with (b) the diamond heat spreader for repetition rates in the range of 100-500 kHz.

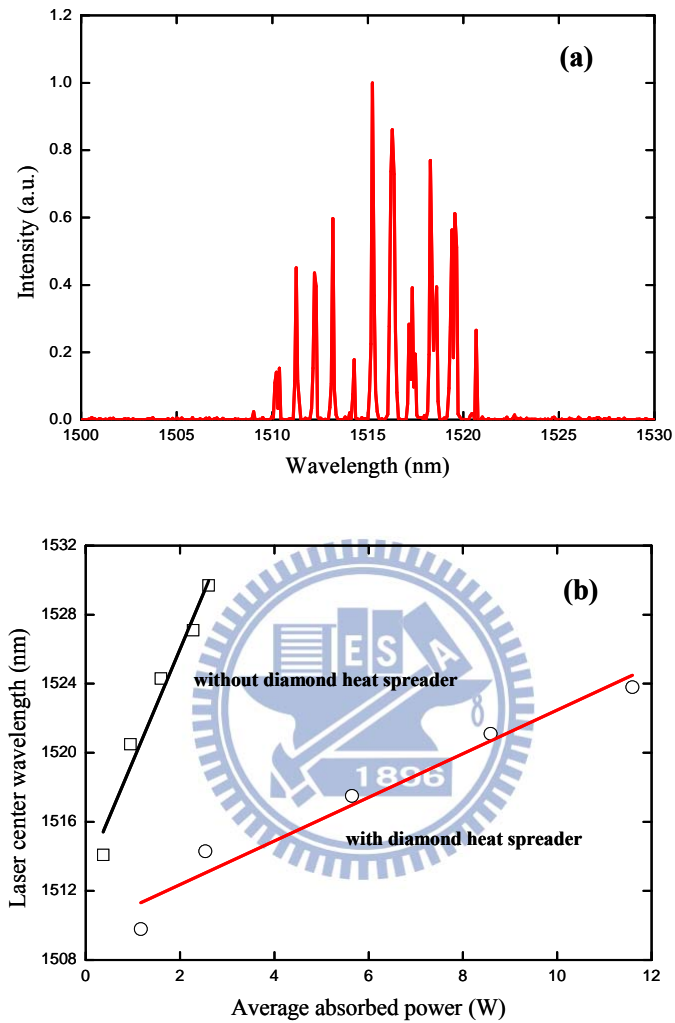


Fig. 3.3-5 (a) Lasing spectrum with the heat spreader under an average absorbed power of 2.5 W at a repetition rate of 100 kHz. (b) Dependence of the red-shift on the absorbed pump power for the laser operation without and with the heat spreader at a repetition rate of 100 kHz.

operation without and with the heat spreader at a repetition rate of 100 kHz. It can be seen that the redshift measured for the laser without using the heat spreader is considerably larger than the result with the heat spreader. This substantial difference also confirms the local heating to be considerably improved by use of the diamond heat spreader.

The temporal behavior of the laser output was recorded with a LeCroy digital oscilloscope (Wave pro 7100, 10 G samples/s, 1 GHz bandwidth). [Figure 3.3-6](#) shows the input and output pulse trains as well as the extended pulse shape of the single pulse for the result obtained with an average absorbed power of 2.5 W at a repetition rate of 200 kHz. It can be seen that the time delay of the output pulse with respect to the input pulse is generally less than a few nanoseconds. The characteristics of the small delay comes from the advantage of the in-well pumping scheme. The peak-to-peak instability was experimentally found to arise from the instability of the pump beam. On the whole, the peak-to-peak fluctuation was generally within $\pm 5\%$.

In summary, we have demonstrated a high-repetition-rate (>100 kHz) nanosecond eye-safe AlGaInAs laser at 1525 nm with an Yb-doped pulsed fiber amplifier as a pump source. A diamond heat spreader bonded to the gain chip was employed to reach an efficient heat removal. With a pump power of 13.3 W, the maximum average output powers at the repetition rates of 200 kHz and 500 kHz were found to be up to 3.12 W and 2.32 W, respectively. Correspondingly, the maximum peak powers at the repetition rates of 200 kHz and 500 kHz are 560 W and 170 W, respectively. To the best of our knowledge, this is the highest frequency achieved in the pulsed eye-safe lasers with the average output powers higher than 2 W.

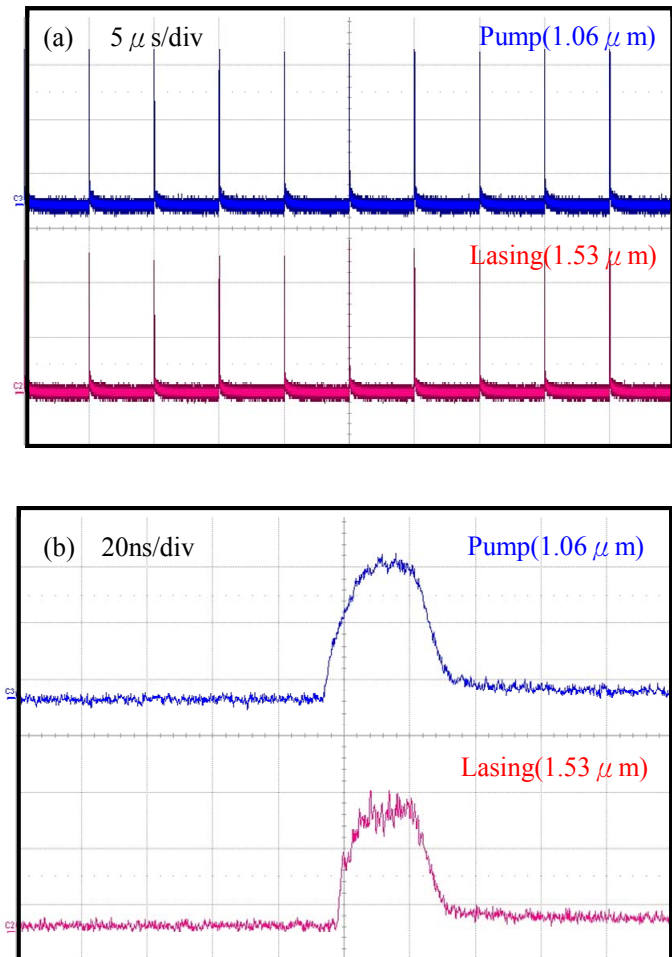


Fig. 3.3-6 (a) Oscilloscope trace of a train of pump and output pulses obtained with an average absorbed power of 2.5 W at a repetition rate of 200 kHz. (b) Expanded shapes of a single pulse.

3.4 Conclusions

In this chapter, an AlGaInAs multiple quantum well structure is first presented as an effective gain medium of the in-well pumped high-peak-power semiconductor disk laser at 1220 nm. This spectral region is in demand as the pump source in the nonlinear frequency conversion to produce yellow-orange light. We use an Yb-doped pulsed fiber amplifier as the pump source to effectively optimize the output characteristics. The maximum average output power of 1.28 W and peak output power of 0.76 kW is obtained at 1225 nm lasing wavelength under 60 kHz pump repetition rate and 28 ns pump pulse width in use of the double gain chip. In the second part we report on a compact efficient high-repetition-rate (>100 kHz) optically pumped AlGaInAs nano-second eye-safe laser at 1525 nm. A diamond heat spreader bonded to the gain chip is employed to improve the heat removal. At a pump power of 13.3 W, the average output power at a repetition rate 200 kHz is up to 3.12 W, corresponding to a peak output power of 560 W. At a repetition rate 500 kHz, the maximum average power and peak power are found to be 2.32 W and 170 W, respectively. Demonstration of these high peak power and high repetition rate OPSLs confirms the efficiency of the realization of gain-switched lasers with the semiconductor MQWs as the gain-switched medium. The detailed introductions of the gain-switched lasers will be brought up in [section 3.1](#).

Reference

- [1] A. J. Maclean, R. B. Birch, P. W. Roth, A. J. Kemp, and D. Burns, "Limits on efficiency and power scaling in semiconductor disk lasers with diamond heatspreaders," *J. Opt. Soc. Am. B* **26**, 2228-2236 (2009).
- [2] M. Schmid, S. Benchabane, F. Torabi-Goudarzi, R. Abram, A. I. Ferguson, and E. Riis, "Optical in-well pumping of a vertical-external-cavity surface-emitting laser," *Appl. Phys. Lett.* **84**, 4860-4862 (2004).

- [3] J. Wagner, N. Schulz, M. Rattunde, C. Ritzenthaler, C. Manz, C. Wild, and K. Köhler, "Barrier- and in-well pumped GaSb-based 2.3 μm VECSELs," *Phys. Stat. Sol. (c)* **4**, 1597-1600 (2007).
- [4] N. Schulz, B. Rösener, R. Moser, M. Rattunde, C. Manz, K. Köhler, and J. Wagner, "An improved active region concept for highly efficient GaSb-based optically in-well pumped vertical-external-cavity surface-emitting lasers," *Appl. Phys. Lett.* **93**, 181113 1-3 (2008).
- [5] H. L. Chang, S. C. Huang, Yi-Fan Chen, K. W. Su, Y. F. Chen, and K. F. Huang, "Efficient high-peak-power AlGaInAs eye-safe wavelength disk laser with optical in-well pumping," *Opt. Express* **17**, 11409-11414 (2009).
- [6] S. Lutgen, T. Albrecht, P. Brick, W. Reill, J. Luft, and W. Späth, "8-W high-efficiency continuous-wave semiconductor disk laser at 1000 nm," *Appl. Phys. Lett.* **82**, 3620-3622 (2003).
- [7] J. H. Lee, J. Y. Kim, S. M. Lee, J. R. Yoo, K. S. Kim, S. H. Cho, S. J. Lim, G. B. Kim, S. M. Hwang, T. Kim, and Y. J. Park, "9.1-W high-efficient continuous-wave end-pumped vertical-external-cavity surface-emitting semiconductor laser," *IEEE Photon. Tech. Lett.* **18**, 2117-2119 (2006).
- [8] B. Rudin, A. Rutz, M. Hoffmann, D. J. H. C. Maas, A.-R. Bellancourt, E. Gini, T. Südmeyer, and U. Keller, "Highly efficient optically pumped vertical-emitting semiconductor laser with more than 20 W average output power in a fundamental transverse mode," *Opt. Lett.* **33**, 2719-2721 (2008).
- [9] T.-L. Wang, Y. Kaneda, J. M. Yarborough, J. Hader, J. V. Moloney, A. Chernikov, S. Chatterjee, S. W. Koch, B. Kunert, and W. Stolz, "High-power optically pumped semiconductor laser at 1040 nm," *IEEE Photon. Tech. Lett.* **22**, 661-663 (2012).
- [10] W. W. Bewley, C. L. Felix, I. Vurgaftman, D. W. Stokes, E. H. Aifer, L. J. Olafsen, J. R. Meyer, M. J. Yang, B. V. Shanabrook, H. Lee, R. U. Martinelli, and A. R. Sugg, "High-temperature continuous-wave 3-6.1 μm "W" lasers with diamond-pressure-bond heat sinking," *Appl. Phys. Lett.* **74**, 1075-1077 (1999).
- [11] W. W. Bewley, C. L. Felix, E. H. Aifer, D. W. Stokes, I. Vurgaftman, L. J. Olafsen, J. R. Meyer, M. J. Yang, and H. Lee, "Thermal characterization of diamond-pressure-bond heat sinking for optically pumped mid-infrared lasers," *IEEE J. Quantum Electron.* **35**, 1597-1601 (1999).
- [12] W. J. Alford, T. D. Raymond, and A. A. Allerman, "High power and good beam

- quality at 980 nm from a vertical external-cavity surface-emitting laser,” *J. Opt. Soc. Am. B* **19**, 663-666 (2002).
- [13] J. E. Hastie, J. M. Hopkins, S. Calvez, C. W. Jeon, D. Burns, R. Abram, E. Riis, A. I. Ferguson, and M. D. Dawson, “0.5-W single transverse-mode operation of an 850-nm diode-pumped surface-emitting semiconductor laser,” *IEEE Photon. Technol. Lett.* **15**, 894-896 (2003).
- [14] A. Härkönen, S. Suomalainen, E. Saarinen, L. Orsila, R. Koskinen, O. Okhotnikov, S. Calvez, and M. Dawson, “4 W single-transverse mode VECSEL utilizing intra-cavity diamond heat spreader,” *Electron. Lett.* **42**, 693-694 (2006).
- [15] V.-M. Korpijärvi, T. Leinonen, J. Puustinen, A. Härkönen, and M. D. Guina, “11 W single gain-chip dilute nitride disk laser emitting around 1180 nm,” *Opt. Express* **18**, 25633-25641 (2010).
- [16] J. Rautiainen, I. Krestnikov, M. Butkus, E. U. Rafailov, and O. G. Okhotnikov, “Optically pumped semiconductor quantum dot disk laser operating at 1180 nm,” *Opt. Lett.* **35**, 694-696 (2010).
- [17] J.-M. Hopkins, S. A. Smith, C. W. Jeon, H. D. Sun, D. Burns, S. Calvez, M. D. Dawson, T. Jouhti, and M. Pessa, “0.6 W CW GaInNAs vertical external-cavity surface emitting laser operating at 1.32 μm ” *Electron. Lett.* **40**, 30-31 (2004).
- [18] H. Lindberg, A. Strassner, E. Gerster, and A. Larsson, “0.8 W optically pumped vertical external cavity surface emitting laser operating CW at 1550 nm,” *Electron. Lett.* **40**, 601-602 (2004).
- [19] S. Calvez, J. E. Hastie, M. Guina, O. G. Okhotnic]kov, and M. D. Dawson, “Semiconductor disk lasers for the generation of visible and ultraviolet radiation,” *Laser & Photon. Rev.* **3**, 407-434 (2009).
- [20] A. J. Kemp, G. J. Valentine, J.-M. Hopkins, J. E. Hastie, S. A. Smith, S. Calvez, M. D. Dawson, and D. Burns, “Thermal management in vertical-external- cavity surface-emitting lasers: Finite-element analysis of a heatspreader approach,” *IEEE J. Quantum Electron.* **41**, 148-155 (2005).
- [21] A. Chernikov, J. Herrmann, M. Koch, B. Kunert, W. Stolz, S. Chatterjee, S. W. Koch, T.-L. Wang, Y. Kaneda, J. M. Yarborough, J. Harder, and J. V. Moloney, “Heat management in high-power vertical-external-cavity surface-emitting laser,” *IEEE J. Sel. Top. Quantum Electron.* **17**, 1772-1778 (2011).

- [22] A. J. Maclean, A. J. Kemp, S. Calvez, J.-Y. Kim, T. Kim, M. D. Dawson, and D. Burns, "Continuous tuning and efficient intracavity second-harmonic generation in a semiconductor disk laser with an intracavity diamond heatspreader," *IEEE J. Quantum Electron.* **44**, 216-225 (2008).
- [23] H. Lindberg, M. Strassner, and A. Larsson, "Improved spectral properties of an optically pumped semiconductor disk laser using a thin diamond heat spreader as an intracavity filter," *IEEE Photon. Tech. Lett.* **17**, 1363-1365 (2005).
- [24] J. E. Hastie, J.-M. Hopkins, S. Calvez, D. Burns, M. D. Dawson, R. Abram, E. Riis, A. I. Ferguson, W. J. Alford, T. D. Raymond, and A. A. Allerman, "Microchip vertical external cavity surface emitting lasers," *Electron. Lett.* **39**, 1324-1326 (2003).
- [25] S. Giet, A. J. Kemp, D. Burns, S. Calvez, M. D. Dawson, S. Suomalainen, A. Härkönen, M. Guina, O. Okhotnikov, and M. Pessa "Comparison of thermal management techniques for semiconductor disk lasers," *Proc. SPIE* **6871**, 687115 1-10 (2008).
- [26] A. J. Maclean, A. J. Kemp, S. Calvez, J. Y. Kim, T. Kim, M. D. Dawson, and D. Burns, "Continuous tuning and efficient intracavity second-harmonic generation in a semiconductor disk laser with an intracavity diamond heatspreader," *IEEE J. Quantum Electron.* **44**, 216-225 (2008).
- [27] R. Q. Fugate, D. L. Fried, G. A. Ameer, B. R. Boeke, S. L. Browne, P. H. Roberts, R. E. Ruane, G. A. Tyler, and L. M. Wopat, "Measurement of atmospheric wavefront distortion using scattered light from a laser guide-star," *Nature* **353**, 144-146 (1991).
- [28] A. D. Singh, M. Nouri, C. L. Shields, J. A. Shields, and N. Perez, "Treatment of retinal capillary hemangioma," *Ophthalmology* **109**, 1799-1806 (2002).
- [29] H. M. Pask and J. A. Piper, "Efficient all-solid-state yellow laser source producing 1.2-W average power," *Opt. Lett.* **24**, 1490-1492 (1999).
- [30] A. Shirakawa, H. Maruyama, K. Ueda, C. B. Olausson, J. K. Lyngso, and J. Broeng, "High-power Yb-doped photonic bandgap fiber amplifier at 1150-1200 nm," *Opt. Express* **17**, 447-454 (2009).
- [31] E. M. Dianov, A. V. Shubin, M. A. Melkumov, O. I. Medvedkov, and I. A. Bufetov, "High-power cw bismuth-fiber lasers," *J. Opt. Soc. Am B* **24**, 1749-1755 (2007).
- [32] A. C. Tropper, H. D. Foreman, A. Garnache, K. G. Wilcox, and S. H. Hoogland,

- “Vertical-external-cavity semiconductor lasers,” *J. Phys. D* **37**, R75-R85 (2004).
- [33] L. Fan, M. Fallahi, J. T. Murray, R. Bedford, Y. Kaneda, J. Harder, A. R. Zakharian, J. V. Moloney, S. W. Koch, and W. Stolz, “Tunable high-power high-brightness linearly polarized vertical-external-cavity surface-emitting lasers,” *Appl. Phys. Lett.* **88**, 021105 1-3 (2006).
- [34] L. Fan, C. Hessenius, M. Fallahi, J. Harder, H. Li, J. V. Moloney, W. Stolz, S. W. Koch, J. T. Murray, and R. Bedford, “Highly strained InGaAs/GaAs multiwatt vertical-external-cavity surface-emitting laser emitting around 1170 nm,” *Appl. Phys. Lett.* **91**, 131114 1-3 (2007).
- [35] V.-M. Korpijärvi, M. Guina, J. Puustinen, P. Tuomisto, J. Rautiainen, A. Härkönen, A. Tukiainen, O. Okhotnikov, and M. Pessa, “MBE grown GaInNAs-based multi-watt disk laser,” *J. Cryst. Growth* **311**, 1868-1871 (2009).
- [36] K. W. Su, S. C. Huang, A. Li, S. C. Liu, Y. F. Chen, and K. F. Huang, “High-peak power AlGaInAs quantum-well 1.3- μm laser pumped by a diode-pumped actively Q-switched solid-state laser,” *Opt. Lett.* **31**, 2009-2011 (2006).
- [37] S. C. Huang, H. L. Chang, K. W. Su, A. Li, S. C. Liu, Y. F. chen, and K. F. Huang, “AlGaInAs/InP eye-safe laser pumped by a Q-switched Nd:GdVO₄ laser,” *Appl. Phys. B* **94**, 483-487 (2009).
- [38] P. Dupriez, A. Piper, A. Malinowski, J. K. Sahu, M. Ibsen, B. C. Thomsen, Y. Jeong, L. M. B. Hickey, M. N. Zervas, J. Nilsson, and D. J. Richardson, “High average power, high repetition rate, picosecond pulsed fiber master oscillator power amplifier source seeded by a gain-switched laser diode at 1060 nm,” *IEEE Photon. Tech. Lett.* **18**, 1013-1015 (2006).
- [39] J. H. Biek, I. H. Choi, B. Lee, W. S. Han, and H. K. Cho, “Precise control of 1.55 μm vertical-cavity surface-emitting laser structure with InAlGaAs/InAlAs Bragg reflectors by in situ growth monitoring,” *Appl. Phys. Lett.* **75**, 1500-1502 (1999).
- [40] N. Nishiyama, C. Caneau, B. Hall, G. Guryanov, M. H. Hu, X. S. Liu, M. J. Li, R. Bhat, and C. E. Zah, “Long-wavelength vertical-cavity surface-emitting lasers on InP with lattice matched AlGaInAs/InP DBR grown by MOCVD,” *IEEE J. Sel. Top. Quantum Electron.* **11**, 990-998 (2005).
- [41] P. Černý, H. Jelínková, P. Zverev, and T. T. Basiev, “Solid state lasers with

- Raman frequency conversion,” *Prog. Quantum Electron.* **28**, 113-143 (2004).
- [42] S. H. Ding, X. Y. Zhang, Q. P. Wang, F. F. Su, P. Jia, S. T. Li, S. Z. Fan, J. Chang, S. S. Zhang, and Z. J. Liu, “Theoretical and experimental study on the self-Raman laser with Nd:YVO₄ crystal,” *IEEE Quantum Electron.* **42**, 927-933 (2006).
- [43] Y. F. Chen, “Efficient 1521-nm Nd:GdVO₄ Raman laser,” *Opt. Lett.* **29**, 2632-2634 (2004).
- [44] J. T. Murray, R. C. Powell, D. Smith, W. Austin, and R. A. Stolzenberger, “Generation of 1.5- μ m radiation through intracavity solid-state Raman shifting in Ba(NO₃)₂ nonlinear crystals,” *Opt. Lett.* **20**, 1017-1019 (1995).
- [45] A. Agnesi, S. Dell’Acqua, and G. Reali, “Diode-pumped quasi-cw intracavity optical parametric oscillator at 1.57 μ m with efficient pulse shortening,” *Appl. Phys. B* **70**, 751-753 (2000).
- [46] Y. F. Chen, S. W. Chen, Y. C. Chen, Y. P. Lan, and S. W. Tsai, “Compact efficient intracavity optical parametric oscillator with a passively Q-switched Nd:YVO₄/Cr⁴⁺:YAG laser in a hemispherical cavity,” *Appl. Phys. B* **77**, 493-495 (2003).
- [47] H. T. Huang, J. L. He, X. L. Dong, C. H. Zuo, B. T. Zhang, G. Qiu, and Z. K. Liu, “High-repetition-rate eye-safe intracavity KTA OPO driven by a diode-end-pumped Q-switched Nd:YVO₄ laser,” *Appl. Phys. B* **90**, 43-45 (2008).
- [48] S. Kück, K. Petermann, U. Pohlmann, U. Schönhoff, and G. Huber, “Tunable room-temperature laser action of Cr⁴⁺-doped Y₃Sc_xAl_{5-x}O₁₂,” *Appl. Phys. B* **58**, 153-156 (1994).
- [49] N. V. Kuleshov, A. A. Lagatsky, A. V. Podlipensky, V. P. Mikhailov, A. A. Kornienko, E. B. Dunina, S. Hartung, and G. Huber, “Fluorescence dynamics, excited-state absorption, and stimulated emission of Er³⁺ in KY(WO₄)₂,” *J. Opt. Soc. Am. B* **15**, 1205-1212 (1998).
- [50] I. Sokólska, E. Heumann, S. Kück, and T. Lukasiewicz, “Laser oscillation of Er³⁺:YVO₄ and Er³⁺, Yb³⁺:YVO₄ crystals in the spectral range around 1.6 μ m,” *Appl. Phys. B* **71**, 893-896 (2000).
- [51] A. Sennaroglu, “Broadly tunable Cr⁴⁺-doped solid-state lasers in the near infrared and visible,” *Proc. Quantum Electron.* **26**, 287-352 (2002).

- [52] J. Rautiainen, J. Lyytikäinen, A. Sirbu, A. Mereuta, A. Caliman, E. Kapon, and O. G. Okhotnikov, “2.6 W optically-pumped semiconductor disk laser operating at 1.57- μm using wafer fusion,” *Opt. Express* **16**, 21881-21886 (2008).



Chapter Four

Simultaneous Q-switching and Wavelength Conversion of the AlGaInAs Multiple-Quantum-Wells

4.1 Simultaneously passively Q-switched and frequency-switched behaviors of the multiple-quantum-wells

The realization of compact, rugged, all-solid-state pulsed laser systems at the near-infrared (NIR) region is of great importance in numerous applications such as remote sensing, range finding, medical treatment, industrial processing and optical communication [1-5]. Nowadays, there are different approaches to obtain suitable laser sources in these fields such as the actively or passively Q-switched solid-state lasers (SSLs) with a variety of doped crystals as the gain medium [6-11]. To achieve more diverse wavelengths, the collocation of Q-switched SSLs and the nonlinear frequency conversion methods including the optical-parametric-oscillation (OPO) or the stimulated-Raman-scattering (SRS) are developed vigorously [12-15]. Even so, the emission wavelengths are still strongly limited by the discrete energy level of the doped ions in the host crystals and the adequate nonlinear crystals. Besides, the high voltage RF drivers used to activate the active Q-switches which need additional heat dissipated apparatus and the insertion of saturable absorbers in the passively Q-switched lasers are all increasing the complexity and enlarging the device dimension of laser systems.

Another way using the composition of an efficient pulsed pump laser module and a frequency down-converted doped crystal laser cavity have been presented as the

pulse-pumped frequency-switched laser [16,17]. As an example, a signal laser cavity with frequency-switched medium of Cr^{4+} :YAG could be inter-cavity pumped by a 1.06 μm pulsed Nd:YAG laser and 1.44 μm pulsed laser output is obtained. But the drawback of these lasers are the restriction of emission wavelengths of the gain-switched materials and the requirement of a promising pump laser module with emission spectrum exactly at the absorption band of the frequency-switched medium. Moreover, these lasers are mostly inter-cavity pumped by a harmonically up-converted pulsed Nd-doped laser module to obtain the ultra-violet to visible laser emission. So far, the pulse-pumped frequency-switched lasers at NIR spectral region with the intra-cavity pump configuration have not been presented and the semiconductor materials also have never been used as the frequency-switched mediums yet.

Recently, as mentioned in section 1.4, the multiple-quantum-well (MQW) structure with flexible choices of modulation wavelength via bandgap engineering is developed to be an efficient saturable absorber in the simple, compact passively Q-switched solid-state lasers [7-11]. Compared to the bulk crystal saturable absorbers the MQW absorber allows the shorter cavity length and has lower nonsaturable loss which are beneficial to the shorter pulse formation and promotion of the Q-switching efficiency, respectively [11,18,19]. The MQW structure is also applied in the optically-pumped semiconductor lasers (OPSLs) as an active medium to provide the high power, low divergence and nearly-diffraction-limited beams with potential spectral range from the ultraviolet to mid-infrared as noted in section 1.3. Numerous OPSLs with inter-cavity quasi-CW or pulsed pumping similar to the pulse-pumped frequency-switched lasers have been presented [20-22]. In Chapter three the semiconductor MQW gain-switched lasers inter-cavity pumped by the Yb-doped fiber

amplifier have been demonstrated. In according to these characteristics we brought up an idea that the MQWs structure has the potential to be designed simultaneously as a saturable absorber and a frequency-switched medium in the intra-cavity pumped solid-state lasers. The dual functionalities of the MQWs not only simplify the fabrication but also have inherently shorter cavity length by decreasing the intra-cavity elements and, the most important, make the realization of the wavelength versatile miniature passively Q-switched laser via the use of semiconductor saturable absorber to be possible. In comparison to the pulse-pumped frequency-switched lasers, the intra-cavity pumping scheme could reserve more energy of the pump light and the synchronous Q-switched behavior of the MQWs also simplifies the composition of pump laser module. Although the Cr, Nd:YAG co-doped crystals have been demonstrated to act as the gain medium and the saturable absorber at the same time in the self Q-switched lasers [23-25], the semiconductor MQW structure has not been applied in this aspect up to now.

In this chapter an AlGaInAs MQW saturable absorber intra-cavity pumped by a diode-pumped Nd:GdVO₄ laser at 1064 nm to produce the passively Q-switched and frequency-switched 1530 nm laser output is presented. Conventionally, the MQW active mediums of OPSLs are pumped by exciting the electrons in the barrier region and the lasing photons are generated by the recombination process of relaxed electrons in the quantum-well region. But the strong absorption of the barrier region leads to the high transparency threshold intensity of the MQWs. This means that the saturable absorption may not happened unless an ultra-high average power of the pump emission is applied. Alternatively, the MQW structure was grown to be in-well pumped at the higher energy level of the quantum-well region in which the activation length is rather short to realize the saturable absorption of pump light in the

Nd:GdVO₄ laser. Under this scheme, the pulsed 1530 nm laser output with maximum average output power of 530 mW at a diode pump power of 21.6 W was obtained with 357 kHz repetition rate and 27 ns pulse duration. The conversion efficiency of the average output power to the pump power was 2.4% and the slope efficiency was 5.6%. To the author's knowledge, it is the first demonstration of the simultaneous Q-switching and wavelength conversion of the AlGaInAs MQWs intra-cavity pumped by a diode-pumped Nd-doped solid-state laser.

4.2 Device fabrication and experimental setup

The MQW structure with emission spectral region at 1.1-1.6 μm is traditionally based on the InGaAsP and AlGaInAs systems. Since the conduction band offset of InGaAsP system is lower, the AlGaInAs system has better carrier confinement. This means that the AlGaInAs MQW structure has better stability and thermal resistance under room temperature operation. Therefore, 30 pairs of AlGaInAs triple quantum-wells were grown on the Fe-doped InP as the 1530 nm active medium via metalorganic chemical-vapor deposition. Each pairs of the MQWs consist of three 8-nm-thick quantum wells and two 10-nm-thick barriers and are spaced at the half-wavelength intervals by the cladding layers to locate the MQWs at the anti-node of the lasing mode. The frequency-switched behavior could be significantly enhanced under this framework which is called the resonant-periodic-gain structure [26,27]. Unlike the typical gain mirrors of the OPSLs and the semiconductor saturable absorber mirrors, the distributed Bragg reflector (DBR) structure in our MQW sample is removed since the lattice-matched DBRs of the InP-based materials to date suffer from the low refractive index contrast, low thermal conductivity or high complexity of growth [28,29]. Alternatively, the Fe-doped InP with higher transmittance than the conventionally used S-doped InP at spectral region over 1 μm is applied as the

substrate to diminish the intracavity loss. As a result, the function of DBRs could be replaced by an external reflective mirror. To prevent the surface recombination and the oxidation an InP window layer was deposited on the top surface of the MQWs. Both sides of the MQW chip were mechanically polished and anti-reflection (AR) coated at the pump and lasing wavelength to reduce the loss and couple-cavity effect.

To solve the problem that the strong absorption in barrier region leads to the high transparency threshold intensity of the MQWs in the passive Q-switching process. The quantum-well region is fabricated to accommodate the pump energy level of 1064 nm and the emission level of 1530 nm. The upper state is served as the nonlinear saturable absorption device at 1064 nm and the lower state is served as the active medium at 1530 nm with additional couple-cavity in the Nd:GdVO₄ laser. The room-temperature absorption spectrum of the AlGaInAs MQW wafer under low power excitation is the same as in Fig. 2.2-5. The lasing wavelength at 1530 nm is located at the first quantum state ($n=1$) and the pump wavelength at 1064 nm is included in the second state ($n=2$). The schematic illustration of saturable absorption and frequency-switching processes are the same as in Fig. 2.2-1 with the operation (1) to be nonlinear saturable absorption, (2) to be noradiative relaxation and (3) to be frequency-switched emission. The hardly transmitted light below 950 nm is due to the strong absorption of the Fe-doped InP substrate. Because the thermal load of the MQW gain chip will result in the red-shift of the emission spectrum and increase the carrier leakage under high power excitation [30,31], to obtain the better performance of semiconductor lasers the thermal management is fairly significant as described in section 3.1. In our experiment, we use the intra-cavity heat spreader method which is mostly applied at spectral range longer than 1 μm to improve the heat dissipation [30,32-37]. The epitaxial side of the cleaved 2.5-mm square piece of MQWs chip was

in contact with a 4.5-mm square, 0.5-mm thick piece of single crystal diamond heat spreader via liquid capillary bonding [38]. Then the whole specimen was clipped by the copper blocks with the indium foil between the interfaces as specified in the section 3.3. The copper heat sinks were hollowed out with a hole of 2-mm diameter and cooled by a thermal-electric cooler with the temperature maintained at 10 °C. The contact uniformity was further confirmed by the interference fringe formed from the minute gap between the MQWs surface and diamond heat spreader.

Figure 4.2-1 shows the experimental configuration of the diode-pumped 1530 nm passively Q-switched Nd:GdVO₄ laser by the use of an AlGaInAs/InP MQW structure which is simultaneously acting the saturable absorption and wavelength conversion. This setup is pumped by a 21.6 W, 808 nm fiber-coupled laser diode with a core diameter of 800 μm and a numerical aperture of 0.16. A focusing lens system was used to reimage the pump light from laser diode into a 0.3 at. % Nd³⁺, 6 mm long Nd:GdVO₄ crystal with 1:2 magnification by a pair of plane-convex lens. The Nd:GdVO₄ crystal was wrapped with indium foil and mounted in a air-cooling copper block. The 1064 nm emission light of the Nd:GdVO₄ crystal is incident on the heat spreader side of the entire gain-switched composite to bypass the thermal load from the diamond in the lateral direction effectively. The surfaces of lens are AR-coated at 808 nm and the coupling efficiency of the pump light is higher than 90%. The rear side of the focusing lens system is flat and high-reflection (HR) coated at 1064 nm (R>99.8%) to served as the front mirror of the Nd:GdVO₄ laser cavity. The flat external reflector of the fundamental cavity is coated with partial-reflection (PR) at 1064 nm (R=93%) on the inner facet and the transmission at 1530 nm is 85%. To simplify the cavity alignment, the front mirror of the 1530 nm cavity is formed by the high-reflection and high-transmission coating at 1530 nm (R>99.8%) and 1064 nm

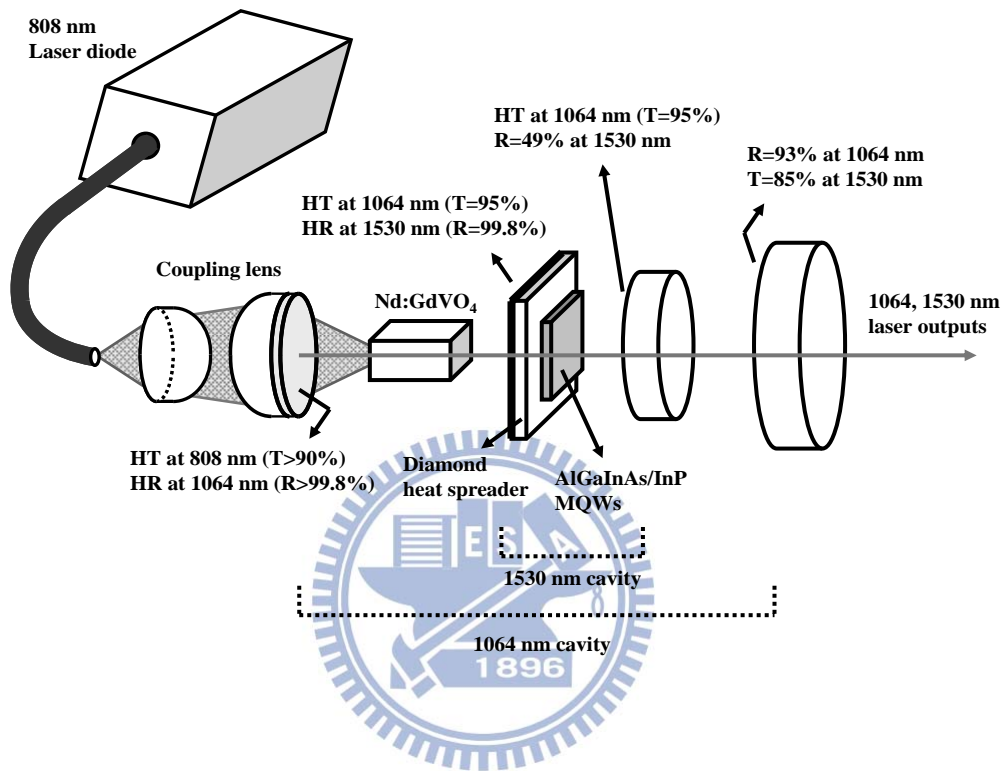


Fig. 4.2-1 Experimental configuration of the diode-pumped Nd:GdVO₄ laser simultaneously passively Q-switched and frequency-switched by the AlGaInAs/InP MQWs.

($T=95\%$) on the pump surface of the diamond heat spreader, respectively. The output coupler is dichroic coated to be partially reflective at 1530 nm ($R=49\%$) and highly transmissive at 1064 nm ($T=95\%$). The overall length of Nd:GdVO₄ laser resonator is 85 mm and the gain-switched cavity length was 2 mm. The location of the AlGaInAs MQW structure was near the external mirror of the pump cavity as compact as possible to lower the Q-switching threshold.

4.3 Experimental results and discussions

In this section the pulsed 1530 nm solid-state laser is presented in use of a simultaneously passively Q-switched and frequency-switched AlGaInAs MQWs structure which is pumped by the Nd:GdVO₄ laser. The laser source with output wavelength beyond 1.44- μm is called the eye-safe laser in which the incident light at this spectral region into the human eyes is strongly absorbed by the ocular fluid of the eye. As a result, the incident light could not reach the sensitive retina and the damage threshold of the eyes is greatly increased. The high repetition rate, high peak power eye-safe lasers are therefore of great interest in the applications like gas sensing, range finding, laser radars, active imaging, and medical treatment [39-41]. At the beginning, a relatively high reflection mirror with $R=93\%$ at 1064 nm is used as the external mirror of the Nd:GdVO₄ laser cavity and, as a result, the dual wavelength exportation was obtained. The average output powers of 1064 nm and 1530 nm versus the pump power at 808 nm are shown in Fig. 4.3-1. It is obvious that the constituent of 1064 nm output is much lower than 1530 nm because most of the photons at 1064 nm are sealed inside the resonator. The threshold pump power is about 12.3 W and the slope efficiency is 5.6% at 1530 nm. Under continuous-wave operation (in which the AlGaInAs MQWs and the couple-cavity are removed) the threshold pump power and the slope efficiency of 1064 nm Nd:GdVO₄ laser output were 5.1 W and 53.5%,

respectively. The rather high threshold and low transition efficiency of the 1530 nm laser output are mainly due to the large non-saturable loss when the excited electrons are relaxed from the $n=2$ to $n=1$ quantum state.

Furthermore, to investigate the influence of the fundamental pump light to the frequency-switched emission we changed the reflectivity of the 1064 nm external mirror from 93% to 30%. The constituent of 1064 nm is increased and 1530 nm is decreased when the reflection of the pump light is lowered. Fig. 4.3-2 depicts the output power characteristics to the pump power at 808 nm with the 30% reflectivity 1064 nm external mirror. The power transition efficiency of 1064 nm exceeded the frequency-switched light of 1530 nm apparently. However, the total average output power of the 93% and 30% output coupler were maintained around a constant value of 630 mW. This indicates that the ratio of the total dual wavelength output could be tuned by varying the reflection of fundamental pump light. Fig. 4.3-3 (a) and (b) show the dual wavelength output spectra of the diode-pumped simultaneously passively Q-switched and frequency-switched Nd:GdVO₄ laser at an incident pump power of 15 W. The spectral information was recorded by an optical spectrum analyzer (Advantest Q8381A) which is using a diffraction monochromator to perform high speed measurement of the pulsed light with resolution of 0.1 nm. The emission spectrum of the Nd:GdVO₄ laser in Fig. 4.3-3 (a) is located at 1064 nm with the bandwidth of 0.2 nm. The lasing spectrum of the frequency-switched light in Fig. 4.3-3 (b) is centered at 1530 nm with 4.8 nm bandwidth and comprises dense longitudinal modes due to the multiple interferences characterized by the interfaces between the MQWs surfaces and the air. The slight red-shift of 8 nm of the 1530 nm lasing spectrum in the whole pump range means that the heating effect is controlled to

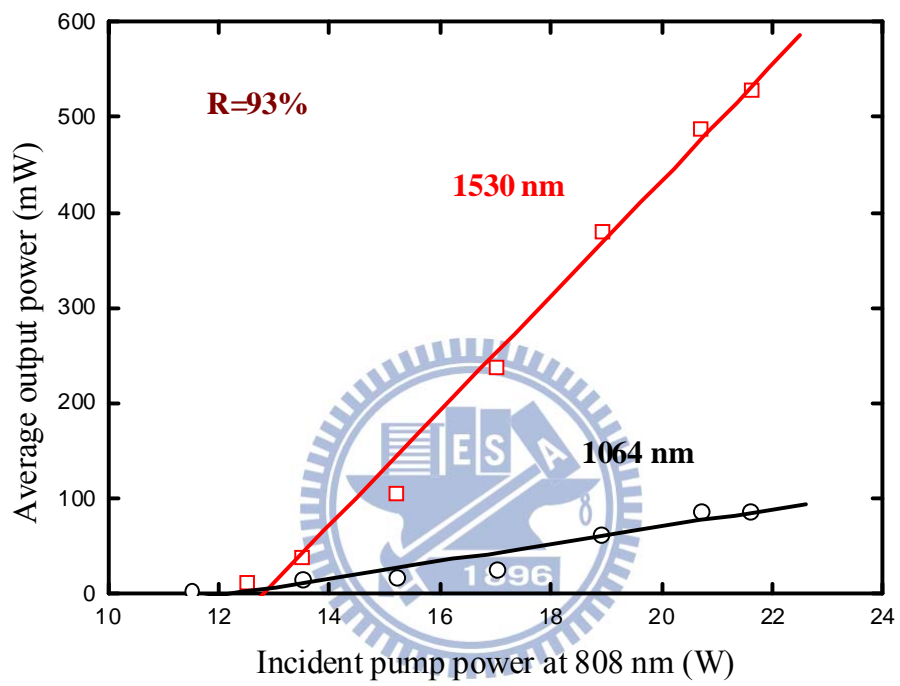


Fig. 4.3-1 Average output powers at 1064 nm and 1530 nm versus the incident pump power with 93% reflectivity of the 1064 nm output coupler.

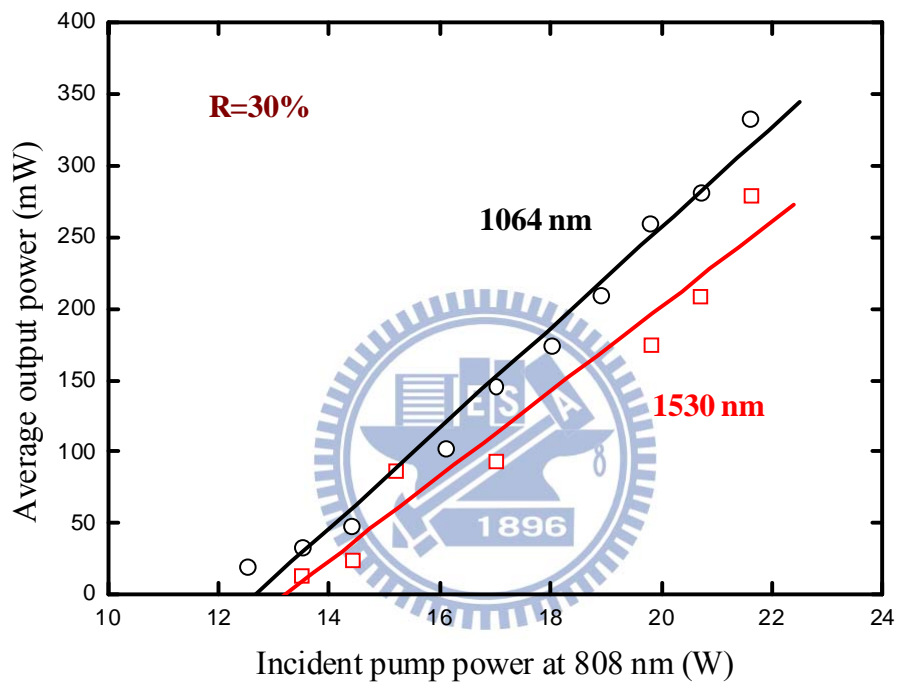


Fig. 4.3-2 Average output powers at 1064 nm and 1530 nm versus the incident pump power with 30% reflectivity of the 1064 nm output coupler.

be insignificant.

The pulse temporal behavior of the dual wavelength laser output was measured by a LeCroy digital oscilloscope (Wave pro 7100, 10 G samples/s, 1 GHz bandwidth) with a fast p-i-n photodiode. When the 93% external reflector of the Nd:GdVO₄ laser cavity was used, the pulse repetition rate was increased from 86 kHz to 357 kHz at the incident pump power ranged from 13.5 W to 21.6 W. The frequency-switched output pulse traced the 1064 nm pump light with a little delay build-up time. Therefore, almost fixed pulse duration of 30 ns at 1064 nm and 27 ns at 1530 nm was produced in the whole pumping range. The typical oscilloscope trace of a train of output pulses and the expanded single pulse shape are shown in Fig. 4.3-4 (a) and (b) at the pump power of 15.2 W. Obviously, the peak-to-peak fluctuation and the pulse-to-pulse timing jitter are very large which may mainly attributed to the inhomogeneous saturation of the large number of MQW pairs. We have also found that if the reflectivity of the external mirror of the 1064 nm resonator is lowered the status of output pulses became fairly stable. The temporal dynamics and the expanded single pulse shape under the identical pump power of 15.2 W by use of the 30% output coupler are shown in Fig. 4.3-5 (a) and (b) for comparison. It is apparent that the pulse amplitude fluctuation and the timing jitter are highly diminished although the constituent ratio of 1530 nm output is reduced. However, the mechanisms of the improvement of temporal behavior are still under further investigations.

In this section, we present what is believed to be the first use of AlGaInAs/InP MQWs structure simultaneously as the saturable absorber and gain medium in a pulsed 1530 nm diode-pumped Nd-doped crystal laser. The 1064 nm emission of the Nd-doped crystal was passively Q-switched by the AlGaInAs/InP MQWs and acted as the pump source of the MQWs in the meantime. As a result, the pulsed 1530 nm laser

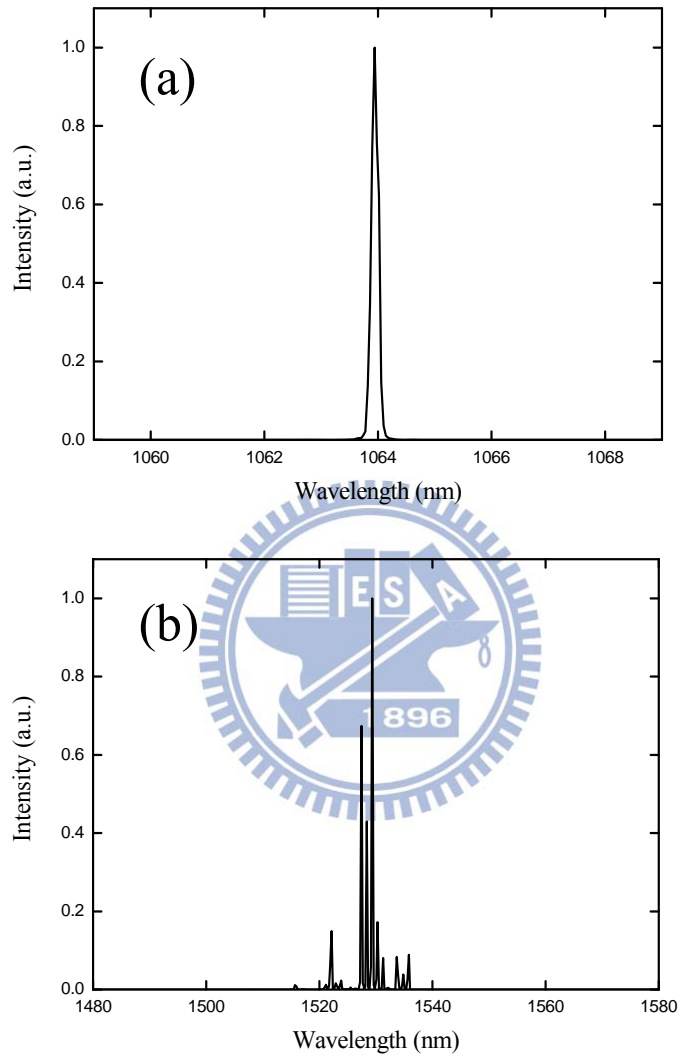


Fig. 4.3-3 Output lasing spectrum at (a) 1064 nm and (b) 1530 nm at incident pump power of 15 W.

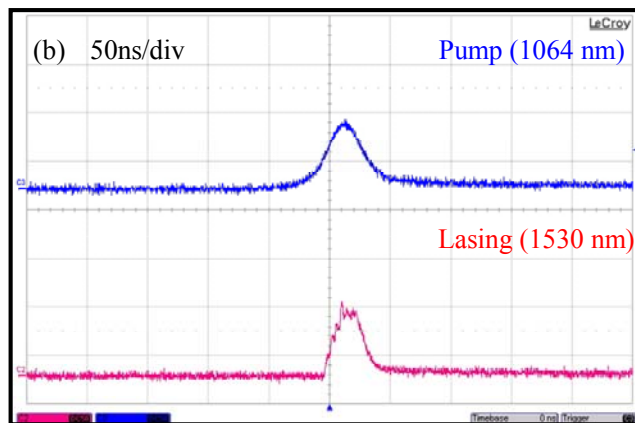
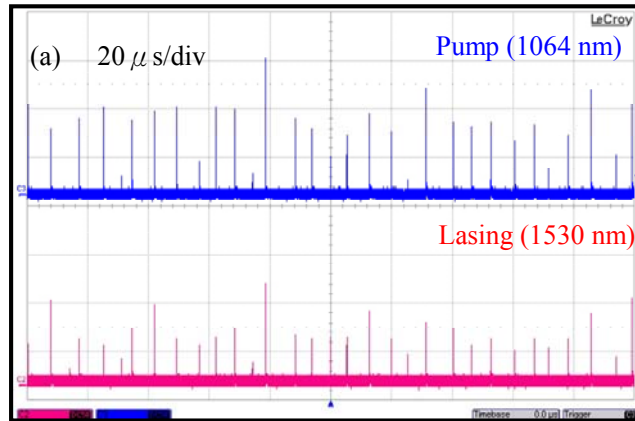


Fig. 4.3-4 Typical oscilloscope trace of the pump and output (a) pulse train and (b) expanded shape of a single pulse with output coupler of 93% reflectivity.

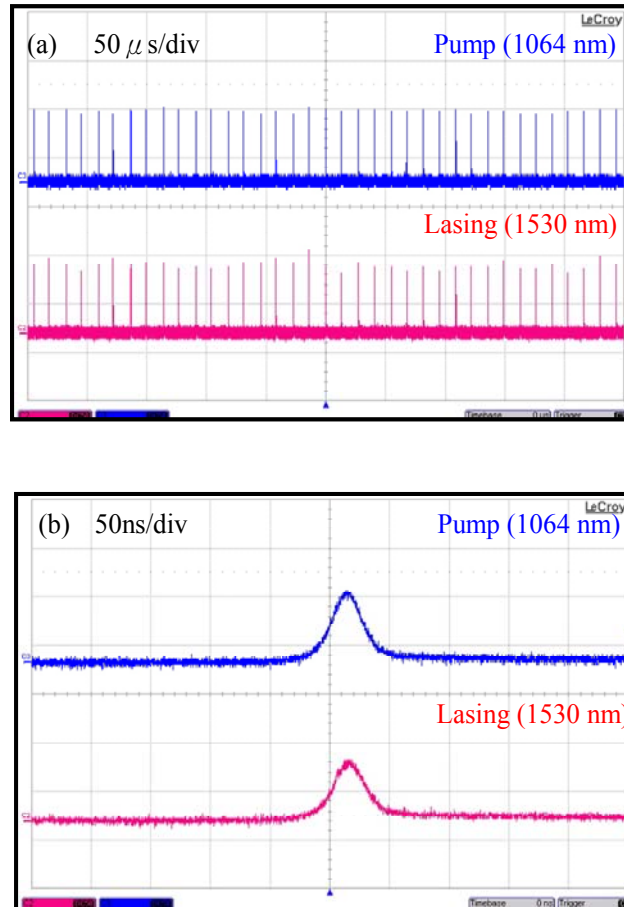


Fig. 4.3-5 Typical oscilloscope trace of the pump and output (a) pulse train and (b) expanded shape of a single pulse with output coupler of 30% reflectivity.

output at the lowest emission state of the MQWs was obtained with the additional coupled-cavity. The maximum average output power of 530 mW was produced at a diode pump power of 21.6 W, and the pulse repetition rate and the pulse duration were operated at 357 kHz and 27 ns, respectively.

4.4 Conclusions

In summary, a diode-pumped Nd:GdVO₄ laser is passively Q-switched and frequency-switched by the AlGaInAs/InP MQWs with the intra-cavity pump scheme to produce a pulsed eye-safe laser output. This laser system combines the advantages of the pulse-pumped solid-state lasers, self-Q-switched lasers and the wavelength versatility of semiconductor heterostructures. The broad potential spectral range via band-gap engineering overcomes the drawbacks in non-linear frequency conversion techniques such as the restriction of emission wavelength due to the limited doped-dielectrics, the suitable nonlinear crystals, the requirement of high-speed, high-voltage electronics and the complexity in fabrication. With the external mirror of 93% reflectivity at 1064 nm, the maximum average output power of 530 mW at 1530 nm was obtained under 357 kHz repetition rate and 27 ns pulse duration. The residual 1064 nm pump light was also exported with relatively lower average output power of 87 mW. By using the 30% reflectivity output coupler the composition ratio of the 1064 nm and 1530 nm output were turned to be nearly equal with invariant total average output power. In addition, the peak-to-peak fluctuation and pulse-to-pulse timing jitter were also highly reduced.

References

- [1] S. D. Jackson, and A. Lauto, "Diode-pumped fiber lasers: A new clinical tools?" *Laser Surg. Med.* **30**, 184-190 (2002).
- [2] J. J. Zayhowski, "Passively Q-switched Nd:YAG microchip lasers and

- applications,” *J. All. Comp.* **303**, 393-400 (2000).
- [3] J. E. Nettleton, B. W. Schilling, D. N. Barr, and J. S. Lei, “Monoblock laser for a low-cost, eyesafe, microlaser range finder,” *Appl. Opt.* **39**, 2428-2432 (2000).
- [4] A. D. Singh, M. Nouri, C. L. Shields, J. A. Shields, and N. Perez, “Treatment of retinal capillary hemangioma,” *Ophthalmology* **109**, 1799-1806 (2002).
- [5] S. M. Spuler, and S. D. Mayor, “Raman shifter optimized for lidar at a 1.5 micron wavelength,” *Appl. Opt.* **46**, 2990-2995 (2007).
- [6] Y. F. Chen, Y. P. Lan, “Diode-pumped passively Q-switched Nd:YAG laser at 1123 nm,” *Appl. Phys. B* **79**, 29-31 (2004).
- [7] Y. P. Huang, H. C. Liang, J. Y. Huang, K. W. Su, A. Li, Y. F. Chen, and K. W. Huang, “Semiconductor quantum-well saturable absorbers for efficient passively Q switching of a diode-pumped 946 nm Nd:YAG laser,” *Appl. Opt.* **46**, 6273-6276 (2007).
- [8] J. Y. Huang, H. C. Liang, K. W. Su, H. C. Lai, Y. F. Chen, and K. F. Huang, “InGaAs quantum-well saturable absorbers for a diode-pumped passively Q-switched Nd:YAG laser at 1123 nm,” *Appl. Opt.* **46**, 239-242 (2007).
- [9] R. Fluck, B. Braun, E. Gini, H. Melchior, and U. Keller, “Passively Q-switched 1.34- μm Nd:YVO₄ microchip laser with semiconductor saturable-absorber mirrors,” *Opt. Lett.* **22**, 991-993 (1997).
- [10] S. C. Huang, S. C. Liu, A. Li, K. W. Su, Y. F. Chen, and K. F. Huang, “AlGaInAs quantum-well as a saturable absorber in a diode-pumped passively Q-switched solid-state laser,” *Opt. Lett.* **32**, 1480-1482 (2007).
- [11] R. Häring, R. Paschotta, R. Fluck, E. Gini, H. Melchior, and U. Keller, “Passively Q-switched microchip laser at 1.5 μm ,” *J. Opt. Soc. Am. B* **18**, 1805-1812 (2001).
- [12] Y. F. Chen, “Efficient subnanosecond diode-pumped passively Q-switched Nd:YVO₄ self-stimulated Raman laser,” *Opt. Lett.* **29**, 1251-1253 (2004).
- [13] W. Chen, Y. Wei, C. Huang, X. Wang, H. Shen, S. Zhai, S. Xu, B. Li, Z. Chen, and G. Zhang, “Second-stokes YVO₄/Nd:YVO₄/YVO₄ self-frequency Raman laser,” *Opt. Lett.* **37**, 1968-1970 (2012).
- [14] Y. T. Chang, K. W. Su, H. L. Chang, and Y. F. Chen, “Compact efficient Q-switched eye-safe laser at 1525 nm with a double-end diffusion-bonded Nd:YVO₄ crystal as a self-Raman medium,” *Opt. Express* **17**, 4330-4335

- (2009).
- [15] H. Zhu, G. Zhang, H. Chen, C. Huang, Y. Wei, Y. Duan, Y. Huang, H. Wang, and G. Qiu, "High-efficiency intracavity Nd:YVO₄/KTA optical parametric oscillator with 3.6 W output power at 1.53 μm ," *Opt. Express* **17**, 20669-20674 (2009).
- [16] J. J. Zayhowski, S. C. Buchter, and A. L. Wilson, "Miniature gain-switched lasers," in *OSA Topics Opt. Photon.—Advanced Solid-State Lasers*. Washington, OSA, **50**, 462-469 (2001).
- [17] J. J. Zayhowski and A. L. Wilson, "Miniature, pulsed Ti:Sapphire laser system," *IEEE J. Quantum Electron.* **38**, 1449-1454 (2002).
- [18] Y. P. Huang, K. W. Su, A. Li, Y. F. Chen, and K. W. Huang, "High-peak-power passively Q-switched Nd:YAG laser at 946 nm," *Appl. Phys. B* **91**, 429-432 (2008).
- [19] J. Y. Huang, W. Z. Zhuang, W. C. Huang, K. W. Su, C. Hu, K. F. Huang, and Y. F. Chen, "Comparative studies for Cr⁴⁺:YAG crystal and AlGaInAs semiconductor used as a saturable in Q-switched Yb-doped fiber lasers," *Opt. Express* **17**, 20800-20805 (2009).
- [20] N. Hempler, J.-M. Hopkins, A. J. Kemp, N. Schulz, M. Rattunde, J. Wagner, M. D. Dawson, and D. Burns, "Pulsed pumping of semiconductor disk lasers," *Opt. Express* **15**, 3247-3256 (2007).
- [21] Y.-Y. Lai, J. M. Yarborough, Y. Kaneda, J. Hader, J. V. Moloney, T. J. Rotter, G. Balakrishnan, C. Hains, and S. W. Koch, "340-W peak power from a GaSb 2- μm optically pumped semiconductor laser (OPSL) grown mismatched on GaAs," *IEEE photon. Tech. Lett.* **22**, 1253-1255 (2010).
- [22] A. Laurain, T.-L. Wang, M. J. Yarborough, J. Harder, J. V. Moloney, S. W. Koch, B. Kunert, and W. Stoltz, "High peak power operation of a 1- μm GaAs-based optically pumped semiconductor laser," *IEEE photon. Tech. Lett.* **24**, 380-382 (2012).
- [23] S. Zhou, K. K. Lee, Y. C. Chen, and S. Li, "Monolithic self-Q-switched Cr,Nd:YAG laser," *Opt. Lett.* **18**, 511-512 (1993).
- [24] L. Lv, L. Wang, P. Fu, X. Chen, Z. Zhang, V. Gaebler, D. Li, B. Liu, H. J. Eichler, S. Zhang, A. Liu, and Z. Zhu, "Diode-pumped self-Q-switched single-frequency 946-nm Nd³⁺,Cr⁴⁺:YAG microchip laser," *Opt. Lett.* **26**, 72-74

(2001).

- [25] M. Jiang, Q. Zhang, K. Qiu, D. Zhang, and B. Feng, "Self-Q-switched Cr, Nd:YAG laser under direct 885 nm diode laser pumping," *Opt. Express* **285**, 3684-3687 (2012).
- [26] M. Y. A. Raja, S. R. J. Brueck, M. Osinski, C. F. Schaus, J. G. McInerney, T. M. Brennan, and B. E. Hammons, "Surface-emitting, multiple quantum well GaAs/AlGaAs laser with wavelength-resonant periodic gain medium," *Appl. Phys. Lett.* **53**, 1678-1680 (1988).
- [27] S. W. Corzine, R. S. Geels, J. W. Scott, R.-H. Yan, and L. A. Coldren, "Design of Fabry-Perot surface-emitting lasers with a periodic gain structure," *IEEE J. Quantum Electron.* **25**, 1513-1524 (1989).
- [28] J. H. Biek, I. H. Choi, B. Lee, W. S. Han, and H. K. Cho, "Precise control of 1.55 μm vertical-cavity surface-emitting laser structure with InAlGaAs/InAlAs Bragg reflectors by *in situ* growth monitoring," *Appl. Phys. Lett.* **75**, 1500-1502 (1999)
- [29] N. Nishiyama, C. Caneau, B. Hall, G. Guryanov, M. H. Hu, X. S. Liu, M. J. Li, R. Bhat, and C. E. Zah, "Long-wavelength vertical-cavity surface-emitting lasers on InP with lattice matched AlGaInAs/InP DBR growth by MOCVD," *IEEE J. Sel. Top. Quantum Electron.* **11**, 990-998 (2005).
- [30] A. J. Maclean, R. B. Birch, P. W. Roth, A. J. Kemp, and D. Burns, "Limits on efficiency and power scaling in semiconductor disk lasers with diamond heat spreaders," *J. Opt. Soc. Am. B* **26**, 2228-2236 (2009).
- [31] S. Calvez, J. E. Hastie, M. Guina, O. G. Okhotnikov, and M. D. Dawson, "Semiconductor disk lasers for the generation of visible and ultraviolet radiation," *Laser & Photon. Rev.* **3**, 407-434 (2009).
- [32] W. J. Alford, T. D. Raymond, and A. A. Allerman, "High power and good beam quality at 980 nm from a vertical external-cavity surface-emitting laser," *J. Opt. Soc. Am. B* **19**, 663-666 (2002).
- [33] T.-L. Wang, Y. Kaneda, J. M. Yarborough, J. Harder, J. V. Moloney, A. Chernikov, S. Chatterjee, A. W. Koch, B. Kunert, and W. Stolz, "High-power optically pumped semiconductor laser at 1040 nm," *IEEE Photon. Tech. Lett.* **22**, 661-663 (2010).
- [34] L. Fan, C. Hassenius, M. Fallahi, J. Harder, H. Li, J. V. Moloney, W. Stolz, S. W.

- Koch, J. T. Murray, and R. Bedford, "Highly strained InGaAs/GaAs multiwatt vertical-external-cavity surface-emitting laser emitting around 1170 nm," *Appl. Phys. Lett.* **91**, 131114(1)-131114(3) (2007).
- [35] J.-M. Hopkins, S. A. Smith, C. W. Jeon, H. D. Sun, D. Burns, S. Calvez, M. D. Dawson, T. Jouhti, and M. Pessa, "0.6 W CW GaInNAs vertical external-cavity surface emitting laser operating at 1.32 μm ," *Electron. Lett.* **40**, 30-31 (2004).
- [36] H. Linberg, M. Strassner, E. Gerster, and A. Larsson, "0.8 W optically pumped vertical external cavity surface emitting laser operating CW at 1550 nm," *Electron. Lett.* **40**, 601-602 (2004).
- [37] J. Rautiainen, J. Lyytikäinen, A. Sirbu, A. Mereuta, A. Caliman, E. Kapon, and O. G. Okhotnikov, "2.6 W optically-pumped semiconductor disk laser operating at 1.57- μm using wafer fusion," *Opt. Express* **16**, 21881-21886 (2008).
- [38] Z. L. Liao, "Semiconductor wafer bonding via liquid capillarity," *Appl. Phys. Lett.* **77**, 651-653 (2000).
- [39] L. R. Marshall, A. D. Hays, J. Kasinski, and R. Burnham, "Highly efficient optical parametric oscillators," *Proc. SPIE* **1419**, 141-152 (1991).
- [40] S. M. Spuler and S. D. Mayor, "Raman shifter optimized for lidar at a 1.5 micron wavelength," *Appl. Opt.* **46**, 2990-2995 (2007).
- [41] A. J. Mcgrath, J. Munch, G. Smith, and P. Veitch, "Injection-seeded, single-frequency, Q-switched erbium:glass laser for remote sensing," *Appl. Opt.* **37**, 5706-5709 (1998).

Chapter Five

Summary and Future Works

5.1 Summary

In summary, we have introduced the luminescence features of MQWs under low and high level excitation, development of MQWs as gain mediums in optically-pumped semiconductor lasers (OPSLs) and semiconductor saturable absorbers in passively Q-switched lasers in [Chapter 1](#). In [Chapter 2](#), an AlGaInAs MQWs structure is fabricated with resonant-periodic-gain configuration to promote the light-QWs interaction. Under this framework, we demonstrate the first observation of room temperature spontaneous emission of the many-body state luminescence induced by the high density electron-hole plasma in the AlGaInAs MQWs. Furthermore, the temperature-dependent luminescence features of this emanation mode with photon energy below the band-edge of ground state has been investigated from 93 to 313 K and the excitation threshold intensity is obtained as low as 198 kW/cm^2 at room temperature of 293 K.

In [Chapter 3](#), an AlGaInAs multiple quantum wells (MQWs) structure is used as an effective gain medium of the in-well pumped high peak power OPSLs with 1220 nm output. The laser is excited by an Yb-doped pulsed fiber amplifier to effectively optimize the output characteristics. The maximum average output power of 1.28 W and peak output power of 0.76 kW is obtained at 1220 nm lasing wavelength under 60 kHz pump repetition rate and 28 ns pump pulse width via the double gain chip regime. Moreover, we further demonstrated a compact efficient high-repetition-rate (>100 kHz) optically pumped AlGaInAs nanosecond eye-safe laser at 1520 nm. A diamond heat spreader bonded to the gain chip is employed to improve the heat removal. At a

pump power of 13.3 W, the average output power at a repetition rate 200 kHz is up to 3.12 W, corresponding to a peak output power of 560 W. At a repetition rate 500 kHz, the maximum average power and peak power are found to be 2.32 W and 170 W, respectively. The realization of these OPSLs confirms that the MQWs structure is suitable as the active medium of the inter-cavity frequency- switched laser which is recommended in [section 4.1](#).

At the end, we present what is believed to be the first use of AlGaInAs/InP MQW structure simultaneously as the saturable absorber and the gain medium in a pulsed 1530 nm diode-pumped Nd-doped crystal laser in [Chapter 4](#). The 1064 nm emission of the Nd-doped crystal was passively Q-switched by the AlGaInAs/InP MQWs and acted as the pump source of the MQWs in the meantime. As a result, the pulsed 1530 nm laser output at the lowest emission state of the MQWs was obtained with the additional coupled-cavity. The maximum average output power of 530 mW was produced at a diode pump power of 21.6 W, and the pulse repetition rate and the pulse duration were operated at 357 kHz and 27 ns, respectively.

5.2 Future works

Compact, simple, economical and high peak power solid-state laser source with sub-nanosecond pulses is of practical importance in many fields such as range finding and 3D imaging in use of the time-of-flight methods, micro-processing and optical communication. Because the pulse energy of mode-locked lasers is limited by the short inter-pulse periods and the device configuration is complex in fabrication, a better way to obtain high peak power laser output is the passively Q-switched (PQS) microchip lasers discussed in [section 1.4](#). Compared to the actively Q-switched microchip lasers, the PQS microchip lasers is simple, low cost and no need of any external high speed and high power consumption drivers and temperature control of

the electro- or acousto-optic Q-switches. But the choices of gain mediums and saturable absorbers are restricted to the suitable doped bulk crystals with matched emission and absorption spectrum. Even though the use of antiresonant Fabry-Perot saturable absorbers (A-FPSAs) or the so-called semiconductor saturable absorber mirrors (SESAMs) with adjustable wavelengths via bandgap engineering in PQS microchip lasers is demonstrated by Braun *et al.* in the spectral region of 1.06- μm , 1.34- μm and 1.5- μm [1-3], the operation wavelengths of these lasers are still mainly limited by the discrete energy levels of the doped ions of gain medium. Alternatively, the passively Q-switched lasers in combination with nonlinear frequency conversion techniques such as the harmonic generation, optical parametric oscillation and stimulated Raman scattering are developed to be the promising pulsed laser sources [4-6]. But the long active length of the nonlinear crystal hinders the application of intra-cavity pumping in which the cavity length should be short enough to afford sub-nanosecond operation.

Based on the contents of this thesis, if we combine simultaneous Q-switching and frequency-switching device and the heat spreader method discussed in [Chapter 4](#) and [section 3.3](#), a compact thin disk PQS microchip laser with intra-cavity wavelength conversion could be achieved via capillary bonding technique. The effectiveness of the use of diamond in contact with the Yb:YAG crystal with 1 mm thickness has been realized in our lab with continuous wave and PQS operation [7]. But the Cr⁴⁺:YAG crystal is separated from the gain chip and is just functioning as a nonlinear saturable absorber. Therefore, the emission wavelength is restricted to the Yb:YAG gain chip of 1030 nm and the cavity length is as long as 8.4 mm. If we take the AlGaInAs MQWs chip as shown in [Chapter 4](#) instead of the Cr⁴⁺:YAG and construct a suppositional

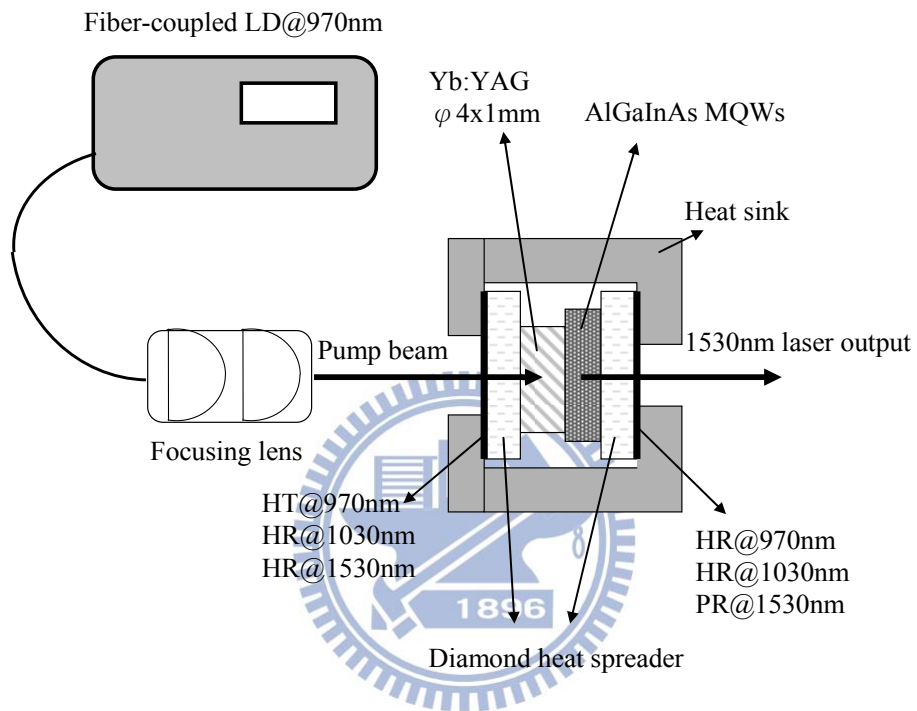


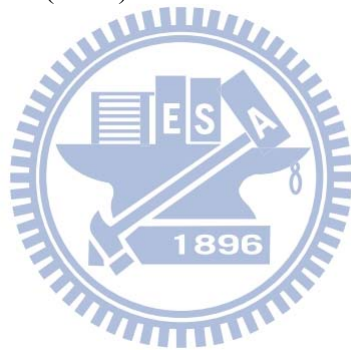
Fig. 5.2-1 Suppositional experimental setup of the simultaneously Q-switched and frequency-switched Yb:YAG/AlGaInAs MQWs microchip laser.

laser configuration as demonstrated in Fig. 5.2-1, we could obtain the 1530 nm pulsed output and the cavity length could be shortened well below 2.5 mm under the nearly equivalent experimental setup. In this framework, the two diamonds are bonded to the Yb:YAG crystal and AlGaInAs MQWs chip with thickness of 0.5 mm to enhance heat dissipation from the pump spot. The diamond wafer in contact with the gain chip is high-reflection (HR) coated at 1030 and 1530 nm and high-transmittance (HT) coated at 970 nm at the entrance side to serve as the front mirror. The other diamond wafer in contact with the AlGaInAs MQWs chip is HR coated at 970 and 1030 nm and partial reflection coated at 1530 nm at the output face to serve as the external mirror. Compared to the PQS laser in combination with the nonlinear wavelength conversion, this laser setup offers several advantages. First, it is capable of intracavity pumping without significantly lengthening the cavity. Second, the fundamental laser emission is no need to be linear polarization. Third, the wavelength conversion efficiency is not strongly depending on the intracavity photon intensity. Four, there is no requirement of phase matching. Therefore, it is a simple, compact, monolithic and low cost potential laser configuration to produce sub-nanosecond near-infrared laser pulses and we are interested in realizing this laser module in the future.

Reference

- [1] B. Braun, F. X. Kärtner, G. Zhang, M. Moser, and U. Keller, "56-ps passively Q-switched diode-pumped microchip laser," *Opt. Lett.* **22**, 381-383 (1997).
- [2] R. Fluck, B. Braun, E. Gini, H. Melchior, and U. Keller, "Passively Q-switched 1.34- μm Nd:YVO₄ microchip laser with semiconductor saturable-absorber mirrors," *Opt. Lett.* **22**, 991-993 (1997).
- [3] R. Fluck, R. Häring, R. Paschotta, E. Gini, H. Melchior, and U. Keller, "Eyesafe pulsed microchip laser using semiconductor saturable absorber mirrors," *Appl. Phys. Lett.* **72**, 3273-3275 (1998).
- [4] R. Bhandari and T. Taira, "> 6MW peak power at 532 nm from passively

- Q-switched Nd:YAG/Cr⁴⁺:YAG microchip laser,” Opt. Express **19**, 19135-19141 (2011).
- [5] H. Zhu, G. Zhang, H. Chen, C. Huang, Y. Wei, Y. Duan, Y. Huang, H. Wang, and G. Qiu, “High-efficiency intracavity Nd:YVO₄/KTA optical parametric oscillator with 3.6 W output power at 1.53 μm,” Opt. Express **17**, 20669-20647 (2009).
- [6] Y. T. Chang, K. W. Su, H. L. Chang, and Y. F. Chen, “Compact efficient Q-switched eye-safe laser at 1525 nm with a double-end diffusion-bonded Nd:YVO₄ crystal as a self-Raman medium,” Opt. Express **17**, 4330-4335 (2009).
- [7] W. Z. Zhang, Yi-Fan Chen, K. W. Su, K. W. Huang, and Y. F. Chen, “Performance enhancement of sub-nanosecond diode-pumped passively Q-switched Yb:YAG microchip laser with diamond surface cooling,” Opt. Express **20**, 22602-22608 (2012).



Curriculum Vitae

Personal Data

Name: Yi-Fan Chen

Birthday: Jan. 7, 1986

Nationality: Taiwan (R.O.C.)

Birthplace: Taipei

Telephone (M): +886-911-202-823

Sex: Male

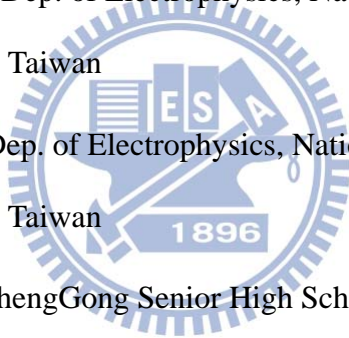
E-mail: ivan.ep97g@nctu.edu.tw

Education

2007~2012 Ph.D. in Dep. of Electrophysics, National Chiao Tung University,
Hsinchu, Taiwan

2004~2007 B.S. in Dep. of Electrophysics, National Chiao Tung University,
Hsinchu, Taiwan

2001~2004 Taipei ChengGong Senior High School, Taipei



Work Experience

2007~2012 T.A. of Fundamental Physics

Speciality

Laser Physics and Optically-Pumped Semiconductor Lasers

Publication List

Journal paper:

- [1] **Y.-F. Chen**, K. W. Su, W. L. Chen, K. F. Huang, and Y. F. Chen, “High-peak-power optically pumped AlGaInAs eye-safe laser at 500-kHz repetition rate with an intracavity diamond heat spreader,” Appl. Phys. B **108**, 319-323 (2012).

IF=2.189 => 點數=2.5x100%=2.5

- [2] **Y.-F. Chen**, Y. C. Lee, S. C. Huang, K. W. Huang, and Y. F. Chen, “AlGaInAs multiple-quantum-well 1.2- μ m semiconductor laser in-well pumped by an Yb-doped pulsed fiber amplifier,” Appl. Phys. B **106**, 57-62 (2012).

IF=2.189 => 點數=2.5x100%=2.5

- [3] W. Z. Zhuang, **Yi-Fan Chen**, K. W. Su, K. F. Huang, and Y. F. Chen, “Performance enhancement of sub-nanosecond diode-pumped passively Q-switched Yb:YAG microchip laser with diamond surface cooling,” Opt. Express **20**, 22602-22608 (2012).

IF=3.587 => 點數=3x70%=2.1

- [4] H. L. Chang, S. C. Huang, **Yi-Fan Chen**, K. W. Su, Y. F. Chen, and K. F. Huang, “Efficient high-peak-power AlGaInAs eye-safe wavelength disk laser with optical in-well pumping,” Opt. Express **17**, 11409-11414 (2009).

IF=3.587 => 點數=3x50%=1.5

- [5] S. C. Huang, H. L. Chang, **Yi-Fan Chen**, K. W. Su, Y. F. Chen, and K. F. Huang, “Diode-pumped passively mode-locked 1342 nm Nd:YVO₄ laser with an AlGaInAs quantum-well saturable absorber,” Opt. Lett. **34**, 2348-2350 (2009).

IF=3.399 => 點數=3x50%=1.5

Conference paper:

- [1] K. W. Su, *Yi-Fan Chen*, S. C. Huang, A. Li, S. C. Liu, Y. F. Chen, and K. F. Huang, “Low-temperature study of lasing characteristics for 1.3- μm AlGaInAs quantum-well laser pumped by an actively Q-switched Nd:YAG laser,” Proc. SPIE **7578**, 75780Z 1-7 (2010).

總點數=2.5+2.5+2.1+1.5+1.5=10.1

High-peak-power optically pumped AlGaInAs eye-safe laser at 500-kHz repetition rate with an intracavity diamond heat spreader

Y.-F. Chen · K.W. Su · W.L. Chen · K.F. Huang · Y.F. Chen

Received: 23 November 2011 / Revised version: 1 February 2012 / Published online: 21 March 2012
© Springer-Verlag 2012

Abstract We report on a compact efficient high-repetition-rate (>100 kHz) optically pumped AlGaInAs nanosecond eye-safe laser at 1525 nm. A diamond heat spreader bonded to the gain chip is employed to improve the heat removal. At a pump power of 13.3 W, the average output power at a repetition rate 200 kHz is up to 3.12 W, corresponding to a peak output power of 560 W. At a repetition rate 500 kHz, the maximum average power and peak power are found to be 2.32 W and 170 W, respectively.

1 Introduction

High-peak-power high-repetition-rate laser sources have been in demand for the applications in the eye-safe wavelength regime near 1.55- μm such as free-space communication, gas sensing, spectroscopy, and medical treatment. The eye-safe laser sources can be realized in several ways including stimulated Raman scattering (SRS) or optical parametric oscillation (OPO) pumped by the high-peak-power Nd-doped lasers [1–7] and the solid state lasers directly use the Er^{3+} -doped or Cr^{4+} -doped gain media [8–11].

Optically-pumped multiple-quantum-wells (MQWs) semiconductor disk lasers have been developed to provide low-divergence, circular, and high quality nearly-diffraction-limited output beams with flexible choices of emission wavelengths via bandgap engineering [12, 13]. The quaternary alloys lattice matched to InP including InGaAsP

and AlGaInAs are developed in the quantum confined structure of the semiconductor lasers for generating the radiation at the NIR region [14–18]. Although the InGaAsP systems were commonly employed in the semiconductor lasers of the NIR region in the early stage [19, 20], the AlGaInAs systems have been verified to have higher conduction band offsets and better carrier confinements. So far, the maximum average output power ever reported for the eye-safe laser based on the AlGaInAs material was found to be 2.6 W at the continuous-wave operation [21].

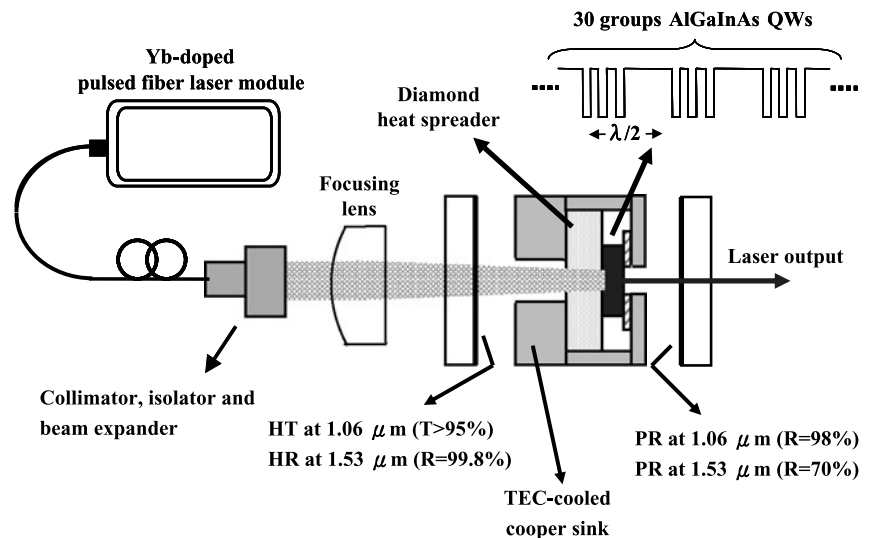
Recently, the AlGaInAs eye-safe pulsed laser was realized with an actively Q-switched 1.06- μm laser as a pump source [22, 23]. However, the average output power and the pulse repetition rate were restricted to 0.52 W and 20 kHz, respectively, due to the poor heat dissipation from the pump area. Here we report, for the first time to our knowledge, on a high-repetition-rate (100–500 kHz) high-power optically pumped AlGaInAs nanosecond eye-safe laser at 1525 nm with an intracavity diamond heat spreader to enhance the heat removal. We employ an Yb-doped pulsed fiber amplifier to be a pump source for providing various pulse repetition rates. With a pump width of 28-ns at a repetition rate of 200 kHz, the average output power and peak output power under an average pump power of 13.3 W are found to be up to 3.12 W and 560 W, respectively. The maximum average power and peak power at a repetition rate 500 kHz are found to be 2.32 W and 170 W, respectively. The overall slope efficiency is maintained as high as 27.3 % at a pulse repetition rate between 100 and 500 kHz.

2 Experimental setup

Figure 1 shows the experimental configuration of the AlGaInAs MQWs laser at the eye-safe region driven by a

Y.-F. Chen · K.W. Su · W.L. Chen · K.F. Huang · Y.F. Chen (✉)
Department of Electrophysics, National Chiao Tung University,
1001 TA Hsueh Road, Hsinchu 30050, Taiwan
e-mail: yfchen@cc.nctu.edu.tw
Fax: +1-886-35-725230

Fig. 1 Experimental setup of AlGaInAs eye-safe laser at 1525 nm with an intracavity diamond heat spreader and using an Yb-doped pulsed fiber amplifier as a pump source



1.06 μm Yb-doped pulsed fiber amplifier (SPI redENERGY G3). The pump source could be operated to provide consecutive pulses with the pulse duration in the range of 9–200 ns and the repetition rate ranging from 10–500 kHz. The pump spot diameter was controlled to be approximately $700 \pm 20 \mu\text{m}$ to have a good spatial overlap with the lasing mode. The laser resonator was designed to be a linear plane-plane cavity which was stabilized by the thermally induced lens of the gain material. The flat mirror at the pump side was coated with antireflection coating at 1.06 μm ($R < 0.2\%$) at the entrance face and with high-reflection coating ($R > 99.8\%$) at 1.53 μm and high-transmission ($T > 95\%$) at 1.06 μm at the other face. The reflectivity of the flat output coupler was 70% at 1.53 μm . The overall cavity length is approximately 15 mm.

The gain structure is composed of 30 groups of triple QWs spaced at half-wavelength intervals by AlGaInAs barrier layers as shown in the inset of Fig. 1. The thickness of the quantum wells are designed to be 8 nm. The AlGaInAs barriers are only used to separate the QWs not used as strain compensation layers. The resonant-periodic-gain (RPG) structure was designed to locate the QWs at the antinodes of the lasing field standing wave [24, 25]. The periodic AlGaInAs QW/barrier layers were grown on a Fe-doped InP transparent substrate by metalorganic chemical-vapor deposition. The Fe-doped InP transparent substrate with high transmission at the pump and lasing wavelength is used to solve the problem of the lack of good distributed Bragg reflectors (DBRs) for the InP-based systems. The function of conventional DBRs was replaced with an external reflective mirror. A window layer of InP was deposited on the gain structure to prevent surface recombination and oxidation. In contrast to the conventional barrier pumping scheme, the present gain medium was designed to be suitable for in-well pumping to enhance the quantum efficiency [26]. It has been

confirmed that the slope efficiency with the in-well pumping scheme was significantly higher than that with the barrier pumping scheme [23]. In the experiment, the single-pass absorption of this gain chip is 81–84% for repetition rate ranged from 30–500 kHz under 28 ns pump pulse width.

A 4.5-mm square, 0.5-mm thick piece of uncoated single crystal diamond heat spreader was bonded to the MQWs side of the cleaved 2.5-mm square piece of the gain chip to improve the heat removal. Although the heat spreader approach has been used in a variety of high power optically pumped semiconductor lasers [27–29], to the best of our knowledge, the diamond heat spreader is for the first time to be applied to the transparent semiconductor gain medium. The other side of the diamond was in contact with a copper heat sink which was cooled by a thermal-electric cooler (TEC), where the temperature was maintained at 15 $^{\circ}\text{C}$. The substrate side of the gain chip was attached tightly to a copper plate with a hole of 2-mm diameter, where an indium foil was employed to be the contact interface. The contact uniformity was further confirmed by inspecting the interference fringe coming from the minute gap between the gain chip and the diamond heat spreader. The package configuration of the gain medium can be seen in Fig. 1.

3 Experimental results and discussion

We fixed the duration of pump pulses to be 28 ns for making a detailed comparison at different pulse repetition rates. The spectral information was monitored by an optical spectrum analyzer (Advantest Q8381A) with a diffraction monochromator which could be used for the high-speed measurement of pulsed light with a resolution of 0.1 nm. Figure 2 shows the room temperature spontaneous-emission spectrum of AlGaInAs MQWs pumped with an average absorbed power

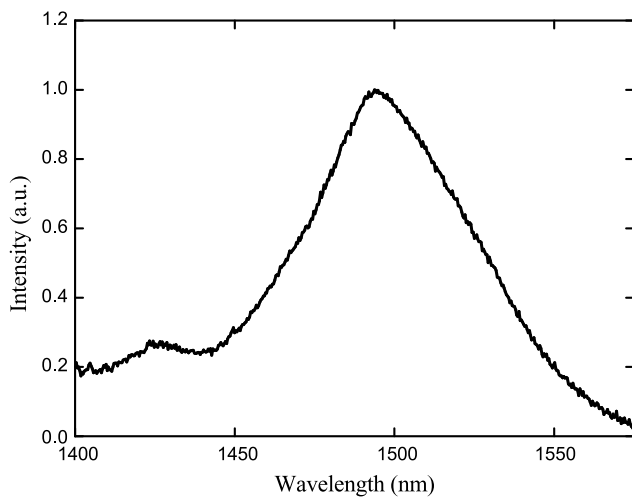


Fig. 2 Room temperature surface emitting spontaneous emission spectrum under a 100-kHz pump repetition rate at an average absorbed power of 0.8 W

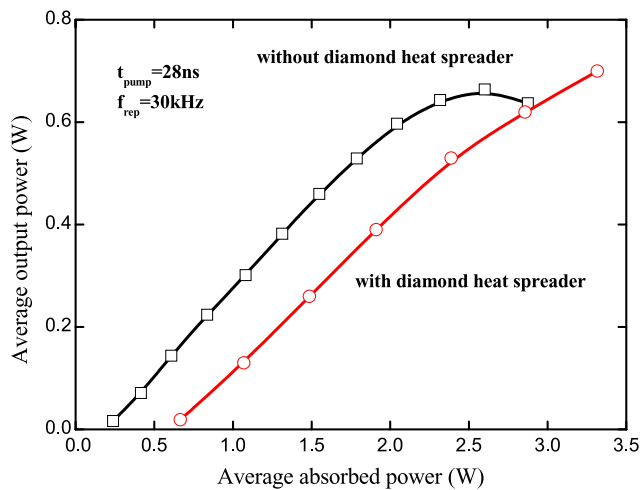


Fig. 3 Output performances of the eye-safe laser without and with the diamond heat spreader at a 30-kHz repetition rate

of 0.8 W at a pulse repetition rate of 100 kHz. It can be seen that the photoluminescence peak at a low pump power was approximately at 1500 nm.

The pump source is a standard commercial product and its maximum output power is dependent on the pulse repetition rate. The maximum output powers of the pump source are approximately 5 W and 20 W for the repetition rates of 30 kHz and 100–500 kHz, respectively. Consequently, we present the experimental results for the laser performance in different figures for the conditions of 30 kHz and 100–500 kHz, respectively. To investigate the losses introduced by the intracavity diamond heat spreader, we make a comparison between the performance of the AlGaInAs eye-safe laser without and with the diamond at the repetition rate of 30 kHz, as shown in Fig. 3. Note that the thermal ef-

fect at the repetition rate of 30 kHz is not significant for the absorbed pump power less than 2 W. It can be seen that the output power without the heat spreader displays a thermally induced roll-over effect for the average absorbed power higher than 2.3 W. In contrast, the slope efficiency obtained with the heat spreader can remain nearly constant for the absorbed pump power up to the maximum pump power of 3.3 W, where the maximum pump power is just limited by the pump source at the repetition rate of 30 kHz. This result confirms the improvement of the power scalability by use of the diamond heat spreader. On the other hand, the slope efficiencies obtained without and with the heat spreader can be found to be 33 % and 28 %, respectively. With these slope efficiencies and the output reflectivity of 70 %, the losses introduced by the heat spreader can be estimated to be 7.5 %. Even though there is a room for improving the introduced losses, the diamond heat spreader can extend the operation frequency up to 500 kHz, as shown in the following results.

Figures 4(a) and (b) show the output performances without and with the diamond heat spreader, respectively, for the repetition rate in the range of 100–500 kHz. The maximum average output powers without the heat spreader can be seen to decrease from 0.45 W down to 0.11 W for the repetition rate increasing from 100 kHz to 500 kHz. On the other hand, the average output powers with the heat spreader can be almost maintained linear for the absorbed pump power reaching the maximum value of 13.3 W at the repetition rate within the range of 200–500 kHz. Since the diamond can effectively reduce the thermal effects, the overall beam quality M2 was found to be better than 1.3 for all the pump powers. The maximum average output powers can be found to be up to 3.12 W and 2.32 W for the repetition rates of 200 kHz and 500 kHz, respectively. The roll-over phenomenon observed in Fig. 4(b) for the case of 100 kHz was attributed to the pump-saturation effect. With an absorbed pump power of 10 W and a pump diameter of 700 μm , the pump intensity for the pump duration of 28 ns at 100 kHz could be calculated to be 0.93 MW/cm². Since the saturation intensity of the MQW absorption was measured to be approximately within 0.8–1.0 MW/cm², the power roll-over phenomenon at 100 kHz was considered to come from the pump-saturation effect.

Figure 5(a) depicts the lasing spectrum with the heat spreader under an average absorbed power of 2.5 W at a repetition rate of 100 kHz. The lasing spectrum can be seen to comprise dense longitudinal modes with the bandwidth to be approximately 10 nm and the center wavelength to be located at 1515 nm. With increasing the average absorbed power, the center wavelength has significant redshifts due to the pump power induced the local heating on the gain medium. Figure 5(b) shows the dependence of the red-shift on the absorbed pump power for the laser operation without and with the heat spreader at a repetition rate of 100 kHz. It

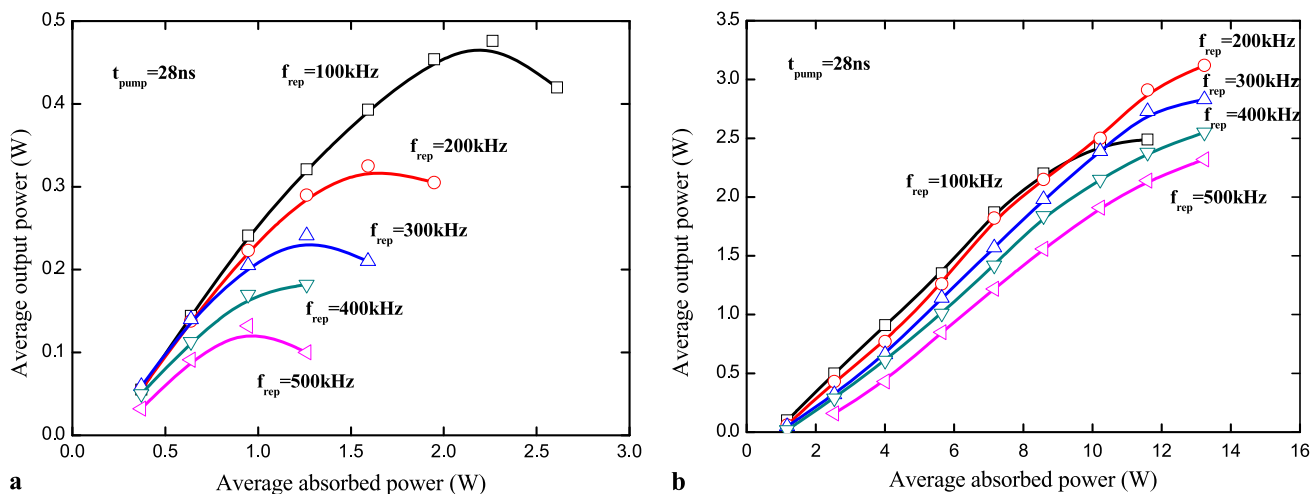


Fig. 4 Output performances without (a) and with (b) the diamond heat spreader for repetition rates in the range of 100–500 kHz

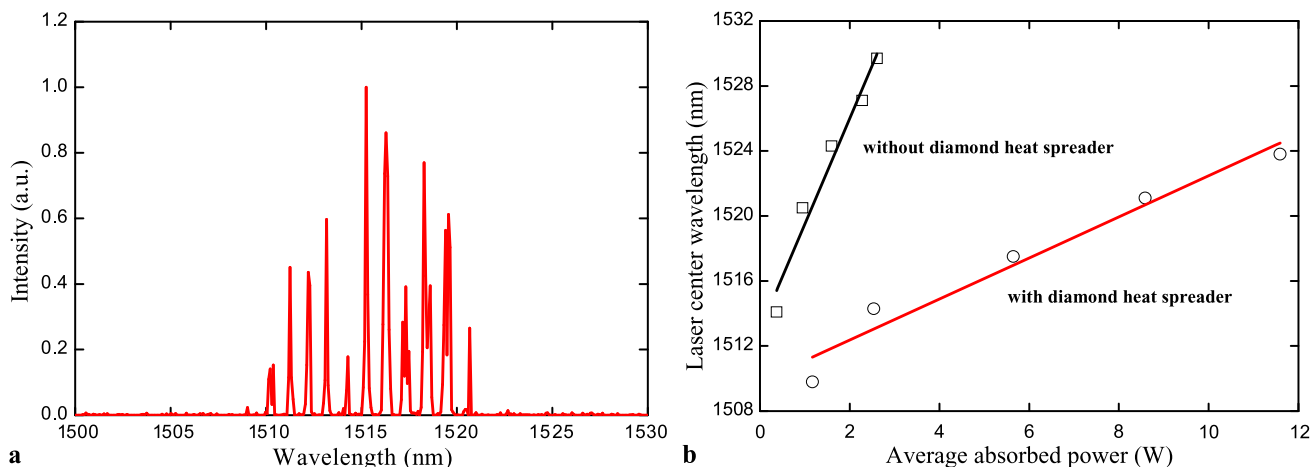


Fig. 5 (a) Lasing spectrum with the heat spreader under an average absorbed power of 2.5 W at a repetition rate of 100 kHz. (b) Dependence of the red-shift on the absorbed pump power for the laser operation without and with the heat spreader at a repetition rate of 100 kHz

can be seen that the redshift measured for the laser without using the heat spreader is considerably larger than the result with the heat spreader. This substantial difference also confirms the local heating to be considerably improved by use of the diamond heat spreader.

The temporal behavior of the laser output was recorded with a LeCroy digital oscilloscope (Wave pro 7100, 10 G samples/s, 1 GHz bandwidth). Figure 6 shows the input and output pulse trains as well as the extended pulse shape of the single pulse for the result obtained with an average absorbed power of 2.5 W at a repetition rate of 200 kHz. It can be seen that the time delay of the output pulse with respect to the input pulse is generally less than a few nanoseconds. The characteristics of the small delay comes from the advantage of the in-well pumping scheme. The peak-to-peak instability was experimentally found to arise from the instability of the pump beam. On the whole, the peak-to-peak fluctuation was

generally within $\pm 5\%$. Finally it is worthwhile to mention that the present gain chip was designed for the high-peak-power operation and could not be used in the CW regime. We currently undertake a design for the gain chip to be applicable for the high-peak-power and CW operations.

4 Summary

In summary, we have demonstrated a high-repetition-rate (>100 kHz) nanosecond eye-safe AlGaInAs laser at 1525 nm with an Yb-doped pulsed fiber amplifier as a pump source. A diamond heat spreader bonded to the gain chip was employed to reach an efficient heat removal. With a pump power of 13.3 W, the maximum average output powers at the repetition rates of 200 kHz and 500 kHz were found to be up to 3.12 W and 2.32 W, respectively. Correspondingly, the maximum peak powers at the repetition

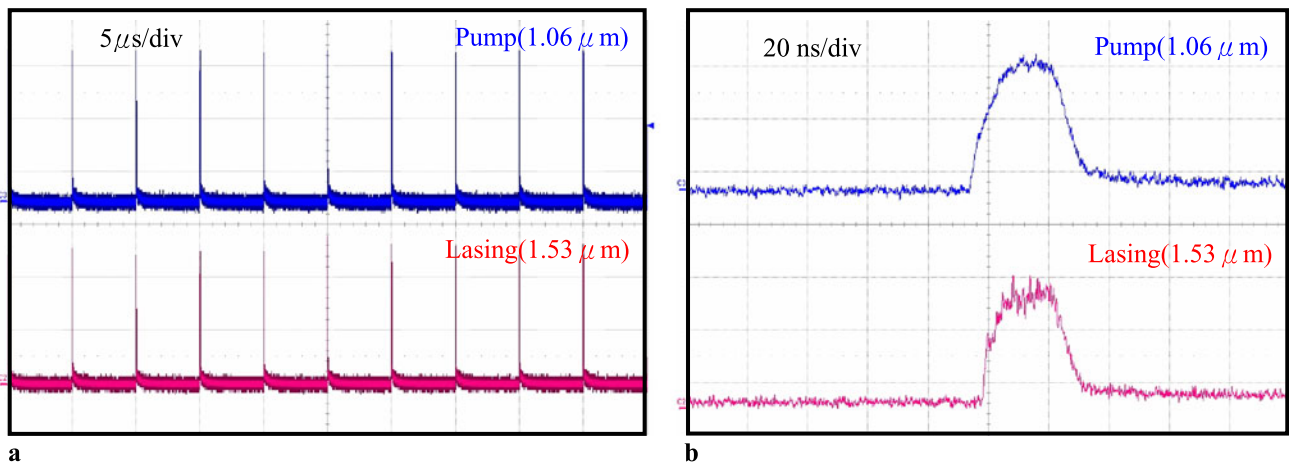


Fig. 6 (a) Oscilloscope trace of a train of pump and output pulses obtained with an average absorbed power of 2.5 W at a repetition rate of 200 kHz. (b) Expanded shapes of a single pulse

rates of 200 kHz and 500 kHz are 560 W and 170 W, respectively. To the best of our knowledge, this is the highest frequency achieved in the pulsed eye-safe lasers with the average output powers higher than 2 W.

Acknowledgements The authors gratefully acknowledge various AlGaInAs/InP gain chips from TrueLight Corporation. The authors also thank the National Science Council for their financial support of this research under Contract No. NSC-100-2628-M-009-001-MY3.

References

- P. Černý, H. Jelínková, P. Zverev, T.T. Basiev, *Prog. Quantum Electron.* **28**, 113 (2004)
- S.H. Ding, X.Y. Zhang, Q.P. Wang, F.F. Su, P. Jia, S.T. Li, S.Z. Fan, J. Chang, S.S. Zhang, Z.J. Liu, *IEEE J. Quantum Electron.* **42**, 927 (2006)
- Y.F. Chen, *Opt. Lett.* **29**, 2632 (2004)
- J.T. Murray, R.C. Powell, D. Smith, W. Austin, R.A. Stolzenberger, *Opt. Lett.* **20**, 1017 (1995)
- A. Agnesi, S. Dell'Acqua, G. Reali, *Appl. Phys. B* **70**, 751 (2000)
- Y.F. Chen, S.W. Chen, Y.C. Chen, Y.P. Lan, S.W. Tsai, *Appl. Phys. B* **77**, 493 (2003)
- H.T. Huang, J.L. He, X.L. Dong, C.H. Zuo, B.T. Zhang, G. Qiu, Z.K. Liu, *Appl. Phys. B* **90**, 43 (2008)
- S. Kück, K. Petermann, U. Pohlmann, U. Schönhoff, G. Huber, *Appl. Phys. B* **58**, 153 (1994)
- N.V. Kuleshov, A.A. Lagatsky, A.V. Podlipensky, V.P. Mikhailov, A.A. Kornienko, E.B. Dunina, S. Hartung, G. Huber, *J. Opt. Soc. Am. B* **15**, 1205 (1998)
- I. Sokólska, E. Heumann, S. Kück, T. Łukasiewicz, *Appl. Phys. B* **71**, 893 (2000)
- A. Sennaroglu, *Prog. Quantum Electron.* **26**, 287 (2002)
- A.C. Tropper, H.D. Foreman, A. Garnache, K.G. Wilcox, S.H. Hoogland, *J. Phys. D* **37**, R75 (2004)
- M. Kuznetsov, F. Hakimi, R. Sprague, A. Mooradian, *IEEE Photonics Technol. Lett.* **9**, 1063 (1997)
- C.E. Zah, R. Bhat, B.N. Pathak, F. Favire, W. Lin, M.C. Wang, N.C. Andreadakis, D.M. Hwang, M.A. Koza, T.P. Lee, Z. Wang, D. Darby, D. Flanders, J.J. Heieh, *IEEE J. Quantum Electron.* **30**, 511 (1994)
- J.P. Donnelly, J.N. Walpole, S.H. Groves, R.J. Bailey, L.J. Missaggia, A. Napoleone, R.E. Reeder, C.C. Cook, *IEEE Photonics Technol. Lett.* **10**, 1377 (1998)
- J. Minch, S.H. Park, T. Keating, S.L. Chuang, *IEEE J. Quantum Electron.* **35**, 771 (1999)
- S.R. Šelmić, G.A. Evans, T.M. Chou, J.B. Kirk, J.N. Walpole, J.P. Donnelly, C.T. Harris, L.J. Missaggia, *IEEE Photonics Technol. Lett.* **14**, 890 (2002)
- J.C.L. Yong, J.M. Rorison, I.H. White, *IEEE J. Quantum Electron.* **38**, 1553 (2002)
- N. Nishiyama, C. Caneau, B. Hall, G. Guryanov, M.H. Hu, X.S. Liu, M.-J. Li, R. Bhat, C.E. Zah, *IEEE J. Sel. Top. Quantum Electron.* **11**, 990 (2005)
- H. Lindberg, A. Larsson, M. Strassner, *Opt. Lett.* **30**, 2260 (2005)
- J. Rautiainen, J. Lytykäinen, A. Sirbu, A. Mereuta, E. Kapon, O.G. Okhotnikov, *Opt. Express* **16**, 21881 (2008)
- S.C. Huang, H.L. Chang, K.W. Su, A. Li, S.C. Liu, Y.F. Chen, K.F. Huang, *Appl. Phys. B* **94**, 483 (2009)
- H.L. Chang, S.C. Huang, Yi-Fan Chen, K.W. Su, Y.F. Chen, K.F. Huang, *Opt. Express* **17**, 11409 (2009)
- M.Y.A. Raya, S.R.J. Brueck, M. Osinsky, C.F. Schaus, J.G. Mcinery, T.M. Brennan, B.E. Hammons, *IEEE J. Quantum Electron.* **26**, 1500 (1989)
- M.Y.A. Raya, S.R.J. Brueck, M.O. Scully, C. Lee, *Phys. Rev. A* **44**, 4599 (1991)
- M. Schmid, S. Benchabane, F. Torabi-Goudarzi, R. Abram, A.I. Ferguson, E. Riis, *Appl. Phys. Lett.* **84**, 4860 (2004)
- J.M. Hopkins, S.A. Smith, C.W. Jeon, H.D. Sun, D. Burns, S. Calvez, M.D. Dawson, T. Jouhti, M. Pessa, *Electron. Lett.* **40**, 30 (2004)
- H. Lindberg, A. Strassner, E. Gerster, A. Larsson, *Electron. Lett.* **40**, 601 (2004)
- V.-M. Korpijärvi, T. Leinonen, J. Puustinen, A. Härkönen, M.D. Guina, *Opt. Express* **18**, 25633 (2010)

AlGaInAs multiple-quantum-well 1.2- μm semiconductor laser in-well pumped by an Yb-doped pulsed fiber amplifier

Y.-F. Chen · Y.C. Lee · S.C. Huang · K.F. Huang ·
Y.F. Chen

Received: 21 March 2011 / Revised version: 17 June 2011 / Published online: 30 July 2011
© Springer-Verlag 2011

Abstract An AlGaInAs multiple quantum well structure is reported as an effective gain medium of the in-well pumped high-peak-power semiconductor disk laser at 1.2 μm . We use an Yb-doped pulsed fiber amplifier as the pump source to effectively optimize the output characteristics. The maximum average output power of 1.28 W and peak output power of 0.76 kW is obtained at 1225 nm lasing wavelength under 60 kHz pump repetition rate and 28 ns pump pulse width.

1 Introduction

High-peak-power all-solid-state lasers operating at 1.14–1.25 μm are desirable for producing yellow-orange lights for many applications such as astronomy community, biomedical optics, and laser absorption spectroscopy [1–3]. Light sources in this spectral range could be realized by Raman-shifted Nd- (Yb-) doped solid-state lasers or Yb- (Bi-) doped fiber lasers [4–6]. However, the performance of solid-state lasers is limited by the discrete energy level of the doped ions. Alternatively, optically pumped semiconductor lasers (OPSLs) have been developed to provide flexible choice of emission wavelength via bandgap engineering [7, 8]. OPSLs also offer a variety of advantages like broad gain curves and a low-divergence, circular, and high quality nearly-diffraction-limited output beam [7–9]. So far, the lasers based on the quantum confined structure with GaAs material systems including InGaAs/GaAs and GaInNAs/GaAs have

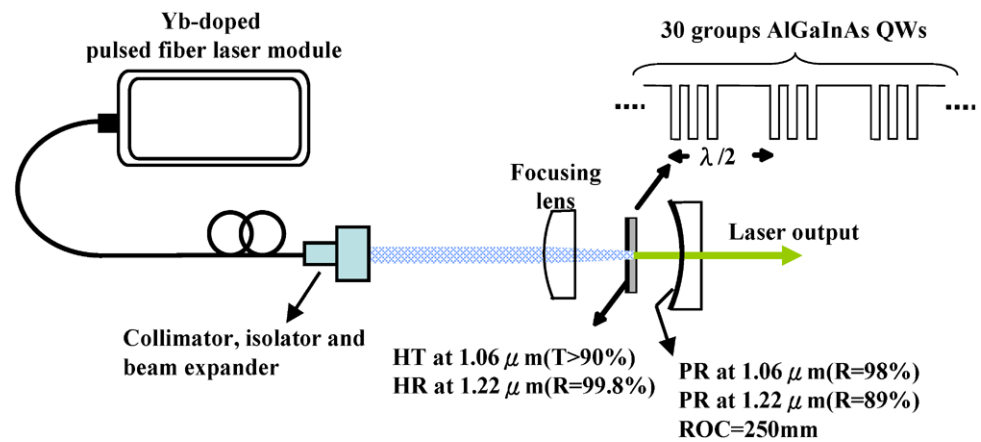
been demonstrated in the 1.14–1.25 μm spectral range under continuous-wave operation [10–13]. However, these lasers are pumped by exciting the electrons from the barrier region and the quantum defect between pump and lasing photons leads to a large amount of heat. Recently, a novel method based on the in-well pumping scheme has been demonstrated to reduce the heat effectively [14, 15]. For the in-well pumping scheme, the electrons are directly excited from the ground state to the excited state in the quantum-well (QW) region. As a result, the thermal load is reduced by lowering the quantum defect. However, OPSLs at 1.14–1.25 μm based on the in-well pumping scheme have not been explored until now.

The quaternary alloys lattice matched to InP such as AlGaInAs and InGaAsP are employed in the semiconductor lasers in the near-infrared (NIR) spectral region. The AlGaInAs systems have been verified to have higher conduction band offset and better carrier confinement than the InGaAsP systems. Several high-peak-power AlGaInAs semiconductor disk lasers have been demonstrated in the NIR region driven by the actively Q-switched (AQS) solid-state lasers [16–18]. However, the pulse width of conventional AQS solid-state lasers depends on the pulse repetition rate and the average pump power. Consequently, it is difficult to optimize the output performance of the semiconductor disk lasers. Therefore, a light source with fixed pulse duration under various repetition rates can be a more suitable pump source for optimizing the performance of OPSLs. High-power pulsed fiber amplifiers are a light source to satisfy this requirement [19].

In this work, we report on a high-peak-power AlGaInAs multiple-quantum-well (MQW) semiconductor laser grown on a Fe-doped InP transparent substrate and pumped by a 1.06 μm Yb-doped pulsed fiber amplifier. With in-well pumping, the thermal and roll-over effect could be reduced

Y.-F. Chen · Y.C. Lee · S.C. Huang · K.F. Huang · Y.F. Chen (✉)
Department of Electrophysics, National Chiao Tung University,
Hsinchu, Taiwan
e-mail: yfchen@cc.nctu.edu.tw
Fax: +886-35-725230

Fig. 1 Experimental setup of AlGaInAs/InP semiconductor disk laser at 1.2 μm pumped by a 1.06 μm Yb-doped pulsed fiber amplifier in the single chip scheme



by lowering the quantum defect. We obtained an average output power of 810 mW at 1225 nm with slope efficiency up to 46.7% to the average absorbed power in the single-chip scheme. The pump conditions of 60 kHz pulse repetition rate and 28 ns pulse width are used. To increase the average absorbed power, the double-chips scheme is used under the same pump conditions. The maximum average output power could be scaled up to 1.28 W with slope efficiency of 37.5% at 1225 nm lasing wavelength. The maximum peak output power of 0.76 kW is obtained with 2.37 kW peak pump power.

2 Device structure and experimental setup

Figure 1 shows the experimental configuration of the AlGaInAs MQW 1.2 μm semiconductor disk laser pumped by a SPI 1.06 μm Yb-doped master oscillator fiber amplifier. This pump source provides 9–200 ns pulse with repetition rate ranged from 10–500 kHz. Compared to the AQS solid-state laser, this laser module can provide fixed pulse width of output pulse even when the output power is changed. We controlled pump spot diameter to be about 800 μm to have efficient spatial overlap with the lasing mode. The gain region is composed of an AlGaInAs QW/barrier structure grown on a Fe-doped InP transparent substrate by metalorganic chemical-vapor deposition. It consisted of 30 groups of triple QWs spaced at half-wavelength intervals by AlGaInAs barrier layers as shown in the inset of Fig. 1. This is a resonant-periodic-gain structure that barrier layers are used to locate the quantum well region at the antinode of the lasing field standing wave. In this structure, the wavelength selection is enhanced [20, 21]. A window layer of InP was deposited on the gain structure to prevent surface recombination and oxidation. In contrast to the conventional barrier pumping scheme, our gain medium is in-well pumped by a 1.06 μm Yb-doped pulsed fiber amplifier. This pumping scheme results in the low absorption (58%) but high conversion efficiency due to the short active region and the

small quantum defect, respectively. In our previous work, we have also verified that the in-well pumping scheme has better slope efficiency than the barrier pumping scheme at equivalent absorbed pump power [18].

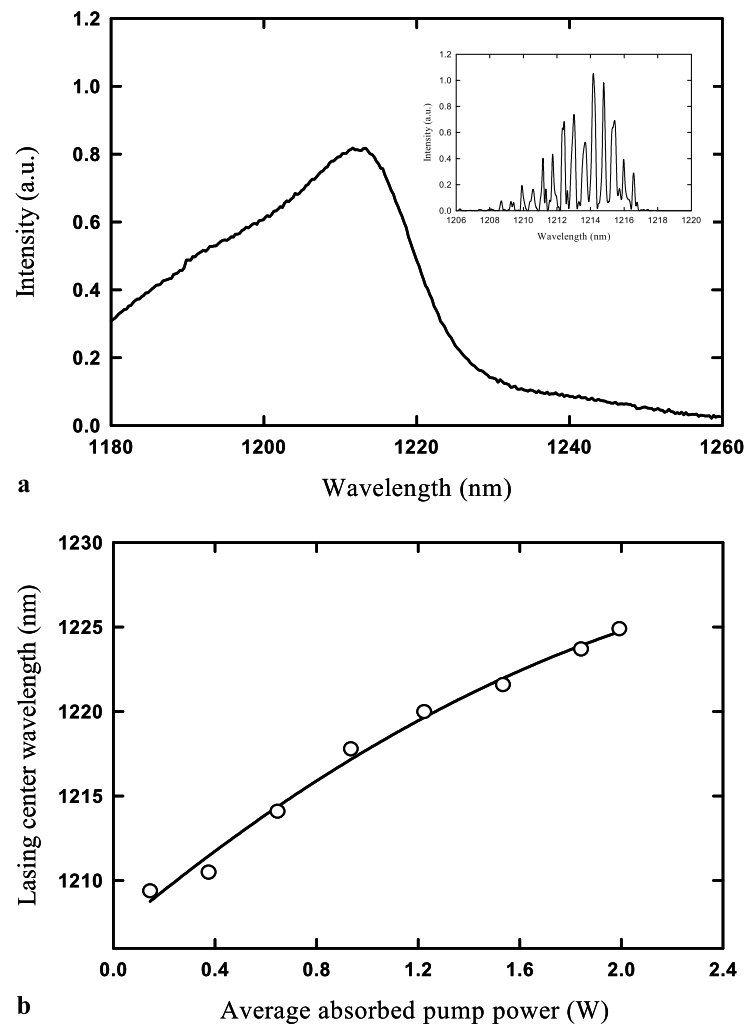
The InP based systems suffer from the lack of good distributed-Bragg-reflector (DBR) and have been challenging to transfer from edge-emitting lasers to surface-emitting lasers. A number of lattice-matched DBRs such as AlGaInAs/AlInAs, AlGaInAs/InP, GaInAsP/InP, AlGaAsSb/AlAsSb, and AlGaAsSb/InP have been demonstrated [22, 23]. Unfortunately, these DBR systems suffer from the low refractive index contrast, low thermal conductivity or high complexity of growth. Therefore, Fe-doped InP with good transparency in the lasing wavelength is chosen as the substrate system instead of conventional S-doped InP with large absorption in the 1.0–2.0 μm spectral region. As a result, the function of DBRs could be replaced by an external mirror. In this configuration, the problem of fabrication of good DBRs has been resolved and the heat dissipation is improved by reducing the length of thermal conduction.

The laser gain medium is fabricated with dielectric coated mirror on the cap layer served as a front mirror. This forms high transmittance at 1.06 μm ($T > 90\%$) and high reflectance between 1.18–1.25 μm ($R > 99.8\%$) on the entrance face. We use an external mirror with radius of curvature of 250 mm and partial reflectance at 1.22 μm ($R = 89\%$) as output coupler. The overall cavity length is about 3 mm. With this plano-concave linear cavity, we could modulate the laser mode volume to have better efficiency. The gain medium is attached on a cooper heat sink with substrate side and is cooled down by water with temperature controlled to be 15°C.

3 Experimental results and discussion

Figure 2(a) shows the room temperature spontaneous-emission spectrum of AlGaInAs MQW with dielectric

Fig. 2 (a) Room temperature surface emitting spontaneous emission spectrum under 60 kHz pump repetition rate and 28 ns pump pulse width at average absorbed power of 0.38 W. *Inset*, the expanded lasing spectrum obtained with 0.85 W average absorbed power under the same pump conditions. (b) Redshift of peak lasing wavelength as a function of average absorbed power under 60 kHz pump repetition rate and 28 ns pump pulse width



coated mirror excited by the 1.06 μm Yb-doped pulsed fiber amplifier with average absorbed power of 0.38 W. The pump repetition rate is 60 kHz and the pump pulse width is 28 ns. This surface emitting photoluminescence (PL) spectrum is captured with the pump beam incident on the dielectric coated side, and the emitted light is collected into the multimode fiber on the other side. The spectral information was monitored by an optical spectrum analyzer (Advantest Q8381A) with a diffraction monochromator which can be used for high-speed measurement of pulsed light with a resolution of 0.1 nm. The PL peak is located at 1215 nm. The expanded lasing spectrum is shown in the inset of Fig. 2(a) at the average absorbed power of 0.85 W. The bandwidth of lasing spectrum is about 9 nm, and it comprises dense longitudinal modes due to the multiple interferences between the cavity mirrors. With increasing average pump power, the lasing spectrum will redshift due to the temperature induced shift of cavity resonance and MQW emission peak. In Fig. 2(b), the degree of redshift of peak lasing wavelength is shown as a function of average absorbed power. It will be

shifted to 1225 nm at average absorbed power of 2.2 W as the roll-over effect happened.

Figure 3 shows the laser output performances with fixed pump pulse width of 28 ns and different pump repetition rates varied from 40–80 kHz. Under 40 kHz pump repetition rate, the average output power begins to saturate with absorbed power exceeded 2 W, i.e., the maximum allowed pump intensity is approximately 0.35 MW/cm². Since the saturation intensity of the MQW absorption was measured to be approximately 0.4 MW/cm², the power roll-over phenomenon at 40 kHz was attributed to the pump-saturation effect. On the other hand, the average output power at 80 kHz is also limited when the average absorbed power increased up to 2 W. This is mainly due to the local heating effect which is resulted from the high pump repetition rate. Consequently, the output performance at fixed pump pulse width of 28 ns can be optimized under 60 kHz pump repetition rate. The maximum average output power of 810 mW at 1225 nm is generated by the average absorbed power of 2 W. The slope efficiency to the average absorbed power is calcu-

Fig. 3 Laser output performances at fixed pump pulse width of 28 ns and different pump repetition rates ranged from 40–80 kHz

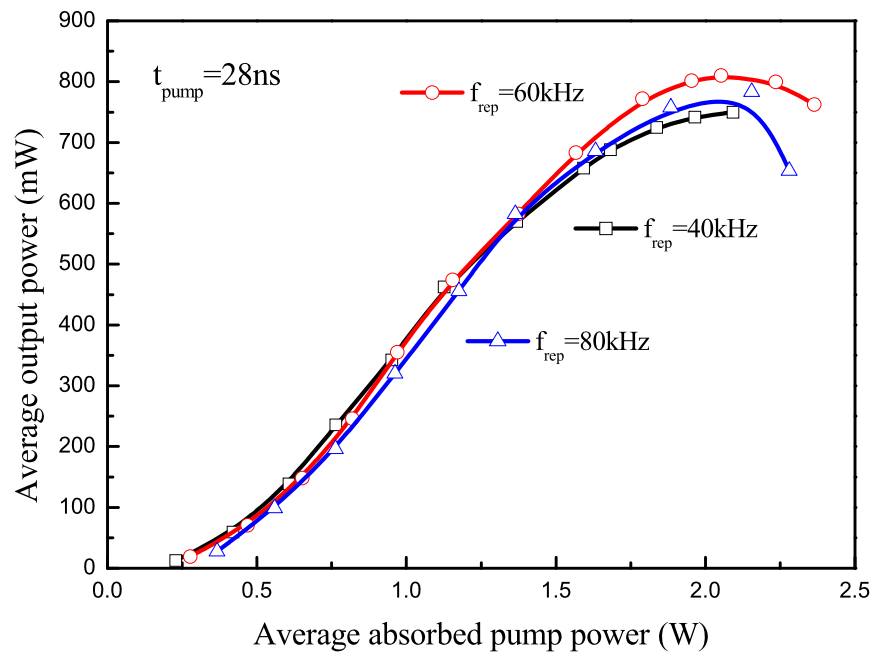
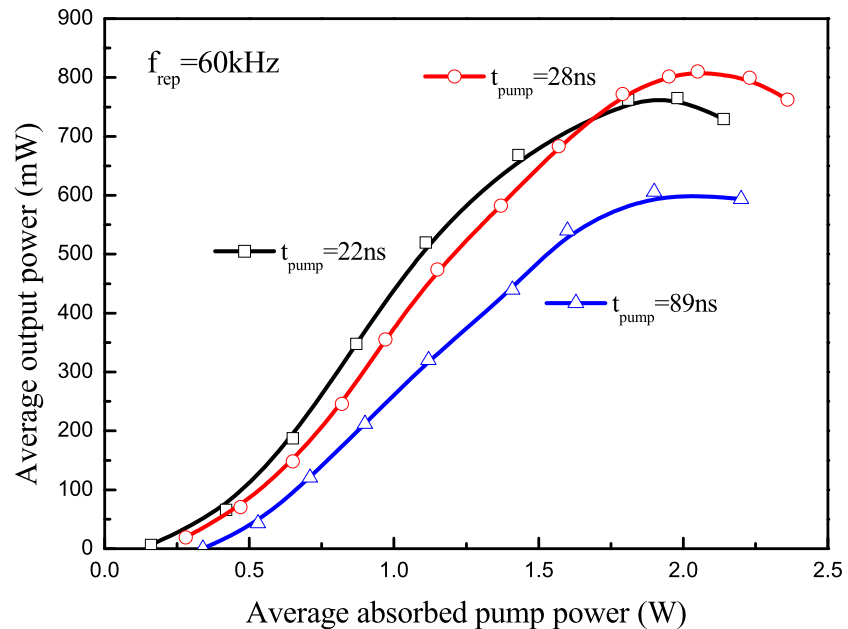


Fig. 4 Laser output performances under 60 kHz pump repetition rate with varied pump pulse width



lated to be 46.7%. The overall beam quality M2 was found to be better than 1.3.

Figure 4 shows the laser output performance with fixed pump repetition rate of 60 kHz and different pump pulse width varied from 22–89 ns. For the given cavity and average absorbed power, the maximum average output power was limited using short pulse width which resulted in the pump-saturation effect [17]. When the pulse duration is long, the roll-over effect appeared due to the thermally induced carrier leakage. As a result, the best performance is obtained under 28 ns pump pulse width. The absorbed satu-

ration intensity of 22 ns and 28 ns pump pulse width is calculated to be 0.3 MW/cm^2 and 0.24 MW/cm^2 , respectively. The slightly lower saturation intensity of 28 ns pump pulse width is due to the larger amount of heat. By contrast, the maximum absorbed intensity of 89 ns pump pulse width is 0.07 MW/cm^2 . This shows that the roll-over is mainly arisen from the considerable heat production with long pump pulse width. Moreover, the conversion efficiency is strongly affected by the thermal load before roll-over effect happens. Hence, the slope efficiency is higher for lower pump pulse width under low average absorbed power.

Fig. 5 (a) Typical oscilloscope trace of a train of pump and output pulses and (b) expanded shapes of a single pulse

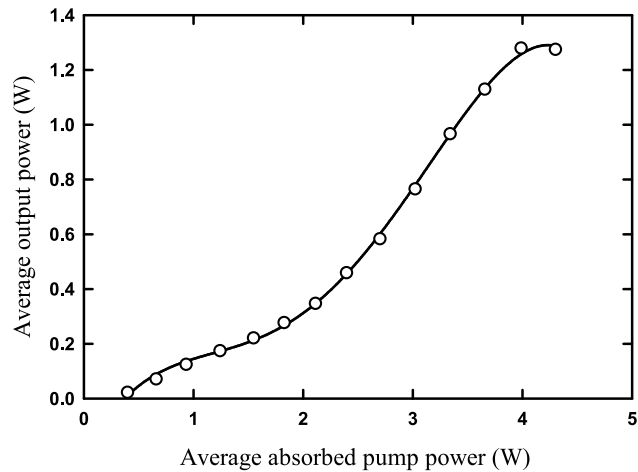
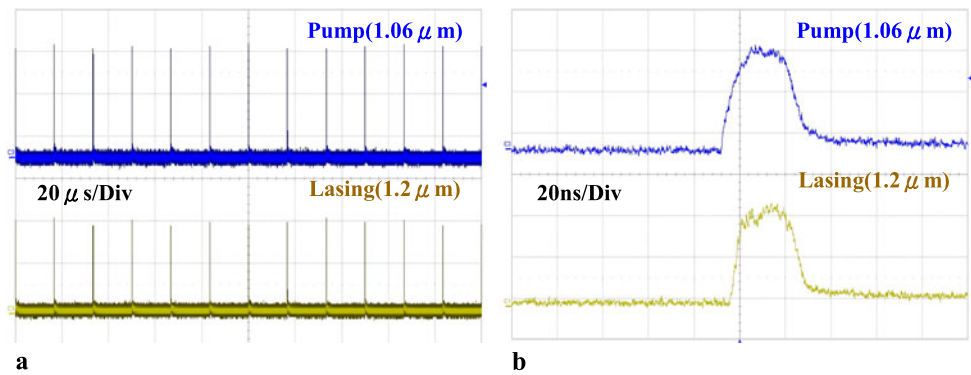


Fig. 6 Output performance with double chips at 60 kHz pump repetition rate and 28 ns pump pulse width

With a LeCroy digital oscilloscope (Wave pro 7100, 10 G samples/s, 1 GHz bandwidth), the typical input and output pulse train as well as the extended pulse shape of single pulse are shown in Fig. 5. It can be seen that the output pulse shape tracked the input pulses with barely delayed turn-on time due to the in-well pump scheme [18]. And the pulse-to-pulse fluctuation was found to be within $\pm 5\%$, which is mainly attributed to the instability of the pump beam.

To increase the average absorbed power of gain medium without the fabrication of more MQW, we insert another gain chip with the same MQW structure but without the dielectric coating and keep the same experimental setup as shown in Fig. 1. The absorption of double-chips scheme (82%) is 1.41 times higher than the single-chip scheme (58%). The highest average absorbed power is increased to 4 W before the roll-over effect appeared. In this setup, the thermal load is distributed to the two chips. Figure 6 shows the output characteristic of double-chips scheme operated under 60 kHz pump repetition rate and 28 ns pump pulse width. The average output power could be scaled to 1.28 W with 4 W average absorbed power at 1225 nm. Although this

method enhanced the absorption and dispersed the generated heat, the asynchronous PL emission due to the inhomogeneous heat distribution and the additional loss make the slope efficiency to be 37.5% which is lower than the single-chip scheme. With this setup, the peak output power is up to 0.76 kW at a peak pump power of 2.37 kW under the same pump conditions.

4 Conclusion

In summary, a high-peak-power semiconductor disk laser at 1.2 μm optically-pumped by a Yb-doped pulsed fiber amplifier has been developed. The gain medium is an AlGaInAs MQW structure grown on a Fe-doped InP substrate by metalorganic chemical-vapor deposition. With in-well pumping, we could reduce the thermal and roll-over effect by lowering the quantum defect. The average output power of 810 mW at 1225 nm lasing wavelength is generated at an average absorbed power of 2 W under 60 kHz pump repetition rate and 28 ns pump pulse width in the single-chip scheme. With the double chips, the average output power could be scaled up to 1.28 W at an average absorbed power of 4 W. The peak output power of 0.76 kW is obtained with 2.37 kW peak pump power.

Acknowledgements The authors gratefully acknowledge various AlGaInAs/InP gain chips from TrueLight Corporation. The authors also thank the National Science Council for their financial support of this research under Contract No. NSC-97-2112-M-009-016-MY3.

References

1. R.Q. Fugate, D.L. Fried, G.A. Ameer, B.R. Boeke, S.L. Browne, P.H. Roberts, R.E. Ruane, G.A. Tyler, L.M. Wopat, *Nature* **353**, 144 (1991)
2. R.E. Fitzpatrick, *Opt. Photonics News* **6**, 24 (1995)
3. A.D. Singh, M. Nouri, C.L. Shields, J.A. Shields, N. Perez, *Ophthalmology* **109**, 1799 (2002)
4. H.M. Pask, J.A. Piper, *Opt. Lett.* **24**, 1490 (1999)
5. A. Shirakawa, H. Maruyama, K. Ueda, C.B. Olausson, J.K. Lyngsø, J. Broeng, *Opt. Express* **17**, 447 (2009)

6. E.M. Dianov, A.V. Shubin, M.A. Melkumov, O.I. Medvedkov, I.A. Bufetov, *J. Opt. Soc. Am. B* **24**, 1749 (2007)
7. A.C. Tropper, H.D. Foreman, A. Garnache, K.G. Wilcox, S.H. Hoogland, *J. Phys. D* **37**, R75 (2004)
8. L. Fan, M. Fallahi, J.T. Murray, R. Bedford, Y. Kaneda, J. Harder, A.R. Zakharian, J.V. Moloney, S.W. Koch, W. Stolz, *Appl. Phys. Lett.* **88**, 021105 (2006)
9. M. Kuznetsov, F. Hakimi, R. Sprague, A. Mooradian, *IEEE Photonics Technol. Lett.* **9**, 1063 (1997)
10. L. Fan, C. Hessianus, M. Fallahi, J. Harder, H. Li, J.V. Moloney, W. Stolz, S.W. Koch, J.T. Murray, R. Bedford, *Appl. Phys. Lett.* **91**, 131114 (2007)
11. V.-M. Korpijärvi, T. Leinonen, J. Puustinen, A. Härkönen, D. Guina, *Opt. Express* **18**, 25633 (2010)
12. V.-M. Korpijärvi, M. Guina, J. Puustinen, P. Tuomisto, J. Rautiainen, A. Härkönen, A. Tukiainen, O. Okhotnikov, M. Pessa, *J. Cryst. Growth* **311**, 1868 (2009)
13. J. Rautiainen, I. Krestnikov, M. Butkus, E.U. Rafailov, O.G. Okhotnikov, *Opt. Lett.* **35**, 694 (2010)
14. M. Schmid, S. Benchabane, F. Torabi-Goudarzi, R. Abram, A.I. Ferguson, E. Riis, *Appl. Phys. Lett.* **84**, 4860 (2004)
15. J. Wagner, N. Schulz, M. Rattunde, C. Ritzenthaler, C. Manz, C. Wild, K. Köhler, *Phys. Status Solidi* **4**, 1594 (2007)
16. K.W. Su, S.C. Huang, A. Li, S.C. Liu, Y.F. Chen, K.F. Huang, *Opt. Lett.* **31**, 2009 (2006)
17. S.C. Huang, H.L. Chang, K.W. Su, A. Li, S.C. Liu, Y.F. Chen, K.F. Huang, *Appl. Phys. B* **94**, 483 (2009)
18. H.L. Chang, S.C. Huang, Y.-F. Chen, K.W. Su, Y.F. Chen, K.F. Huang, *Opt. Express* **17**, 11409 (2009)
19. P. Dupriez, A. Piper, A. Malinowski, J.K. Sahu, M. Ibsen, B.C. Thomsen, Y. Jeong, L.M.B. Hickey, M.N. Zervas, J. Nilsson, D.J. Richardson, *IEEE Photonics Technol. Lett.* **18**, 1013 (2006)
20. M.Y.A. Raya, S.R.J. Brueck, M. Osinsky, C.F. Schaus, J.G. Mcinery, T.M. Brennan, B.E. Hammons, *IEEE J. Quantum Electron.* **26**, 1500 (1989)
21. M.Y.A. Raya, S.R.J. Brueck, M.O. Scully, C. Lee, *Phys. Rev. A* **44**, 4599 (1991)
22. J.H. Biek, I.H. Choi, B. Lee, W.S. Han, H.K. Cho, *Appl. Phys. Lett.* **75**, 1500 (1999)
23. N. Nishiyama, C. Caneau, B. Hall, G. Guryanov, M.H. Hu, X.S. Liu, M.J. Li, R. Bhat, C.E. Zah, *IEEE J. Sel. Top. Quantum Electron.* **11**, 990 (2005)

Performance enhancement of sub-nanosecond diode-pumped passively Q-switched Yb:YAG microchip laser with diamond surface cooling

W. Z. Zhuang, Yi-Fan Chen, K. W. Su, K. F. Huang, and Y. F. Chen*

Department of Electrophysics, National Chiao Tung University, Hsinchu, Taiwan

*yfchen@cc.nctu.edu.tw

Abstract: We experimentally confirm that diamond surface cooling can significantly enhance the output performance of a sub-nanosecond diode-end-pumped passively Q-switched Yb:YAG laser. It is found that the pulse energy obtained with diamond cooling is approximately 1.5 times greater than that obtained without diamond cooling, where a Cr⁴⁺:YAG absorber with the initial transmission of 84% is employed. Furthermore, the standard deviation of the pulse amplitude peak-to-peak fluctuation is found to be approximately 3 times lower than that measured without diamond cooling. Under a pump power of 3.9 W, the passively Q-switched Yb:YAG laser can generate a pulse train of 3.3 kHz repetition rate with a pulse energy of 287 μ J and with a pulse width of 650 ps.

©2012 Optical Society of America

OCIS codes: (140.3480) Lasers, diode-pumped; (140.3320) Laser cooling; (140.3540) Lasers, Q-switched.

References and links

1. R. Bhandari and T. Taira, "> 6 MW peak power at 532 nm from passively Q-switched Nd:YAG/Cr⁴⁺:YAG microchip laser," *Opt. Express* **19**(20), 19135–19141 (2011).
2. Z. Zhuo, S. G. Li, T. Li, C. X. Shan, J. M. Jiang, B. Zhao, J. Li, and J. Z. Chen, "Diode-end-pumped passively Q-switched Nd:Y_{0.8}Lu_{0.2}VO₄ laser with Cr⁴⁺:YAG crystal," *Opt. Commun.* **283**(9), 1886–1888 (2010).
3. B. Y. Zhang, J. L. Xu, G. J. Wang, J. L. He, W. J. Wang, Q. L. Zhang, D. L. Sun, J. Q. Luo, and S. T. Yin, "Continuous-wave and passively Q-switched laser performance of a disordered Nd:GYSGG crystal," *Opt. Commun.* **284**(24), 5734–5737 (2011).
4. W. Z. Zhuang, W. C. Huang, Y. P. Huang, K. W. Su, and Y. F. Chen, "Passively Q-switched photonic crystal fiber laser and intracavity optical parametric oscillator," *Opt. Express* **18**(9), 8969–8975 (2010).
5. J. Liu, U. Griebner, V. Petrov, H. Zhang, J. Zhang, and J. Wang, "Efficient continuous-wave and Q-switched operation of a diode-pumped Yb:KLu(WO₄)₂ laser with self-Raman conversion," *Opt. Lett.* **30**(18), 2427–2429 (2005).
6. J. Dong, K. Ueda, and A. A. Kaminskii, "Efficient passively Q-switched Yb:LuAG microchip laser," *Opt. Lett.* **32**(22), 3266–3268 (2007).
7. D. S. Sumida and T. Y. Fan, "Effect of radiation trapping on fluorescence lifetime and emission cross section measurements in solid-state laser media," *Opt. Lett.* **19**(17), 1343–1345 (1994).
8. H. W. Bruesselbach, D. S. Sumida, R. A. Reeder, and R. W. Byren, "Low-heat high-power scaling using InGaAs-diode-pumped Yb:YAG lasers," *IEEE J. Sel. Top. Quantum Electron.* **3**(1), 105–116 (1997).
9. J. Dong, K. Ueda, A. Shirakawa, H. Yagi, T. Yanagitani, and A. A. Kaminskii, "Composite Yb:YAG/Cr⁴⁺:YAG ceramics picosecond microchip lasers," *Opt. Express* **15**(22), 14516–14523 (2007).
10. J. Dong, A. Shirakawa, K. Ueda, H. Yagi, T. Yanagitani, and A. A. Kaminskii, "Near-diffraction-limited passively Q-switched Yb:Y₃Al₅O₁₂ ceramic lasers with peak power >150kW," *Appl. Phys. Lett.* **90**(13), 131105 (2007).
11. J. Dong, A. Shirakawa, and K. Ueda, "Sub-nanosecond passively Q-switched Yb:YAG/Cr⁴⁺:YAG sandwiched microchip laser," *Appl. Phys. B* **85**(4), 513–518 (2006).
12. J. M. Hopkins, S. A. Smith, C. W. Jeon, H. D. Sun, D. Burns, S. Calvez, M. D. Dawson, T. Jouhti, and M. Pessa, "0.6 W CW GaInNAs vertical external-cavity surface emitting laser operating at 1.32 μ m," *Electron. Lett.* **40**(1), 30–31 (2004).
13. Y. Tzuk, A. Tal, S. Goldring, Y. Glick, E. Lebiush, G. Kaufman, and R. Lavi, "Diamond cooling of high-power diode-pumped solid-state lasers," *IEEE J. Quantum Electron.* **40**(3), 262–269 (2004).
14. P. Millar, A. J. Kemp, and D. Burns, "Power scaling of Nd:YVO₄ and Nd:GdVO₄ disk lasers using synthetic diamond as a heat spreader," *Opt. Lett.* **34**(6), 782–784 (2009).
15. P. Millar, R. B. Birch, A. J. Kemp, and D. Burns, "Synthetic diamond for intracavity thermal management in compact solid-state lasers," *IEEE J. Quantum Electron.* **44**(8), 709–717 (2008).

16. W. Koehler, *Solid State Laser Engineering* (Springer, 2006).
17. Y. Kalisky, C. Labbe, K. Waichman, L. Kravchik, U. Rachum, P. Deng, J. Xu, J. Dong, and W. Chen, "Passively Q-switched diode-pumped Yb:YAG laser using Cr⁴⁺-doped garnets," *Opt. Mater.* **19**(4), 403–413 (2002).
18. Q. Hao, W. Li, H. Pan, X. Zhang, B. Jiang, Y. Pan, and H. Zeng, "Laser-diode pumped 40-W Yb:YAG ceramic laser," *Opt. Express* **17**(20), 17734–17738 (2009).
19. J. Dong, J. Ma, Y. Cheng, Y. Y. Ren, K. Ueda, and A. A. Kaminskii, "Comparative study on enhancement of self-Q-switched Cr,Yb:YAG lasers by bonding Yb:YAG ceramic and crystal," *Laser Phys. Lett.* **8**(12), 845–852 (2011).
20. J. Dong, J. Li, S. Huang, A. Shirakawa, and K. Ueda, "Multi-longitudinal-mode oscillation of self-Q-switched Cr,Yb:YAG laser with a plano-concave resonator," *Opt. Commun.* **256**(1-3), 158–165 (2005).
21. J. Dong, A. Shirakawa, K. I. Ueda, and A. A. Kaminskii, "Effect of ytterbium concentration on cw Yb:YAG microchip laser performance at ambient temperature - Part I: Experiments," *Appl. Phys. B* **89**(2-3), 359–365 (2007).
22. J. Dong, A. Shirakawa, K. I. Ueda, and A. A. Kaminskii, "Effect of ytterbium concentration on cw Yb:YAG microchip laser performance at ambient temperature - Part II: Theoretical modeling," *Appl. Phys. B* **89**(2-3), 367–376 (2007).
23. D. C. Brown, "Ultrahigh-average-power diode-pumped Nd:YAG and Yb:YAG lasers," *IEEE J. Quantum Electron.* **33**(5), 861–873 (1997).
24. Q. Liu, X. Fu, M. Gong, and L. Huang, "Effects of the temperature dependence of the absorption coefficients in edge-pumped Yb:YAG slab lasers," *J. Opt. Soc. Am. B* **24**(9), 2081–2089 (2007).
25. J. Dong, M. Bass, Y. Mao, P. Deng, and F. Gan, "Dependence of the Yb³⁺ emission cross section and lifetime on temperature and concentration in yttrium aluminum garnet," *J. Opt. Soc. Am. B* **20**(9), 1975–1979 (2003).
26. T. Kasamatsu, H. Sekita, and Y. Kuwano, "Temperature dependence and optimization of 970-nm diode-pumped Yb:YAG and Yb:LuAG lasers," *Appl. Opt.* **38**(24), 5149–5153 (1999).
27. J. Dong and K. Ueda, "Temperature-tuning Yb:YAG microchip lasers," *Laser Phys. Lett.* **2**(9), 429–436 (2005).
28. M. Ostermeyer and A. Straesser, "Theoretical investigation of feasibility of Yb:YAG as laser material for nanosecond pulse emission with large energies in the Joule range," *Opt. Commun.* **274**(2), 422–428 (2007).
29. C. Li, Q. Liu, M. Gong, G. Chen, and P. Yan, "Q-switched operation of end-pumped Yb:YAG lasers with non-uniform temperature distribution," *Opt. Commun.* **231**(1-6), 331–341 (2004).
30. Y. F. Chen, K. W. Su, W. L. Chen, K. F. Huang, and Y. F. Chen, "High-peak-power optically pumped AlGaInAs eye-safe laser at 500-kHz repetition rate with an intracavity diamond heat spreader," *Appl. Phys. B* (to be published), doi:10.1007/s00340-012-4954-4.
31. Y. F. Chen, "High-power diode-pumped Q-switched intracavity frequency-doubled Nd:YVO₄ laser with a sandwich-type resonator," *Opt. Lett.* **24**(15), 1032–1034 (1999).
32. W. A. Clarkson and D. C. Hanna, "Efficient Nd:YAG laser end pumped by a 20-W diode-laser bar," *Opt. Lett.* **21**(12), 869–871 (1996).
33. J. J. Zayhowski, C. Dill III, C. Cook, and J. L. Daneu, "Mid-and high-power passively Q-switched microchip lasers," in *Proceeding of Advanced Solid-State Lasers*, M. M. Fejer, H. Injeyan, and U. Keller, eds., Vol. 26 of OSA Trends in Optics and Photonic Series (Optical Society of America, Washington, D. C., 1999), pp. 178–186.
34. J. J. Zayhowski, "Microchip lasers," *Opt. Mater.* **11**(2-3), 255–267 (1999).
35. J. J. Zayhowski, "Passively Q-switched Nd:YAG microchip lasers and applications," *J. Alloy. Comp.* **303–304**, 393–400 (2000).

1. Introduction

High-energy, compact diode-pumped passively Q-switched (PQS) solid state lasers with sub-nanosecond pulses have a variety of applications such as nonlinear frequency conversion, industrial processing, and remote sensing. Since Cr⁴⁺:YAG crystals possess high damage thresholds and high optical and thermal stabilities, they have been extensively applied as saturable absorbers in PQS laser systems such as Nd³⁺-doped lasers [1–3] and Yb³⁺-doped lasers [4–6]. Comparing with Nd:YAG crystals, Yb:YAG crystals have longer fluorescence lifetimes [7], smaller emission cross sections [8], low quantum defects, and broad absorption bandwidths [8]. Therefore, the Yb:YAG microchips have been employed to construct high-pulse-energy light sources with stability, compactness, and reliability [9–11].

The scaling of power and energy in Yb:YAG lasers are strongly impeded by the thermal effect because the quasi-three-level property of the Yb:YAG crystal causes the population on the lower level to significantly increase with rising temperatures. Therefore, efficient thermal management is highly desirable for enhancing the output performance of Yb:YAG PQS lasers. Recently, it has been demonstrated that the synthetic diamond is a promising heat spreader for thermal management in semiconductor disk lasers [12] and Nd-doped vanadate lasers [13–15] due to its excellent optical and mechanical properties together with high thermal conductivity. In addition, cooling along the direction of pumping is practically useful for reducing the thermal lensing and stress in microchip lasers [16, 17]. Even so, the

feasibility of cooling Yb:YAG microchip PQS lasers with diamond heat spreaders has never been explored thus far.

In this work, we explore the performance improvement of diode-end-pumped PQS Yb:YAG lasers with diamond windows as surface heat spreaders. Comparing with the results obtained without the diamond heat spreader, the pulse energy obtained with the diamond cooling is found to be enhanced by 1.5 times, where a Cr⁴⁺:YAG absorber with the initial transmission of 84% is used. Furthermore, the standard deviation of the pulse amplitude peak-to-peak fluctuation is approximately 3 times lower than that obtained without the diamond heat spreader. Under a pump power of 3.9 W, the passively Q-switched Yb:YAG laser can generate a pulse train of 3.3 kHz repetition rate with a pulse energy of 287 μ J and with a pulse width of 650 ps. More importantly, the optical-to-optical efficiencies are improved up to 58% and 25% for the continuous-wave (CW) and PQS operations, respectively.

2. Experimental setup

Figure 1 presents the schematic experimental setup. The gain medium was a 1-mm-long, 4 mm in diameter, and 11 at.% doped Yb:YAG crystal. One of the end facet of the crystal was coated with highly reflectivity (HR, R>98%) at 1030 nm and high-transmission (HT, T>95%) at 970 nm served as the front mirror, the other facet was with high-transmission (HT, T>95%) at 1030 nm and highly reflectivity (HR, R>95%) at 970 nm to increase the absorption efficiency of the pump power. The Cr⁴⁺:YAG crystal with initial transmission (T_0) of 84% and 1.4 mm in length was used as the saturable absorber. Both end facets of the Cr⁴⁺:YAG crystal were anti-reflection coated (AR, R<0.2%) at 1030 nm. The output coupler was a flat mirror with partially reflection at 1030 nm (R = 30%). The total cavity length was about 8.4 mm. The uncoated, single crystal synthetic diamond of 4.5 mm square and 0.5 mm thickness was used as the heat spreader and bounded to the front mirror side of the gain medium. The diamond plate was polished to laser quality with flatness of $\lambda/8$ at 632.8 nm and roughness of Ra smaller than 30 nm. The other side of the diamond was in contact with a copper heat sink cooled by a thermal-electric cooler at the temperature of 16°C. The side of the Yb:YAG crystal with the coating of HT at 1030 nm and HR at 970 nm was attached tightly to a copper plate with a hole of 2-mm diameter, where an indium foil was used to be the contact interface. The contact uniformity of the bounded interface between the diamond and the Yb:YAG crystal was further confirmed by means of inspecting the interference fringe resulting from the minute gap between the diamond heat spreader and the gain medium. The birefringence of the single crystal diamond was smaller than 5×10^{-4} . The transmittance of the diamond heat spreader was about 70% at 970 nm owing to the high refractive index contrasts of the air/diamond and diamond/Yb:YAG interfaces (The refractive index of the single crystal diamond is 2.432). The Cr⁴⁺:YAG crystal was wrapped within indium foil and mounted in a copper heat sink cooled by water at the temperature of 16°C. The pump source was an 8-W 970-nm fiber-coupled laser diode with a core diameter of 200 μ m and a numerical aperture of 0.20. Focusing lens with 25 mm focal length and 87% coupling efficiency is used to reimage the pump beam into the laser crystal. The pump diameter is approximately 120 μ m. Considering the coupling efficiency of the focusing lens, the transmittance of the diamond, and the effective absorption of the gain medium, the maximum available absorbed pump power is found to be 3.9 W. Note that without using the diamond heat spreader the maximum available absorbed pump power can be up to 5.6 W. The laser spectrum was measured by an optical spectrum analyzer with 0.1 nm resolution (Advantest Q8381A). The pulse temporal behavior was recorded by Agilent digital oscilloscope (infiniium DSO81204B; 40G samples/sec; 12 GHz bandwidth) with a fast InGaAs photodiode of 12.5 GHz bandwidth.

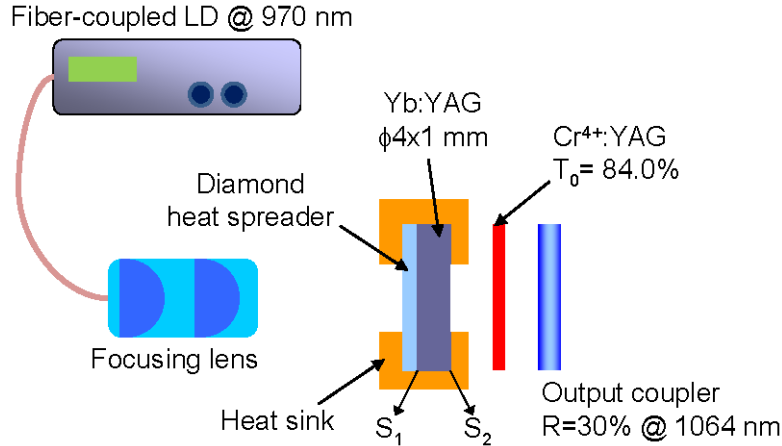


Fig. 1. The schematic diagram of the PQS Yb:YAG/Cr⁴⁺:YAG laser experimental setup. (S₁: HT at 970 nm, HR at 1030 nm; S₂: HT at 1030 nm, HR at 970 nm; HT: high transmission; HR: high reflection).

3. Experimental results and discussion

We firstly investigate the performance of the Yb:YAG laser with the diamond heat spreader under CW operation without the Cr⁴⁺:YAG crystal in place. Here, we use the output coupler with reflectivity of 80% at 1030 nm to maximize the output power around the wavelength of 1031 nm under CW operation. Figure 2 shows the average power with and without the diamond heat spreader with respect to the absorbed pump power. Without the diamond heat spreader, the output power was 1.3 W under an absorbed pump power of 3.9 W which corresponds to the optical-to-optical efficiency of 33% and the slope efficiency of 50%. The output power started to saturate and the slope efficiency decreased to 17% for an absorbed pump power of 5.6 W. The thermal effects induced power degradation has been widely observed in Yb-doped lasers [18–21] and has been theoretically confirmed [22]. Increasing the pump power, the detrimental effects in the Yb:YAG crystal become more severe including the decrease of the thermal conductivity [22] and the increase of the thermal expansion coefficient [23]. Furthermore, the absorption cross section and the emission cross section of the transitions between the manifolds ²F_{5/2} and ²F_{7/2} in the Yb:YAG crystal are significantly decreased with the increased temperature [24, 25] which lead to the reduction of the laser efficiency [16]. In contrast, the maximum output power was enhanced to 2.25 W under the pump power of 3.9 W when a diamond heat spreader was employed for surface cooling. The optical-to-optical efficiency and the slope efficiency were up to 58% and 86%, respectively.

Under the PQS operation, we change the reflectivity of the output coupler to be 30% at 1030 nm to prevent coating damages of the crystals due to the high intracavity intensity which have been observed in PQS Yb:YAG/Cr⁴⁺:YAG lasers [11]. Figure 3(a) depicts the averaged output power versus absorbed pump power under the PQS operation. Without the diamond heat spreader, the maximum output power was found to be limited at 0.47 W under the absorbed pump power of 5.6 W. Like the CW operation, the averaged output power without diamond cooling began to saturate when the absorbed pump power was greater than 4.5 W. On the contrary, the average output power with diamond cooling was 0.96 W at an absorbed pump power of 3.9 W, corresponding to the optical efficiency of 25% and the slope efficiency of 60%. Lower temperature in the Yb:YAG crystal can achieve lower threshold pump power [26] and higher optical efficiency [27] in Yb:YAG lasers. The lower threshold pump power (2.3 W for with diamond heat spreader and 2.8 W for without diamond heat spreader) and higher optical efficiency (25% for with diamond heat spreader and 8.3% for without diamond heat spreader) attained in our results show the effective thermal management of the diamond heat spreader. In comparison with the earlier results such as the self-Q-switched laser that

uses composite Yb:YAG/Cr⁴⁺:YAG ceramics [9] and the mechanical contacted Yb:YAG/Cr⁴⁺:YAG microchip lasers that adopt ceramics [10] or crystals [11], the diamond cooling scheme is confirmed to enhance the performance significantly. The lasing spectra for CW and PQS operations with the diamond heat spreader were quite similar with the peaks near 1031.7 nm and bandwidths to be approximately 0.2 nm, as shown in the inset of Fig. 3(a).

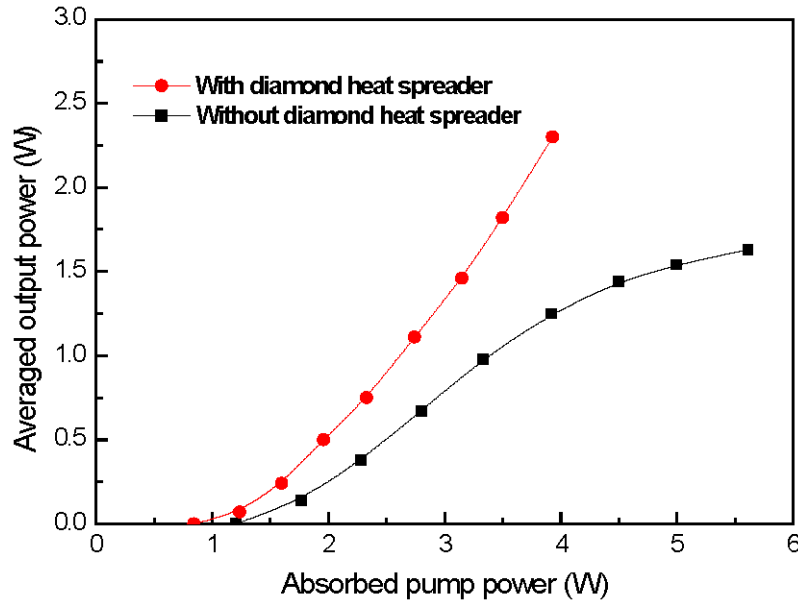


Fig. 2. Dependence of the averaged output power on the absorbed pump power under the CW operation.

Figure 3(b) shows the pulse energies obtained with and without the diamond heat spreader with respect to the absorbed pump power. It can be seen that the maximum pulse energies obtained without and with diamond cooling are approximately 190 μ J and 287 μ J, respectively. The Yb:YAG crystal, as a quasi-three-level laser gain medium, certainly suffers from the increase of the fractional thermal population on the lower laser level and the decrease of the fractional population on the upper laser level which decrease the maximum stored energy in the Yb:YAG crystal [28] for increasing the pump power. Furthermore, the strong thermal lensing in the end-pumped Yb:YAG microchip laser which results from the thermal gradients within the gain medium [17] usually leads to a smaller cavity mode size that will reduce the output pulse energy [29]. Millar et al. [15] and our previous results [30] in semiconductor disk lasers which use diamond heat spreader for thermal management of the gain medium have evidence its effectualness. Smaller red-shift in wavelength when the diamond heat spreader was in place [15, 30] confirms that the gain medium heating to be considerably improved by using the diamond heat spreader. By using the same diamond heat spreader and the same bounding method of the diamond/gain medium composite as in this experiment, our previous result [30] shows that the gain medium temperature rise per unit pump power ($\Delta T/\Delta P$) are 20.5 K/W and 3.3 K/W for without and with the diamond heat spreader. The temperature rise in the diamond-gain medium composite is 6.2 times lower than in the gain medium without a diamond heat spreader, emphasizing the efficiency of the diamond heat spreader for thermal management. Besides, Millar et al. [15] theoretically simulates that using the diamond heat spreader can effectively reduce the maximum temperature rise together with temperature gradients and decrease the thermal stress and distortion in Yb:YAG lasers. Our experimental results confirm that diamond cooling is truly an efficient thermal management for the Yb:YAG microchip laser to enhance the output

performance. To the best of our knowledge, this is the highest pulse energy obtained with Yb:YAG/Cr⁴⁺:YAG microchip laser. The overall pulse energy scaling was 1.9 times as high as the one in Ref [9], 5.7 times as that in Ref [10], and 22 times as that in Ref [11]. The diamond heat spreader not only reduces the maximum temperature rise in the gain medium to enhance the laser efficiency but also decreases the thermal-induced bending and bowing of the gain medium to improve the beam distortion [15, 16]. Furthermore, bounding the diamond heat spreader to the pumped side of the gain medium makes the temperature distribution more uniform [16] that reduces the thermal lens in the Yb:YAG crystal and prevents the cavity mode size from shrinking as the result of the thermal lens effect [31, 32].

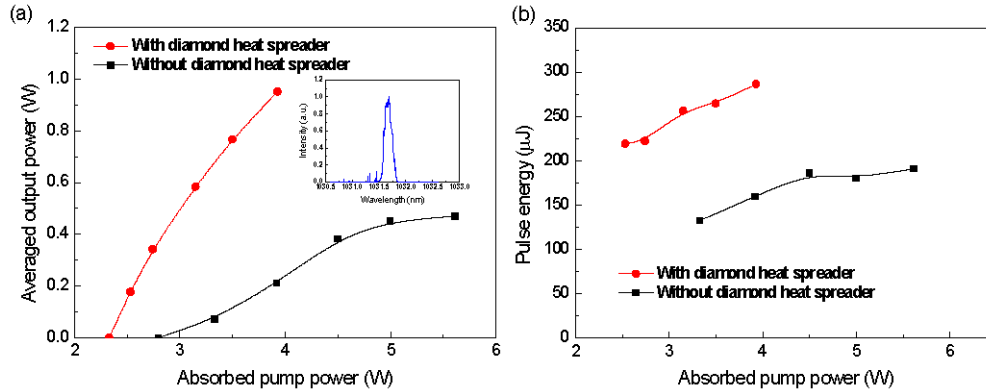


Fig. 3. (a) Dependence of the averaged output power on the absorbed pump power under the PQS operation, the inset: typical lasing spectrum. (b) Dependence of the pulse energy on the absorbed pump power.

Figures 4(a) and 4(b) show the oscilloscope traces obtained with and without diamond cooling, respectively, for the single pulse of the PQS Yb:YAG/Cr⁴⁺:YAG laser at the maximum absorbed pump powers. The pulse widths can be seen to be 650 ps and 764 ps for the operations with and without diamond cooling, respectively. With the pulse energy shown in Fig. 3(b), the peak powers obtained with and without diamond cooling can be calculated to be 442 kW and 262 kW, respectively. In other words, diamond cooling enhances the peak power by a factor of 1.7 times.

Zayhowski et al. demonstrated PQS microchip lasers constructed of diffusion-bounded Nd:YAG/Cr⁴⁺:YAG crystals [33–35]. By optically bounding a 4-mm-long Nd:YAG crystal doped with 1.1 at.% Nd³⁺ ions and a 2.25-mm-thick Cr⁴⁺:YAG, laser pulses with pulse energy of 250 μJ and pulse width of 380 ps at the pulse repetition rate of 1 kHz were obtained under 15 W of pump power, the corresponding peak power of 565 kW was attained. Compared to our result of Yb:YAG/Cr⁴⁺:YAG laser, although the pulse width achieved by Nd:YAG/Cr⁴⁺:YAG laser was shorter than ours owing to the shorter laser resonator, the optical-to-optical efficiency was less than 2% which was much inferior to ours of 25%. Besides, the Nd:YAG/Cr⁴⁺:YAG laser can only be pulse pumped which limited the pulse repetition rate to be merely up to 1 kHz as the result of the thermal effects. At higher repetition rates, the pulse energy of the Nd:YAG/Cr⁴⁺:YAG laser decreased due to the cavity mode shrinking induced by the thermal lens effect. The output pulses start to bifurcate with varied pulse amplitudes in different longitudinal and polarization modes when the laser was CW pumped [33]. Our results provide the solution for improved thermal management by using a diamond heat spreader in the Yb:YAG/Cr⁴⁺:YAG laser, nevertheless, this method also can be expected to be useful in the Nd:YAG/Cr⁴⁺:YAG system.

Figures 5(a) and 5(b) depict the typical oscilloscope traces measured with and without the diamond heat spreader, respectively, for the Q-switched pulse trains at the maximum absorbed pump powers. The standard deviations of the pulse amplitude peak-to-peak fluctuations are analyzed to be approximately 3% and 9% for the operations with and without

the diamond heat spreader, respectively. The pulse amplitude fluctuation with the heat spreader is also superior to the earlier results such as 6% in Ref [9], and 8% in Ref [10], demonstrating an effective improvement in the PQS stability.

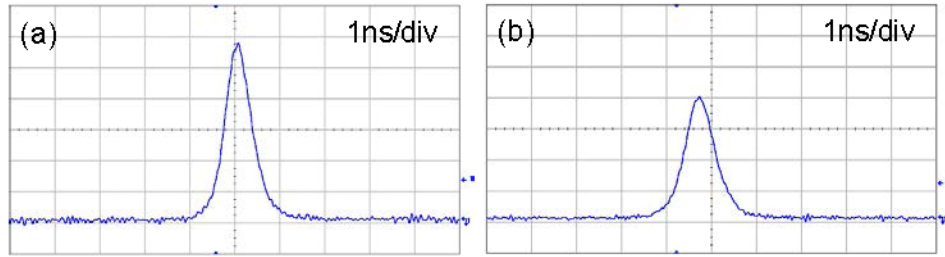


Fig. 4. Oscilloscope traces of a single pulse of the output pulse of (a) with the diamond heat spreader, (b) without the diamond heat spreader.

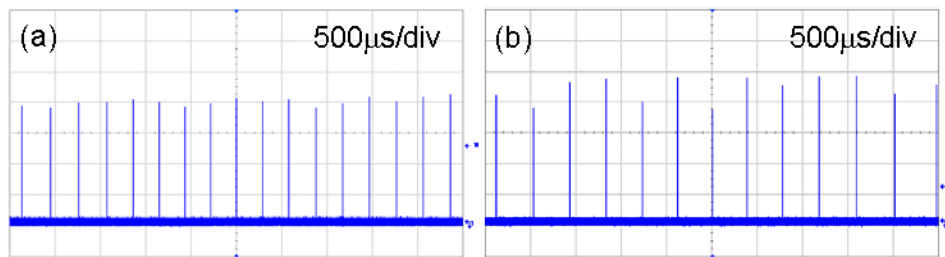


Fig. 5. Oscilloscope traces of a train of output pulses of (a) with the diamond heat spreader, (b) without the diamond heat spreader.

4. Conclusions

We have experimentally confirmed that employing diamond windows as surface heat spreaders can remarkably improve the performance of diode-end-pumped PQS Yb:YAG lasers. The pulse energy obtained with the diamond cooling was found to be 1.5 times higher than that obtained without the diamond heat spreader, where a Cr⁴⁺:YAG absorber with the initial transmission of 84% was employed in experiment. Under a pump power of 3.9 W, a pulse train of 3.3 kHz repetition rate could be efficiently generated from the passively Q-switched Yb:YAG laser with a pulse energy of 287 μ J and with a pulse width of 650 ps. In addition, the optical-to-optical efficiencies were found to be improved up to 58% and 25% for the CW and PQS operations, respectively. The standard deviations of the pulse amplitude peak-to-peak fluctuations were measured to be approximately 3% and 9% for the operations with and without the diamond heat spreader, respectively. This result indicates that the amplitude fluctuation obtained with diamond cooling was approximately 3 times lower than that obtained without diamond cooling.

Acknowledgments

The author thanks the National Science Council for their financial support of this research under Contract No. NSC100-2628-M-009-001-MY3.

Efficient high-peak-power AlGaInAs eye-safe wavelength disk laser with optical in-well pumping

H. L. Chang, S. C. Huang, Yi-Fan Chen, K. W. Su*, Y. F. Chen*, and K. F. Huang

Department of Electrophysics, National Chiao Tung University, Hsinchu 30013, Taiwan

**sukuanwei@mail.nctu.edu.tw, yfchen@cc.nctu.edu.tw*

Abstract: We have demonstrated an efficient high-peak-power AlGaInAs eye-safe wavelength disk laser at 1555 nm. The quantum defect and the thermal load are significantly reduced by pumping the quantum well directly. The overall conversion efficiency is enhanced over three times compared with the barrier pumping method. With a pump peak power of 3.7 kW, an output peak power of 0.52 kW is generated at a pulse repetition rate of 20 kHz.

©2009 Optical Society of America

OCIS codes: (140.3380) Laser materials; (140.3480) diode-pumped; (140.3538) Lasers, pulsed

References and links

1. S. M. Spuler, and S. D. Mayor, "Raman shifter optimized for lidar at a 1.5 microm wavelength," *Appl. Opt.* **46**(15), 2990–2995 (2007).
2. G. S. Mecherle, ed., *Free-Space Laser Communication Technologies XIII*, San Jose, CA, 24 to 25 January 2001, *Proc. SPIE* **4272** (2001).
3. A. J. McGrath, J. Munch, G. Smith, and P. Veitch, "Injection-seeded, single-frequency, q-switched erbium:glass laser for remote sensing," *Appl. Opt.* **37**(24), 5706–5709 (1998).
4. S. Taccheo, P. Laporta, S. Longhi, O. Svelto, and C. Svelto, "Diode-pumped bulk erbium–ytterbium lasers," *Appl. Phys. B* **63**, 425–436 (1996).
5. I. Sokólska, E. Heumann, S. Kück, and T. Łukasiewicz, "Laser oscillation of Er³⁺:YVO₄ and Er³⁺, Yb³⁺:YVO₄ crystals in the spectral range around 1.6 μm," *Appl. Phys. B* **71**, 893–896 (2000).
6. S. Kück, K. Petermann, U. Pohlmann, and G. Huber, "Near-infrared emission of Cr⁴⁺-doped garnets: Lifetimes, quantum efficiencies, and emission cross sections," *Phys. Rev. B* **51**(24), 17323–17331 (1995).
7. F. F. Su, X. Y. Zhang, Q. P. Wang, S. H. Ding, P. Jia, S. T. Li, S. Z. Fan, C. Zhang, and B. Liu, "Diode pumped actively Q-switched Nd:YVO₄ self-Raman laser," *J. Phys. D Appl. Phys.* **39**(10), 2090–2093 (2006).
8. S. H. Ding, X. Y. Zhang, Q. P. Wang, F. F. Su, P. Jia, S. T. Li, S. Z. Fan, J. Chang, S. S. Zhang, and Z. J. Liu, "Theoretical and experimental study on the self-Raman laser with Nd:YVO₄ crystal," *IEEE J. Quantum Electron.* **42**(9), 927–933 (2006).
9. H. Jianhong, L. Jipeng, S. Rongbing, L. Jinghui, Z. Hui, X. Canhua, S. Fei, L. Zongzhi, Z. Jian, Z. Wenrong, and L. Wenxiong, "Short pulse eye-safe laser with a stimulated Raman scattering self-conversion based on a Nd:KGW crystal," *Opt. Lett.* **32**(9), 1096–1098 (2007).
10. H. T. Huang, J. L. He, X. L. Dong, C. H. Zuo, B. T. Zhang, G. Qiu, and Z. K. Liu, "High-repetition-rate eye-safe intracavity KTA OPO driven by a diode-end-pumped Q-switched Nd:YVO₄ laser," *Appl. Phys. B* **90**(1), 43–45 (2008).
11. Y. F. Chen, S. W. Chen, Y. C. Chen, Y. P. Lan, and S. W. Tsai, "Compact efficient intracavity optical parametric oscillator with a passively Q-switched Nd:YVO₄/Cr⁴⁺:YAG laser in a hemispherical cavity," *Appl. Phys. B* **77**(5), 493–495 (2003).
12. Y. F. Chen, and L. Y. Tsai, "Comparison between shared and coupled resonators for passively Q-switched Nd:GdVO₄ intracavity optical parametric oscillators," *Appl. Phys. B* **82**(3), 403–406 (2006).
13. C. E. Zah, R. Bhat, B. N. Pathak, F. Favire, W. Lin, M. C. Wang, N. C. Andreadakis, D. M. Hwang, M. A. Koza, T. P. Lee, Z. Wang, and D. Darby, D. Flanders, and J. J. Heieh, "High-performance uncooled 1.3-μm Al Ga In As/InP strained-layer quantum-well lasers for subscriberloop applications," *IEEE J. Quantum Electron.* **30**(2), 511–521 (1994).
14. J. Minch, S. H. Park, J. Minch, and S. L. Chuang, "Theory and Experiment of InGaAsP and InGaAlAs long-wavelength strained quantum-well lasers," *IEEE J. Quantum Electron.* **35**, 771–782 (1999).
15. S. R. Šelmić, G. A. Evans, T. M. Chou, J. B. Kirk, J. N. Walpole, J. P. Donnelly, C. T. Harris, and L. J. Missaggia, "Single frequency 1550-nm AlGaInAs-InP tapered high-power laser with a distributed Bragg reflector," *IEEE Photon. Technol. Lett.* **14**(7), 890–892 (2002).
16. N. Nishiyama, C. Caneau, B. Hall, G. Guryanov, M. Hu, X. Liu, M. J. Li, R. Bhat, and C. E. Zah, "Long-wavelength vertical-cavity surface-emitting lasers on InP with lattice matched AlGaInAs-InP DBR grown by MOCVD," *IEEE J. Sel. Top. Quantum Electron.* **11**(5), 990–998 (2005).

17. N. J. M. Hopkins, A. J. Kemp, N. Schulz, M. Rattunde, J. Wagner, M. D. Dawson, and D. Burns, "Pulsed pumping of semiconductor disk lasers," *Opt. Express* **3**, 3247–3256 (2007).
18. S. Calvez, N. Laurand, H. D. Sun, J. Weda, D. Burns, M. D. Dawson, A. Harkonen, T. Jouhti, M. Pessa, M. Hopkinson, D. Poitras, J. A. Gupta, C. G. Leburn, C. T. A. Brown, and W. Sibbett, "GaInNAs(Sb) surface normal devices," *Phys. Status Solidi* **205**(1), 85–92 (2008).
19. S. C. Huang, H. L. Chang, K. W. Su, A. Li, S. C. Liu, Y. F. Chen, and K. F. Huang, "AlGaInAs/InP eye-safe laser pumped by a Q-switched Nd:GdVO₄ laser," *Appl. Phys. B* **94**(3), 483–487 (2009).
20. M. Schmid, S. Benchabane, F. Torabi-Goudarzi, R. Abram, A. I. Ferguson, and E. Riis, "Optical in-well pumping of a vertical-external-cavity surface-emitting laser," *Appl. Phys. Lett.* **84**(24), 4860–4862 (2004).
21. J. Wagner, N. Schulz, M. Rattunde, C. Ritzenthaler, C. Manz, C. Wild, and K. Köhler, "Barrier- and in-well pumped GaSb-based 2.3 μm VECSELs," *Phys. Status Solidi* **4**(5), 1594–1600 (2007).
22. J. J. Zayhowski, and A. Mooradian, "Single-frequency microchip Nd lasers," *Opt. Lett.* **14**(1), 24–26 (1989).
23. G. J. Dixon, L. S. Lingvay, and R. H. Jarman, "Properties of close coupled monolithic, lithium neodymium, tetrphosphate lasers," *Proc. SPIE* **1104**, 107 (1989).

1. Introduction

High-peak-power lasers operated at the eye-safe region near 1.5-1.6 μm have been attracting versatile interesting applications including laser radars, range finders, active imaging, and telemetry [1–3]. The radiation within this spectral region is absorbed mainly in the ocular fluid of the eye before the retina such that the damage threshold of the eye is greatly increased. There are several ways in realizing eye-safe laser sources. Directly utilizing gain materials such as Er:Yb:glass [4,5] or Cr⁴⁺:YAG [6] in solid-state lasers for generating 1.54-μm radiation are commonly used while the poor thermal conductivity of Erbium glass restricts their use for high power pumping. Stimulated Raman scattering (SRS) lasers pumped by pulsed neodymium (Nd) lasers operating at the 1064 nm or 1340 nm lines [7–9], and optical parametric oscillators (OPO) pumped by high peak power Nd lasers [10–12] are alternative methods for generating high-peak-power eye-safe lasers.

The lasers based on semiconductor quantum-well (QW) materials including InGaAsP, AlGaInAs, and GaInAsSb system [13–18] provide another practical method for generating the radiation at the eye-safe region. Recently, an optically pumped high-peak-power AlGaInAs eye-safe laser at 1.57 μm pumped by an actively-Q-switched 1064-nm laser was demonstrated [19]. In the gain region of AlGaInAs QW/barrier, the electrons are excited from the ground state to an excited state in the barrier region with band-gap wavelength around 1064 nm, and emit photons with wavelength of 1.57 μm in the QW region. Such a scheme could generate high peak power of hundreds of watt with quite low lasing threshold. However, the quantum defect between the pump photon and lasing photon would give rise to heat generation and influence the performance for the operation of high repetition rate and high pump power.

Recently, the quantum defect and the thermal load were confirmed to be significantly reduced by pumping the QW directly [20,21]. In this work, we employ the in-well pumping scheme to excite AlGaInAs QWs for efficient eye-safe emission at 1.56 μm. The gain medium is an AlGaInAs QW structure grown on a Fe-doped InP transparent substrate and is pumped by an actively Q-switched 1342 nm laser which directly excites the electrons to an excited state in the QW region rather than in the barrier region. As depicted in Fig. 1, electrons are excited in the QW region and the quantum defect between pump photon and lasing photon is reduced from 32% to 14% compared with a pump source at 1064 nm. As a result, the thermal effect is significantly reduced. Experimental result shows that the optical conversion efficiency is up to 30% and is enhanced over three times compared with the barrier pumping method. A high peak output power of 0.52 kW can be generated at a pulse repetition rate of 20 kHz and a pump peak power of 3.7 kW.

2. Device fabrication and experimental setup

Figure 2 shows the experimental configuration for the AlGaInAs QWs 1555-nm laser pumped by a diode-pumped actively Q-switched Nd:YVO₄ laser at 1342 nm. The pump source provides 20~110-ns pulse width between 20 kHz and 100 kHz. For comparison, a 1064-nm Q-switched laser was used in barrier-pumping scheme. The pump spot radius was controlled to be 70-100 μm by a focusing lens to maintain the spatial overlapping between lasing mode and

pump mode. To simplify the cavity structure, the resonator is designed to be a flat-flat cavity stabilized by thermal lens effect of gain medium [22,23]. Although the thermal lens is reduced in in-well pumping, the effect is still strong enough to stabilize the cavity. For the pump power between 0.4 W and 1.7 W, the mode to pump size was experimentally measured to be 0.6-0.9. The front mirror of resonator is a flat mirror coated with anti-reflection coating at pumping wavelength ($R < 0.2\%$) on the entrance surface, and with high-reflection coating at 1555 nm ($R > 90\%$) as well as high-transmission coating at pumping wavelength ($T > 80\%$) on the other surface. The output coupler is a flat mirror with partial reflection of 90% at 1555nm and 60% at pumping wavelength. The overall laser cavity length is approximately 5 mm.

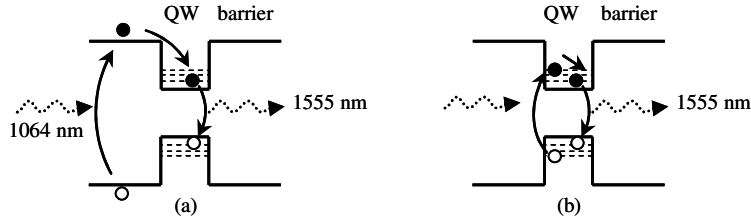


Fig. 1. Schematic explanation of energy diagrams of (a) barrier pumping and (b) in-well pumping.

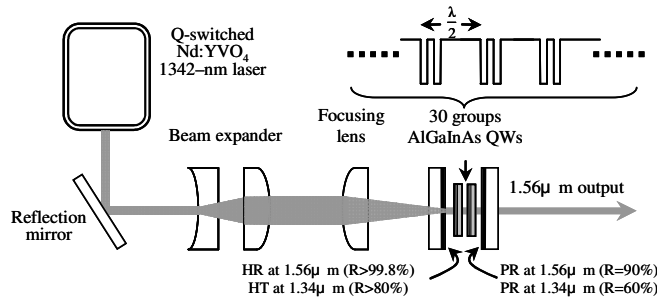


Fig. 2. The schematic of the AlGaInAs/InP eye-safe laser at 1555 nm. HR: high reflection; HT: high transmission; PR: partial reflection.

The gain medium is a structure of AlGaInAs QW/barrier grown on a Fe-doped InP substrate by metalorganic chemical-vapor deposition. The optically active region consists of 30 pairs of AlGaInAs QW/barrier. Each pair contains two 8-nm-thick QWs and 10-nm-thick barrier. The band-gap wavelength of barrier is around 1064 nm and of quantum well is around 1555 nm. In order to get a resonant periodic gain, each group of quantum wells is designed to be located at the antinodes of the lasing mode, or to have intervals of half-wavelength separated by barriers. A window layer of InP was deposited on the gain structure to prevent surface recombination and oxidation. Both surfaces of the gain chip were coated to have anti-reflection coating at pumping and lasing wavelength. The active gain medium was adhered to a water-cooled copper heat sink and the temperature was controlled by water feedback. Figure 3(a) depicts the transmission spectrum of the gain medium and Fig. 3(b) shows the room-temperature spectrum of photoluminescence (PL) obtained by pulse excitation at 1342 nm. It can be seen that there is a high absorption at the pump wavelength of 1342 nm and the spectrum of emission extends more than 200 nm with a peak at the wavelength of 1555 nm.

It is worthwhile to mention that due to the shorter effective thickness of quantum well, the active gain region has lower absorption at 1342-nm pump wavelength than at 1064 nm which has single pass absorption higher than 95%. In order to increase the absorption efficiency, double chips were further used in the serial experiments. The advantage of directly using multiple chips is that could reduce the difficulty of fabrication of gain medium with more quantum wells. The experimental result shown in Fig. 3(c) reveals that the single pass

absorption efficiency was increased from 45% to 65% when double chips were employed. Total effective absorption efficiency in the cavity could be estimated to be 60% and 79%, respectively. On the other hand, the effective absorption efficiency for single chip could be up to 70% by using an output coupler with retro-reflection at pump wavelength.

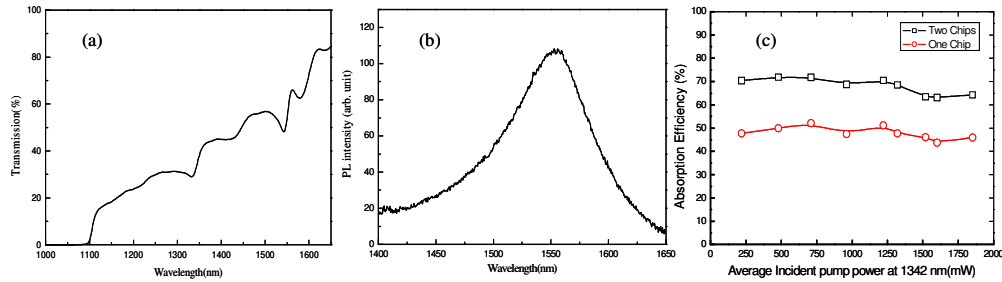


Fig. 3. (a) The transmission spectrum of AlGaInAs QWs. (b) the room-temperature spectrum of photoluminescence pumped by an actively Q-switched Nd:YVO₄ 1342-nm laser. (c) The single pass absorption efficiency of single and double AlGaInAs QW chips.

3. Experimental results and discussions

Figure 4 shows the comparison of average output power of single gain chip with in-well and barrier pumping for the operation of 40 kHz repetition rate and 12°C temperature. The maximum values shown in the two curves were measured for the comparable incident pumping power. The solid lines are fourth order polynomial fitting curves. It can be seen that employing the 1342-nm laser as a pump source exhibits good performance in conversion efficiency. This significant improvement result is contributed from the heat reduction by lowering the quantum defect which is diminished from 32% to 14%. However, since the absorption efficiency of gain medium at 1342 nm is lower than at 1064 nm, the available pump power is restricted. Double gain chips, accordingly, were investigated to improve the absorption efficiency. The earlier onset of thermal rollover in in-well pumping shows that further thermal management may be desired to delay the thermal rollover such as lower operating temperature or bonding a diamond heat spreader.

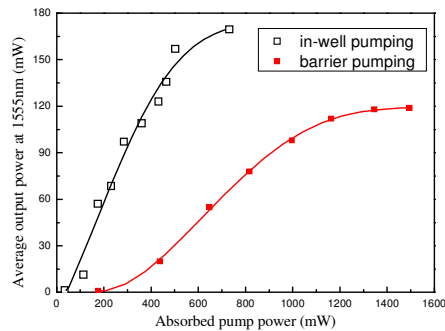


Fig. 4. The performance of single-chip AlGaInAs 1555-nm laser for 40 kHz and 12°C operation in the scheme of barrier and in-well pumping, respectively. The solid lines are fourth order polynomial fitting curves. The in-well pumping scheme exhibits good performance in conversion efficiency.

Figure 5(a) shows the performance of the optically pumped AlGaInAs eye-safe laser with double gain chips operated at 12°C for different pump repetition rate from 20 kHz to 100 kHz in 20 kHz interval. The corresponding average pump pulse width ranges from 20 ns to 110 ns with increasing repetition rate and therefore a decreasing peak power of pulse is corresponded. In the process of increasing the repetition rate for the given cavity and absorbed pump power, the conversion efficiency was limited by instantaneous high peak power which resulted in a rapid temperature rise in low repetition rate and limited by high average power

which resulted in an average temperature rise in high repetition rate. Therefore, there was an optimum repetition rate for obtaining the maximum average output power. This conclusion is coincident to the result of the experiment and the published research [19]. From the experimental results shown in Fig. 5(a), the optimum repetition rate was between 40 kHz and 60 kHz. Figure 5(b) shows the typical lasing spectrum for the operation of 40-kHz repetition rate with average pump power of 0.65 W. The spectral bandwidth was approximately 17 nm. The filamented spectrum may result from multiple interferences between cavity mirrors and chips and it could also be observed in single chip operation.

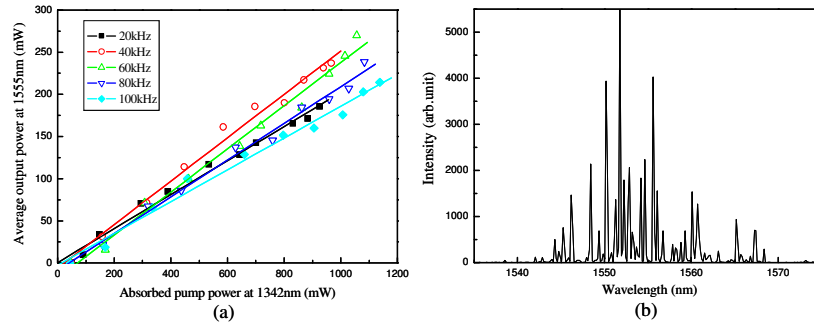


Fig. 5. Performance of double chips: (a) Experimental results for the optically pumped AlGaInAs eye-safe laser operated at 12 °C for several pulse repetition rates. The repetition rate for optimum performance of conversion efficiency was between 40 kHz and 60 kHz. (b) Typical lasing spectrum at repetition rate of 40 kHz and average pump power of 0.65 W

In order to further realize the influence of thermal effect, the average output power versus pump power was measured for different operating temperature, 9 °C, 15 °C, 20 °C, and 25 °C, at 50 kHz repetition rate and the result was shown in Fig. 6. Increase of temperature leads to the reduction of conversion efficiency and this result demonstrates the reduction of quantum defect is a practical way to improve optical conversion efficiency. The optical conversion efficiency could be up to 30% under the operating temperature of 9 °C. Compared with barrier pumping which shows an optimum efficiency in 30 kHz repetition rate, the optical conversion efficiency exceeds 3 times and over 20% of enhancement was obtained.

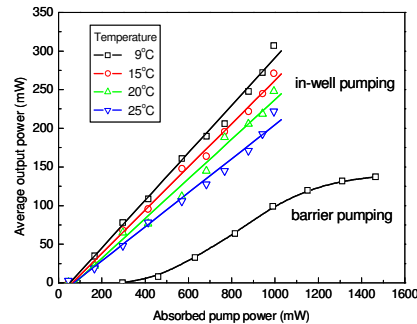


Fig. 6. The output characteristics of double chips in in-well pumping and of single chip in barrier pumping were measured for the operation of different temperature. In-well pumping was operated in 50 kHz repetition rate, while barrier pumping in 30 kHz for optimum conversion efficiency. The result shows the influence of thermal effect on conversion efficiency.

The operation of 20-kHz pulse repetition rate was chosen to evaluate the performance of output peak power due to shorter pulse and available maximum pump peak power. For the operation at the temperature of 9 °C, the output peak power from double chips at 1555 nm versus the absorbed pump power at pulse repetition rate of 20 kHz was measured and shown in Fig. 7. At the pump peak power of 3.7 kW, the maximum output peak power up to 0.52 kW was generated. The typical pump and output pulse train as well as extended pulse shape of

single pulse was recorded by a Lecroy digital oscilloscope (Wave pro 7100, 10G samples/sec, 1 GHz bandwidth) and shown in Fig. 8. The output pulse with long tail follows in the characteristic of pump source. But the turn-on time of output pulse is slightly different between in-well and barrier pumping [19], where the former has a nearly 10-ns advance. The output peak power fluctuates within 10% variation and it mainly comes from the fluctuation of pump source. Experimental result shows that the output beam possesses an excellent beam quality. The half divergence angle of output beam was measured by using knife-edge method to be approximately 0.01 rad. Consequently, the M square value was estimated to be smaller than 1.3.

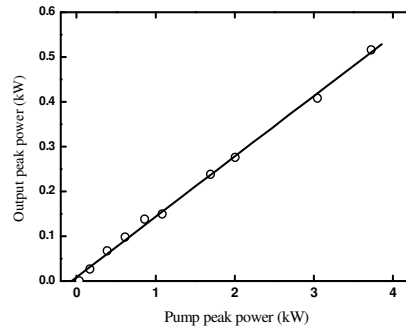


Fig. 7. The output peak power of double-chip AlGaInAs eye-safe laser at repetition rate of 20 kHz. At the pump peak power of 3.7 kW, the output peak power is up to 0.52 kW.

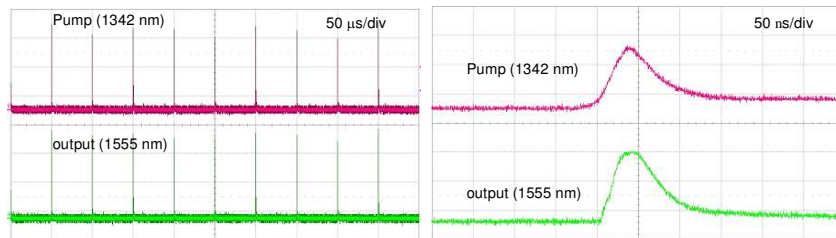


Fig. 8. The typical pump and output pulse train and the expanded pulse shape of a single pulse.

4. Conclusions

We have demonstrated an optically pumped high-peak-power AlGaInAs/InP eye-safe laser by using a pump method with lower quantum defect. The pump source is an actively Q-switched 1342-nm laser. With lower quantum defect, the thermal effect in gain medium decreases and results in improvement of optical conversion efficiency. The conversion efficiency is enhanced over three times compared with conventional pumping method. Double gain chips were used to increase the absorption efficiency of pump laser and a high peak output power of 0.52 kW was generated at a pulse repetition rate of 20 kHz and peak pump power of 3.7 kW.

Acknowledgments

The authors gratefully acknowledge various AlGaInAs/InP gain chips from TrueLight Corporation. The authors also thank the National Science Council for their financial support of this research under Contract No. NSC-95-2745-M-009-001.

Diode-pumped passively mode-locked 1342 nm Nd:YVO₄ laser with an AlGaInAs quantum-well saturable absorber

S. C. Huang, H. L. Cheng, Yi-Fan Chen, K. W. Su, Y. F. Chen,* and K. F. Huang

Department of Electrophysics, National Chiao Tung University, Hsinchu 300, Taiwan

*Corresponding author: yfchen@cc.nctu.edu.tw

Received May 26, 2009; revised July 9, 2009; accepted July 10, 2009;
posted July 16, 2009 (Doc. ID 111900); published July 29, 2009

We demonstrate what we believe to be the first use of AlGaInAs quantum wells (QWs) as a saturable absorber for a diode-pumped passively mode locked Nd:YVO₄ laser at 1342 nm. The QWs are grown on a Fe-doped InP substrate that is transparent at lasing wavelength. At an incident pump power of 13.5 W an average output power of 1.05 W with a continuous mode-locked pulse duration of 26.4 ps at a repetition rate of 152 MHz was generated. © 2009 Optical Society of America

OCIS codes: 140.4050, 140.3580, 140.3480.

Diode-pumped solid-state lasers at 1.3 μm have a wide variety of applications such as telecommunication, fiber sensing, ranging, and data storage. As a potentiality, numerous Nd-doped crystals have been employed for developing 1.3 μm lasers at cw or pulsed operation [1–6]. Passive mode locking with GaAs-based semiconductor saturable absorber mirrors (SESAMs) has been extensively used for the generation of ultrashort pulses in the 0.8–1.1 μm spectral range [7,8]. However, it is rather difficult to design InGaAs SESAMs for 1.3 μm lasers, because the required indium concentrations are beyond the critical strain-thickness limit. So far, two new schemes based on the GaAs substrate have been exploited to design SESAMs near 1.3 and 1.5 μm . One approach is the use of the quaternary alloy GaInNAs quantum wells (QWs) with low nitrogen concentrations in the active region [9–11]; the other technique is the use of the InAs/GaAs quantum-dot (QD) multilayer structures [12]. Nevertheless, the characteristic of the GaInNAs QWs is subject to drastic bandgap blueshift when exposed to annealing. On the other hand, the epi-wafer of the InAs QDs usually suffers from the uniformity of optical characteristics. Therefore it is highly desirable to develop a superior saturable absorber for passively mode-locked lasers in the 1.3–1.6 μm spectral range.

Since the quaternary alloys of InGaAsP and AlGaInAs can be grown epitaxially on an InP substrate without lattice mismatch in the 0.84–1.65 μm spectral region, they have been confirmed to be promising materials for optoelectronic devices [13,14]. The InGaAsP QWs have been used as saturable absorbers in Q-switched lasers at 1.34 μm [15,16] and mode-locked lasers at 1.55 μm [17]. Compared with InGaAsP materials, the AlGaInAs quaternary alloy with a larger conduction band offset can provide a better electron confinement covering the same wavelength region [18,19]. Although AlGaInAs/InP QWs have been designed to passively Q-switch lasers at 1.06 μm and 1.56 μm [20,21], to our knowledge they have not yet been exploited to mode lock a laser. In this Letter we design and fabricate AlGaInAs QWs to

be a saturable absorber in a diode-pumped Nd:YVO₄ laser at 1.34 μm . With an incident pump power of 13.5 W, we obtain an average output power of 1.05 W with a stable continuous-mode-locked pulse train at a repetition rate of 152 MHz. The pulse duration is found to be approximately 26.4 ps.

The AlGaInAs QWs, used as a saturable absorber in a mode-locked 1.34 μm laser, was grown on Fe-doped InP substrate by metal-organic chemical-vapor deposition. Instead of the conventional S-doped InP substrate (with a carrier concentration around $5 \times 10^{18} \text{ cm}^{-3}$), a semi-insulating Fe-doped InP substrate was used, because it almost has no absorption for the light wavelength greater than 940 nm [22–24]. Since the Fe-doped InP substrate is transparent at 1.34 μm , the function of the distributed Bragg reflector in the SESAM device can be replaced by an external mirror. The saturable absorber is formed by two 8 nm AlGaInAs QWs with the bandgap wavelength near 1.34 μm , spaced at quarter-wavelength intervals by AlGaInAs barrier layers with the bandgap wavelength around 1.07 μm . The backside of the substrate was mechanically polished after growth. The both sides of the SESAM were coated for antireflection (AR) at 1.34 μm to reduce the couple cavity effects. Unlike for the saturable absorber based on InAs/GaAs QDs [12], the peak wavelength of the photoluminescence spectrum for AlGaInAs QWs almost does not vary with the position of the wafer. In other words, the uniformity of the optical property of AlGaInAs QWs is significantly superior to that of InAs/GaAs QDs. The initial transmission of the SESAM device at the wavelength of 1.34 μm was measured to be approximately 97.5%. Figure 1 shows the transmittance spectrum at room temperature for the AR-coated AlGaInAs/InP saturable absorber. A Q-switched Nd:YVO₄ laser at 1.34 μm was used to measure the modulation depth of the QW saturable absorber with the z-scan method. The pump pulse energy and pulse width were 40 μJ and 40 ns, respectively. The pump fluence was varied in the range of 0.5–50 $\mu\text{J}/\text{cm}^2$. Note that

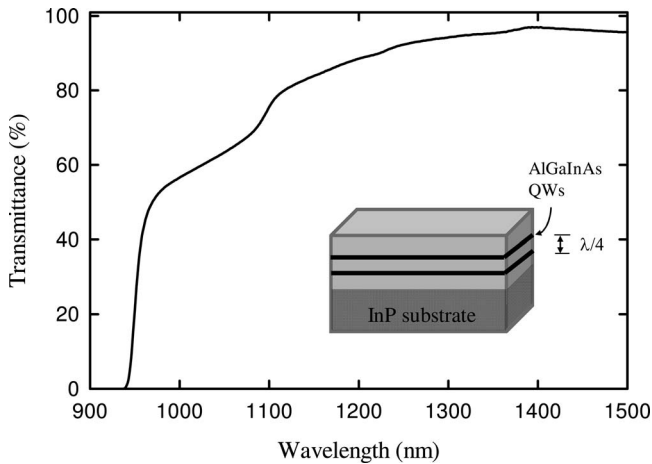


Fig. 1. Transmittance spectrum at room temperature for the AR-coated AlGaInAs saturable absorber. Inset, schematic diagram of the AlGaInAs QW structure, where λ is the value of lasing wavelength.

we cannot measure the absorber recovery time because of no suitable probe beam. The total nonsaturable loss introduced by the SESAM was found to be less than 0.7%. According to the experimental results, the saturation fluence is estimated to be in the range of $20 \mu\text{J}/\text{cm}^2$, and the modulation depth is about 1.8%.

Figure 2 depicts the experimental configuration for a continuously mode-locked $1.34 \mu\text{m}$ Nd:YVO₄ laser with AlGaInAs QWs as a saturable absorber. The gain medium was a 0.3 at. % Nd:YVO₄ crystal with a length of 9 mm. Both sides of the laser crystal were coated for AR at $1.34 \mu\text{m}$ ($R < 0.2\%$) and a wedge-cut angle 0.5° . The laser crystal was wrapped with indium foil and mounted in a water-cooled copper block, and the water temperature was maintained at 20°C . The pump source was a 16 W fiber-coupled laser diode at 808 nm with a core diameter of $800 \mu\text{m}$ and an NA of 0.16. Focusing lenses with 17.5 mm focal length and 85% coupling efficiency were used to reimage the pump beam into the laser crystal. The pump spot radius was approximately $350 \mu\text{m}$. The laser cavity consisted of one input mirror; two high-reflection (HR) concave mirrors, M1 and M2, at lasing wavelength ($R > 99.8\%$); and an output coupler with reflectivity of 94% and a wedge-cut angle of 2° . The input mirror was a 500 mm radius of curvature concave mirror with an AR coating at 808 nm ($R < 0.2\%$) on the entrance face, an HR coating at the lasing wavelength ($R > 99.8\%$), and a high-

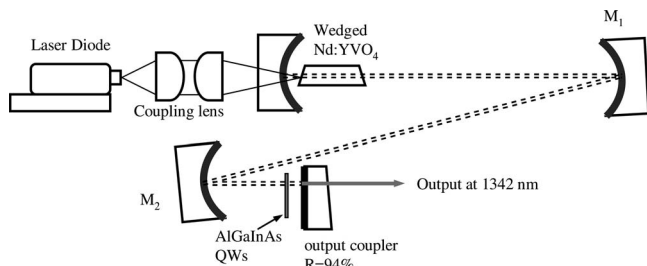


Fig. 2. Schematic of a diode-pumped self-starting continuous-mode-locked Nd:YVO₄ laser at 1342 nm.

transmission coating at 808 nm ($T > 90\%$) on the other face. Note that the laser crystal was placed closed to the input mirror for spatial overlap of the transverse mode structure and radial pump power distribution. The radii of curvature of mirror M1 and M2 were 500 mm and 100 mm, respectively. M1 and M2 were separated by 600 mm; the overall cavity length was approximately 100 cm. The laser mode radii were $350 \mu\text{m}$ inside the laser crystal and $50 \mu\text{m}$ on the QW saturable absorber.

Prior to performing the mode-locked operation, we first studied the cw performance for the laser system with different reflectivity of 92%, 94%, 96%, and 98% at 1342 nm. The optimum reflectivity of the output coupler was found to be 94%. Figure 3 depicts the average output power at 1342 nm with respect to the incident pump power in cw operation and in cw mode-locked operation. In the cw regime the laser had a slope efficiency of 21.4%; the output power reached 2.3 W at an incident pump power of 13 W. With a AlGaInAs QWs saturable absorber, the laser self-started the cw mode-locked operation at pump powers greater than 4.5 W. Experimental results revealed that the stable cw mode locking could be realized within the range of the pump power from 4.5 W to 12.3 W. As shown in Fig. 3, the laser had a slope efficiency of 11%; the output power reached 1.05 W at an incident pump power of 12.3 W. If the pump power was increased beyond 12.3 W, the mode-locked pulse train exhibited unstable behavior because of the thermal effects. It is worth noting that we did not observe any optical damage in the AlGaInAs saturable absorber during the experiment.

The cw mode-locked pulse train was recorded by a LeCroy digital oscilloscope (Wavepro 7100; 10 G sample/s, 1 GHz bandwidth) with a fast p-i-n photodiode. Figure 4(a) shows a typical pulse train of the cw mode-locked laser. It can be seen that the pulse period of 6.6 ns is consistent with the round-trip time of the cavity length. The pulse duration at the cw mode-locked operation was measured with an autocorrelator (APE pulse check, Angewandte physik & Elektronik GmbH). With the Gaussian-fitted profile, the pulse duration was found to be approxi-

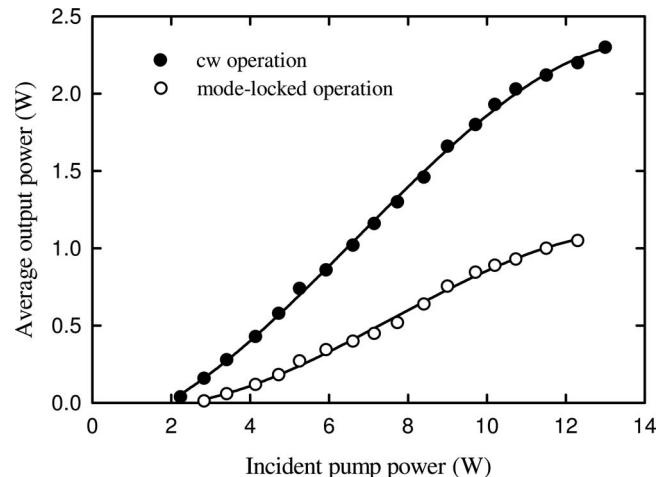


Fig. 3. Average output power at 1342 nm versus incident pump power in cw and mode-locked operations.

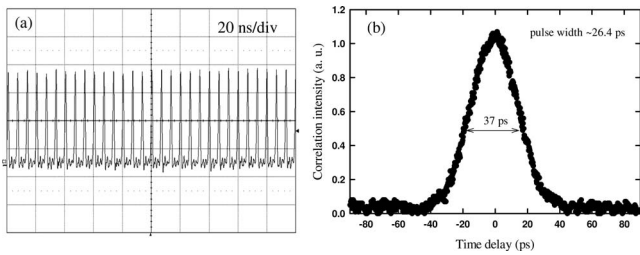


Fig. 4. (a) Typical oscilloscope trace of a train of mode-locked output pulses, (b) autocorrelation trace of the output pulses.

mately 26.4 ps, as shown in Fig. 4(b). The spectral properties of the laser were monitored by an optical spectrum analyzer (Advantest Q8347) with a resolution of 0.005 nm. The spectral bandwidth (FWHM) was found to be 0.12 nm. This result indicates a time–bandwidth product of 0.48. The narrower bandwidth might arise from the etalon effect of the thin AlGaInAs QWs device. It is expected that the etalon effect can be effectively reduced by use of a high-quality AR coating on the both surface of the InP wafer.

In conclusion, we have designed AlGaInAs QWs grown on the Fe-doped InP substrate to be a saturable absorber for self-starting continuous-mode-locked Nd:YVO₄ laser at 1342 nm. Stable mode-locked pulses of 26.4 ps duration with a repetition rate of 152 MHz were generated within the range of incident pump power from 4.5 W to 12.3 W. The average output power for the cw mode-locked operation was 1.05 W at an incident pump power of 12.3 W. The present result confirms that the AlGaInAs QWs structures can be utilized to be saturable absorbers for the passively mode-locked lasers in the spectral region near 1.3 μm .

The authors gratefully acknowledge receipt of AlGaInAs/InP QW devices from TrueLight Corporation. The authors also thank the National Science Council for its financial support of this research under contract NSC-97-2112-M-009-016-MY3.

References

1. R. Fluck, G. Zhang, U. Keller, K. J. Weingarten, and M. Moser, *Opt. Lett.* **21**, 1378 (1996).
2. O. Musset and J. P. Boquillon, *Appl. Phys. B* **64**, 503 (1997).
3. H. J. Zhang, J. H. Liu, J. Y. Wang, X. G. Xu, and M. H. Jiang, *Appl. Opt.* **44**, 7439 (2005).
4. H. T. Huang, J. L. He, C. H. Zuo, H. J. Zhang, J. Y. Wang, and H. T. Wang, *Appl. Phys. B* **89**, 319 (2007).
5. Y. F. Chen, L. J. Lee, T. M. Huang, and C. L. Wang, *Opt. Commun.* **163**, 198 (1999).
6. R. Zhou, S. C. Ruan, C. L. Du, and J. Q. Yao, *Opt. Commun.* **282**, 605 (2009).
7. U. Keller, D. A. B. Miller, G. D. Boyd, T. H. Chiu, J. F. Ferguson, and M. T. Asom, *Opt. Lett.* **17**, 505 (1992).
8. U. Keller, K. J. Weingarten, F. X. Kärtner, D. Kopf, B. Braun, I. D. Jung, R. Fluck, C. Hönninger, N. Matuschek, and J. Aus Der Au, *IEEE J. Sel. Top. Quantum Electron.* **2**, 435 (1996).
9. M. Kondow, K. Uomi, A. Niwa, T. Kitatani, S. Watahiki, and Y. Yazawa, *Jpn. J. Appl. Phys.* **35**, 1273 (1996).
10. H. D. Sun, G. J. Valentine, R. Macaluso, S. Calvez, D. Burns, and M. D. Dawson, *Opt. Lett.* **27**, 2124 (2002).
11. G. J. Spühler, L. Krainer, V. Liverini, R. Grange, M. Haiml, S. Pawlik, B. Schmidt, S. Schön, and U. Keller, *IEEE Photon. Technol. Lett.* **17**, 1319 (2005).
12. K. W. Su, H. C. Lai, A. Li, Y. F. Chen, and K. F. Huang, *Opt. Lett.* **30**, 1482 (2005).
13. H. Temkin, D. Coblenz, R. A. Logan, J. P. van der Ziel, T. Tanbun-Ek, R. D. Yadvish, and A. M. Sergent, *Appl. Phys. Lett.* **62**, 2402 (1993).
14. N. Nishiyama, C. Caneau, B. Hall, G. Guryanov, M. H. Hu, X. S. Liu, M.-J. Li, R. Bhat, and C. E. Zah, *IEEE J. Sel. Top. Quantum Electron.* **11**, 990 (2005).
15. A. Li, S. C. Liu, K. W. Su, Y. L. Liao, S. C. Huang, Y. F. Chen, and K. F. Huang, *Appl. Phys. B* **84**, 429 (2006).
16. R. Fluck, B. Braun, E. Gini, H. Melchior, and U. Keller, *Opt. Lett.* **22**, 991 (1997).
17. B. C. Barnett, L. Rahman, M. N. Islam, Y. C. Chen, P. Bhattacharya, W. Riha, K. V. Reddy, A. T. Howe, K. A. Stair, H. Iwamura, S. R. Friberg, and T. Mukai, *Opt. Lett.* **20**, 471 (1995).
18. K. Alavi, H. Temkin, W. R. Wagner, and A. Y. Cho, *Appl. Phys. Lett.* **42**, 254 (1983).
19. W. T. Tsang and N. A. Olsson, *Appl. Phys. Lett.* **42**, 922 (1983).
20. S. C. Huang, S. C. Liu, A. Li, K. W. Su, Y. F. Chen, and K. F. Huang, *Opt. Lett.* **32**, 1480 (2007).
21. J. Y. Huang, S. C. Huang, H. L. Chang, K. W. Su, Y. F. Chen, and K. F. Huang, *Opt. Express* **16**, 3002 (2008).
22. R. Fornari and J. Kumar, *Appl. Phys. Lett.* **56**, 638 (1990).
23. L. P. Gonzalez, J. M. Murray, S. Krishnamurthy, and S. Guha, *Opt. Express* **17**, 8741 (2009).
24. T. Kawase, R. Shiomi, and M. Yamada, *Mater. Sci. Semicond. Process.* **9**, 362 (2006).

Low-temperature study of lasing characteristics for 1.3- μm AlGaInAs quantum-well laser pumped by an actively Q-switched Nd:YAG laser

K. W. Su, Yi-Fan Chen, S. C. Huang, A. Li, S. C. Liu, Y. F. Chen, and K.F. Huang
Department of Electrophysics, National Chiao Tung University, Hsinchu, Taiwan

ABSTRACT

We report a low-temperature 1.3 μm AlGaInAs quantum-well laser pumped by a 1.06 μm active Q-switched laser quenched by a low-temperature vacuum system. An average power of 330 mW is achieved at temperature as low as 233 K compared to the average power of 50 mW obtained at room-temperature without cooling device both at pumping repetition rate of 30 kHz. And the average rate of gain peak shift was found to be 0.47 nm/K between 293-133 K.

Keywords: VECSEL ; AlGaInAs ; quantum well

1. INTRODUCTION

High-peak-power all-solid-state laser sources in the 1.3-1.6 μm spectral region are of particular interest in remote sensing, eye-safe optical ranging, fiber sensing, and communication^[1-4]. To achieve this, diode pumped solid state lasers (DPSSLs) has advantage points of relatively compact size, high power, excellent beam quality, long lifetime, and low heat production have been widely used for various applications including industry, pure science, medical diagnostics, and entertainment^[5]. Unfortunately, the spectral range of DPSSLs is limited by the properties of doped ion in crystals and glasses. Vertical-external-cavity Surface-emitting semiconductor lasers (VECSELs) which combines both advantages of DPSSLs and semiconductor lasers allows for flexible choice of emission wavelength via bandgap engineering have successfully conquered this situation. Typically this structure

consists of a highly reflecting distributed reflector (DBR) grown on a lattice-matched substrate with resonant-periodic-gain structure that comprises a series of barriers to provide the pump absorption, quantum wells to provide gain, and cap layers to prevent surface recombination and oxidation.

The long wavelength (1.3-1.55 μm) semiconductor laser occurred at spectral range covered by lasers based on GaAs and InP substrates. For InGaAs/GaAs system, at an operation over 1 μm there would be too much scattering loss to have good efficiency due to compressed strain. But the introduction of strain-compensating GaAsP layers as buffer layer could improve the high power operation [6]. On the other hand, laser gain structure based on InP substrate like InGaAsP solid solution system [7,8] suffers from poor temperature characteristic due to their small conduction band offset. To conquer this, an alternative of using AlGaInAs material system with deeper conduction band offset has brought up. But there still have difficulties forming DBRs like low refractive index contrast, low thermal conductivity or high complexity of growth [9-11]. Another way to achieve long wavelength range is using GaInNAs/GaAs system with high contrast GaAs/AlGaAs DBRs and larger conduction band offset [12]. Adding a few of nitrogen will result in the redshift of absorption wavelength and a reduction of lattice mismatch to GaAs [13]. So we can adjust the ratio of indium and nitrogen content to reach the wavelength we want. Because nitrogen is too small in this quaternary alloys, there is a drawback that too many nitrogen content will introduce large number of nonradiative defects. As a result it is difficult to fabricate this compound for long wavelength range. In this work, we use AlGaInAs/InP MQWs as our gain region of optically pumped VECSEL and with cooling temperature at 283K we obtained 140mW output power at the repetition rate of 10kHz and 1.2W input power [14]. Raising input power will decrease the lasing efficiency and a roll-over effect came into existence. However, the temperature dependent laser performance and physics have not been realized. But we believed that it mainly caused by the diffusion of carrier from the gain region due to the heat produced by the high absorbed power. To study the optical characteristics under low temperature, we made a simple cavity put in a vacuum system cooled by liquid nitrogen and heated by Lake Shore 331 Temperature Controller and the temperature is controlled at the suitable degree.

In this article we present a low-temperature 1.3 μm AlGaInAs quantum-well laser pumped by a 1.06 μm Nd:YAG active Q-switch laser quenched by liquid nitrogen. An average power of 330mW is achieved at temperature as low as 233K compared to the average power of 50mW obtained at room-temperature without cooling device both at pumping repetition rate of 30 kHz. And the average rate of gain peak shift was found to be 0.47 nm/K between 293-133 K.

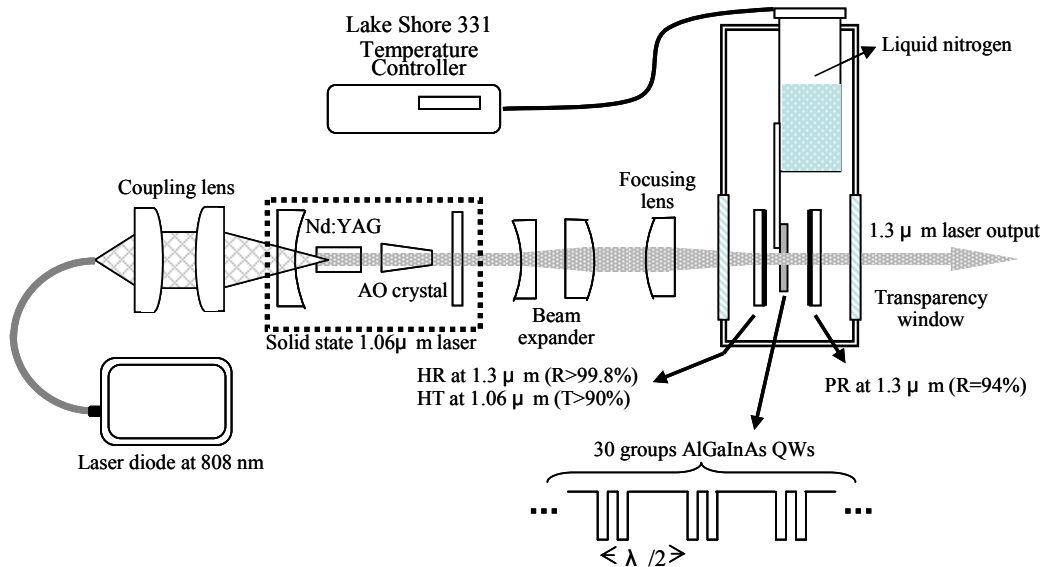


Fig. 1 Experimental setup of low temperature AlGaInAs/InP semiconductor disk laser at 1.3 μ m pumped by a 1.06 μ m A-O Q-switched laser and quenched by a low-temperature vacuum cooling system

2. EXPERIMENTAL SETUP

Fig. 1 shows the experimental configuration of the low-temperature 1.3 μ m AlGaInAs quantum-well laser pumped by a 1.06 μ m Nd:YAG active Q-switched laser. The pumping source provides 20-60 ns pulses at repetition rate between 20 and 60 kHz. We controlled pump spot diameter to be about 420 μ m to have efficient spatial overlap with lasing mode. The gain region consists of 30 groups of two QWs spaced at half-wavelength intervals by AlGaInAs barrier layers with the bandgap around 1070 nm. This is a RPG structure that barrier layers are used not only to absorb pumping light but also to locate the quantum well region at the anti-node of the lasing field standing wave and it can enhance the wavelength selection^[15-17], and we obtained the peak luminescence wavelength around 1365 nm.

The laser resonator is a plano-plano cavity with front mirror which has anti-reflection coating on the entrance face at 1064 nm ($R < 0.2\%$), high-reflection coating at 1365 nm ($R > 99.8\%$), and high transmission coating at 1064 nm ($T > 90\%$) on the other face. The reflectivity of the output coupler is 94% at 1365 nm and the overall cavity length is about 5mm. This flat-flat cavity is stabilized by the thermal induced lens in the gain medium^[18,19]. It is an attractive design because it reduces complexity and makes the system compact and rugged. The gain medium is cooled down by liquid nitrogen and the temperature is controlled by Lake Shore 331 Temperature Controller. The whole structure of laser cavity is inside the Janis VPF-100 cryogenic vacuum equipment to avoid the fog of steam on the

window. And the two transparency windows have high transmittance for spectral range of both lasing and pumping wavelength.

The gain medium was composed of an AlGaInAs QW/barrier structure grown on a Fe-doped InP transparent sub-structure by metalorganic chemical-vapor deposition. Compared to the conventional S-doped InP which has strong absorption in the 1.0-2.0 spectral region, Fe-doped InP has better transparency at lasing wavelength. It is worth mentioning that In-P based systems suffer from the lack of good DBR and has been challenging to transfer from edge-emitting lasers to surface-emitting lasers. By the use of Fe-doped InP, we could replace DBRs in the VECSEL by an external mirror. An InP window layer was deposited on the gain structure to avoid surface recombination and oxidation. The back side of the substrate was mechanically polished after growth. Both sides of the gain chip were anti-reflection coated at lasing and pumping wavelengths to reduce backreflections and coupled-cavity effects. And the total residual reflectivity of the AR-coated sample is approximately 5%.

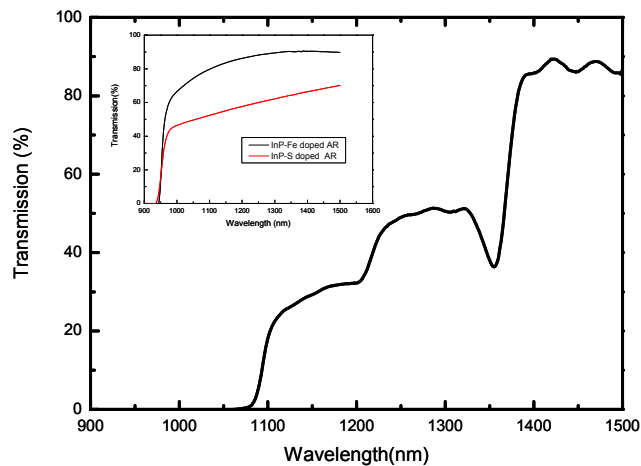


Fig. 2 Transmittance spectrum of AR-coated AlGaInAs/InP MQWs gain chip at room temperature. Inset, room temperature transmittance spectrum of S-doped and Fe-doped InP chip with anti-reflection coating.

Figure 2 shows the transmittance for the AR-coated AlGaInAs/InP gain chip at room temperature. It can be seen that the strong absorption of the barrier layers leads to low transmittance near 1070 nm. The total absorption efficiency of the barrier layers at 1064 nm was found to be approximately 95% for the pulse pumping. On the other hand, an abrupt change in transmittance near 1365 nm comes from the absorption of the AlGaInAs QWs. The inset of Figure 2 shows the transmittance of Fe-doped and S-doped InP with anti-reflection coating. We could observe that the transmittance is about 90% for Fe-doped InP and 60% for S-doped InP near 1365 nm.

3. RESULT AND DISCUSSION

Fig. 3 shows the performance of the optically-pumped 1.3 μm AlGaInAs MQWs laser operated with different cooling temperature ranged from 293 K to 233 K at repetition rate of 15 kHz at low power and 30 kHz at high power. The pulse width at repetition rate of 15 kHz and 30 kHz are ranged from 50 ns to 30 ns and 120 ns to 52 ns respectively. The transverse mode was measured to be the fundamental mode over the complete output power range. The beam quality factor was determined by the Gaussian fit to the laser beam waist and the divergence angle which was found to be less than 1.5. We can see that the slope efficiency is increasing with decreasing temperature, and the maximum output power of 293 K and 233 K are 50 mW and 330 mW respectively. From the past work of our group [14,20,21], we know that the roll-over of output power at low repetition rate is resulted from the gain saturation or the transparency induced by the pumping beam. Although the pumping energy density is larger than the lasing energy density, the gain-saturation effect is more conspicuous than the nonlinear transparency of the barrier due to its long absorption length. So we could still observe the roll-over of output power at 1.8W pumping power even at temperature as low as 293 K.

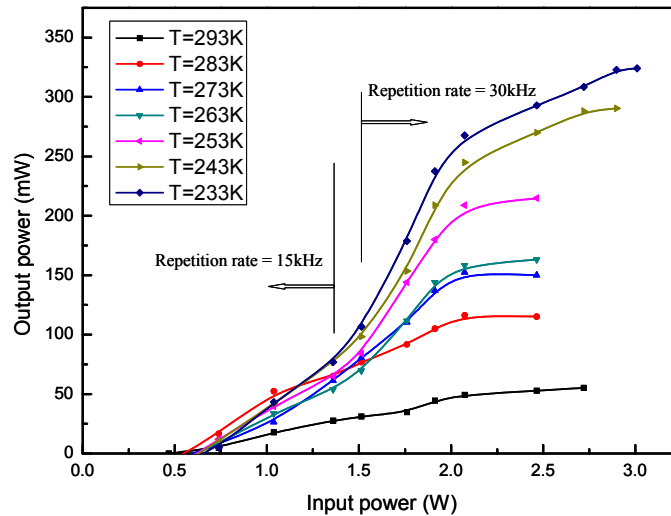


Fig. 3 Experimental results of AlGaInAs 1.3 μm MQWs laser pumped by an 1.06 μm active Q-switched Nd:YAG laser at different cooling temperature. It shows the output power of 15 kHz repetition rate at low input power and 30kHz at high input power.

Fig 4 is the photoluminescence of AlGaInAs MQWs wafer excited by a 1.06 μm active Q-switched laser with 1.2 W pumping power and 800 μm pumping spot size at 30 kHz and cooled from 293 K to 133 K. There are two peaks at about 1350 nm and 1245 nm due to the $n=1$ and $n=2$ transition at 293 K respectively. The $n=1$ peak wavelength shifts from 1350 nm to 1275 nm with the

slope of 0.47 nm/K and the $n=2$ peak disappears gradually. The line-width of $n=1$ peak became narrower with decreasing temperature due to the reduction of collision broadening.

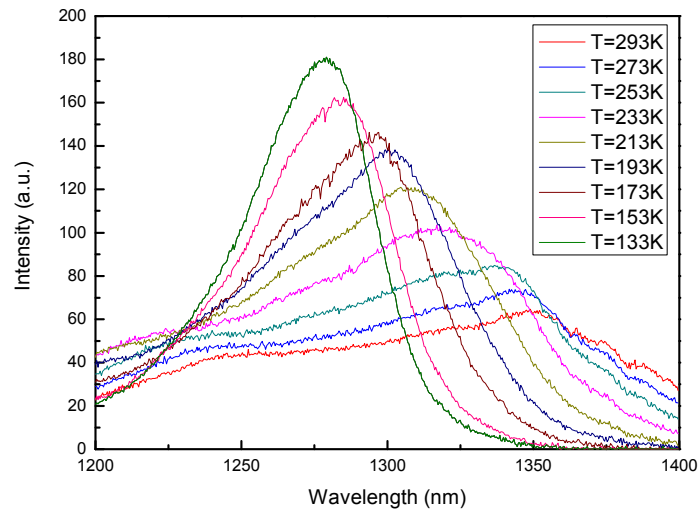


Fig. 4 Experimental results of photoluminescence pumped at input power of 1.2W and repetition rate of 30kHz at different cooling temperature.

REFERENCE

- [1] Gratchikov, A. S., Kuzmin, A. N., Lisinetskii, V. A., Orlovich, V. A., Demidovich, A. A., Yumashev, K. V., Kuleshov, N. V., Eichler, H. J., and Danalov, M. V., "Passively Q-switched 1.35 μm diode pumped Nd:KGW laser with V:YAG saturable absorber," *Opt. Mater.* 16, 349 (2001)
- [2] Fluck, R., Harling, R., Paschotta, R., Gini, R., Melchior, H., and Keller, U., "Eyesafe pulsed microchip laser using semiconductor saturable absorber mirrors," *Appl. Phys. Lett.* 72, 3273 (1998)
- [3] Stultz, R. D., Leyva, V., and Spariosu, K., "Short pulse, high-repetition rate, passively Q-switched Er:yttrium-aluminum-garnet laser at 1.6 microns," *Appl. Phys. Lett.* 87, 241118 (2005)
- [4] Savitski, V. G., Posnov, N. N., Prokoshin, P. V., Malyarevich, A. M., Yumashev, K. V., Demchuk, M. I., and Lipovski, A. A., "PbS-doped phosphate glasses saturable absorbers for 1.3- μm neodymium lasers," *Appl. Phys. B* 75, 841 (2002)
- [5] Spies, D. L., "Highly efficient neodymium:yttrium aluminum garnet laser end pumped by a semiconductor laser array," *Appl. Phys. Lett.* 47, 74 (1985)
- [6] Keller, U., "Ultrafast all-solid-state laser technology," *Appl. Phys. B* 58, 347 (1994)
- [7] Symonds, C., Sagnes, I., Garnache, A., Hoogland, S., Saint-Girons, G., Tropper, A. C., Oudar, J. L., "Continuous-wave operation of monolithically grown 1.5- μm optically pumped

- vertical-external-cavity surface-emitting-lasers,” *Appl. Opt.* 42, 6678 (2003)
- [8] Kurdi, M. E., Bouchoule, S., Bousseksou, A., Sagnes, I., Plais, A., Strassner, M., Symonds, C., Garnache, A., Jacquet, J., “Room-temperature continuous-wave laser operation of electrically 1.55 μm VECSEL,” *Electron. Lett.* 40, 671 (2004)
- [9] Lambert, B., Toudic, Y., Rouillard, Y., Gauneau, M., Baudet, M., Alard, F., Valiente, I., Simon, J. S., “High reflectivity 1.55 μm (Al)GaAsSb/AlAsSb Bragg reflector lattice matched on InP substrates,” *Appl. Phys. Lett.* 66, 442 (1995)
- [10] Baek, J. H., Choi, I. H., Lee, B., Han, W. S., Cho, H. K., “Precise control of 1.55 μm vertical-cavity surface-emitting laser structure with InAlGaAs/InAlAs Bragg reflectors by situ growth monitoring,” *Appl. Phys. Lett.* 75, 1500 (1999)
- [11] Nishiyama, N., Caneau, C., Hall, B., Guryanov, G., Hu, M. H., Liu, X. S., Li, M. J., Bhat, R., Zah, C. E., “Long-wavelength vertical-cavity surface-emitting laser on InP with lattice matched AlGaInAs-InP DBR grown by MOCVD,” *IEEE J. Sel. Top. Quantum Electron.*
- [12] Kondow, M., Uomi, K., Niwa, A., Kitatani, T., Watahiki, S., and Yazawa, Y., “GaInNAs: A novel material for long-wavelength-range laser diodes with excellent high-temperature performance,” *Jpn. J. Appl. Phys. Part 1* 35, 1273 (1996)
- [13] Keller, U., Toppo, A. C., “Passively mode locked surface-emitting semiconductor lasers,” *Physics Reports* 429, 67 (2006)
- [14] Su, K. W., Huang, S. C., Li, A., Liu, S. C., Chen, Y. F., and Huang, K. F., “High-peak-power AlGaInAs quantum-well 1.3- μm laser pumped by a diode-pumped actively Q-switched solid-state laser,” *Opt. Lett.* 31, 2009 (2006)
- [15] Raya, M. Y. A., Brueck, S. R. J., Osinsky, M., Schaus, C. F., McInery, J. G., Brennan, T. M., Hammons, B. E., “Resonant periodic gain surface-emitting semiconductor lasers,” *IEEE J. Quantum Electron.* 26, 1500 (1989)
- [16] Raya, M. Y. A., Brueck, S. R. J., Scully, M. O., Lee, C., “Resonant periodic-gain surface-emitting semiconductor lasers and correlated emission in a ring cavity,” *Phys. Rev. A* 44, 4599 (1991)
- [17] Zhou, J., Cada, M., He, J., Makino, T., “Analysis and design of combined distributed-feedback/Fabry-Perot structures for surface-emitting semiconductor lasers,” *IEEE J. Quantum Electron.* 32, 417 (1996)
- [18] Zayhowski, J. J., Mooradian, “Single-frequency microchip Nd lasers,” *Appl. Opt.* 14, 24 (1989)
- [19] Dixon, G. J., Liang, L. S., Jarmann, R. H., “Properties of closely coupled monolithic, lithium neodymium, tetraphosphate lasers,” *Proc. SPIE* 1104, 107 (1989)
- [20] Huang, S. C., Chang, H. L., Su, K. W., Li, A., Liu, S. C., Chen, Y. F., Huang, K. F., “AlGaInAs/InP eye-safe laser pumped by a Q-switched Nd:GdVO₄ laser,” *Appl. Phys. B* 94, 483 (2009)
- [21] Chang, H. L., Huang, S. C., Chen, Yi-Fan, Su, K. W., Chen, Y. F., Huang, K. F., “Efficient high-peak-power AlGaInAs eye-safe wavelength disk laser with optical in-well pumping,” *Opt. Express* 17, 11409 (2009)